

Improving the Foundation Layers for Concrete Pavements

TECHNICAL REPORT:

Pavement Foundation Layer Reconstruction with Cement Treated Base Underlain by Geotextile – Michigan I-96 Field Study



November 2015

Sponsored by

Federal Highway Administration (DTFH 61-06-H-00011 (Work Plan #18))

FHWA TPF-5(183): California, Iowa (lead state), Michigan, Pennsylvania, Wisconsin

**National Concrete Pavement
Technology Center**



CENTER FOR

CEER

**EARTHWORKS ENGINEERING
RESEARCH**

IOWA STATE UNIVERSITY
Institute for Transportation

About the National CP Tech Center

The mission of the National Concrete Pavement Technology (CP Tech) Center is to unite key transportation stakeholders around the central goal of advancing concrete pavement technology through research, tech transfer, and technology implementation.

About CEER

The mission of the Center for Earthworks Engineering Research (CEER) at Iowa State University is to be the nation's premier institution for developing fundamental knowledge of earth mechanics, and creating innovative technologies, sensors, and systems to enable rapid, high quality, environmentally friendly, and economical construction of roadways, aviation runways, railroad embankments, dams, structural foundations, fortifications constructed from earth materials, and related geotechnical applications.

Disclaimer Notice

The contents of this report reflect the views of the authors, who are responsible for the facts and the accuracy of the information presented herein. The opinions, findings and conclusions expressed in this publication are those of the authors and not necessarily those of the sponsors.

The sponsors assume no liability for the contents or use of the information contained in this document. This report does not constitute a standard, specification, or regulation.

The sponsors do not endorse products or manufacturers. Trademarks or manufacturers' names appear in this report only because they are considered essential to the objective of the document.

Iowa State University Non-Discrimination Statement

Iowa State University does not discriminate on the basis of race, color, age, ethnicity, religion, national origin, pregnancy, sexual orientation, gender identity, genetic information, sex, marital status, disability, or status as a U.S. veteran. Inquiries regarding non-discrimination policies may be directed to Office of Equal Opportunity, Title IX/ADA Coordinator, and Affirmative Action Officer, 3350 Beardshear Hall, Ames, Iowa 50011, 515-294-7612, email eooffice@iastate.edu.

Iowa Department of Transportation Statements

Federal and state laws prohibit employment and/or public accommodation discrimination on the basis of age, color, creed, disability, gender identity, national origin, pregnancy, race, religion, sex, sexual orientation or veteran's status. If you believe you have been discriminated against, please contact the Iowa Civil Rights Commission at 800-457-4416 or the Iowa Department of Transportation affirmative action officer. If you need accommodations because of a disability to access the Iowa Department of Transportation's services, contact the agency's affirmative action officer at 800-262-0003.

The preparation of this report was financed in part through funds provided by the Iowa Department of Transportation through its "Second Revised Agreement for the Management of Research Conducted by Iowa State University for the Iowa Department of Transportation" and its amendments.

The opinions, findings, and conclusions expressed in this publication are those of the authors and not necessarily those of the Iowa Department of Transportation or the U.S. Department of Transportation Federal Highway Administration.

Technical Report Documentation Page

1. Report No. DTFH 61-06-H-00011 Work Plan 18	2. Government Accession No.	3. Recipient's Catalog No.	
4. Title and Subtitle Improving the Foundation Layers for Concrete Pavements: Pavement Foundation Layer Reconstruction with Cement Treated Base Underlain by Geotextile – Michigan I-96 Field Study		5. Report Date November 2015	
		6. Performing Organization Code	
7. Author(s) David J. White, Pavana K. R. Vennapusa, Heath H. Gieselman, Alexander J. Wolfe, Alexander E. Johnson, Rachel Franz, La Zhao		8. Performing Organization Report No. InTrans Project 09-352	
9. Performing Organization Name and Address National Concrete Pavement Technology Center and Center for Earthworks Engineering Research (CEER) Iowa State University 2711 South Loop Drive, Suite 4600 Ames, IA 50010-8664		10. Work Unit No. (TRAIS)	
		11. Contract or Grant No.	
12. Sponsoring Organization Name and Address Federal Highway Administration U.S. Department of Transportation 1200 New Jersey Avenue SE Washington, DC 20590		13. Type of Report and Period Covered Technical Report	
		14. Sponsoring Agency Code TPF-5(183)	
15. Supplementary Notes Visit www.cptechcenter.org or www.ceer.iastate.edu for color PDF files of this and other research reports.			
16. Abstract <p>This technical project report is one of the field project technical reports developed as part of the TPF-5(183) and FHWA DTFH 61-06-H-00011:WO18 studies.</p> <p>This report presents results and analysis from a field study conducted on an interstate highway I-96 reconstruction project near Lansing, Michigan. The existing I-96 section with portland cement concrete (PCC) pavement was removed and replaced with a twenty-year design life jointed PCC underlain by a cement treated base (CTB) layer consisting of recycled PCC and existing or new sand subbase with a geotextile separator at the CTB/subbase interface. The Iowa State University (ISU) research team conducted field testing on the new pavement foundation layers during construction to compare with the design assumed values. Field testing was conducted by spacing measurements about 50–100 m apart along the alignment and also in a dense grid pattern (spaced at about 0.9 to 3.0 m) to capture spatial variability over a small area. Geostatistical analysis was performed to analyze the test data from the dense grid pattern testing to characterize and quantify spatial non-uniformity of the foundation layer properties. Field measurements indicated composite modulus of subgrade reaction values ranging from 101 kPa/mm (370 pci) to 327 kPa/mm (1200 pci), which were about 0.74 times and 2.4 times the design assumed values. The lower bound value was based on the average in situ 406 mm (16 in.) thick subbase (including CTB base and sand subbase) layer modulus and in situ subgrade layer resilient modulus (M_r) from falling weight deflectometer (FWD) measurements. The upper bound value was based on average subbase layer modulus from FWD and average M_r determined from dynamic cone penetrometer measurements. Both laboratory and field measurements indicated that the quality of the drainage layer can be rated as excellent according to AASHTO (1993), which exceeds the good rating assumed in the design.</p> <p>Laboratory resilient modulus testing was conducted on homogenous and layered composite samples. Results indicated that on average, the resilient modulus of layered composite samples was about 20% lower than that of a homogenous subbase layer sample with similar density, and the reduction is attributed to the weaker subgrade layer. Compressive strength testing of CTB samples indicated that 12 of 13 samples tested (by both ISU and MDOT) met the project specifications.</p>			
17. Key Words concrete pavement—pavement foundation—quality assurance—quality control—subbase—subgrade		18. Distribution Statement No restrictions.	
19. Security Classification (of this report) Unclassified.	20. Security Classification (of this page) Unclassified.	21. No. of Pages 126	22. Price NA

IMPROVING THE FOUNDATION LAYERS FOR CONCRETE PAVEMENTS: PAVEMENT FOUNDATION LAYER RECONSTRUCTION WITH CEMENT TREATED BASE UNDERLAIN BY GEOTEXTILE – MICHIGAN I-96 FIELD STUDY

Technical Report
November 2015

Research Team Members

Tom Cackler, David J. White, Jeffery R. Roesler, Barry Christopher, Andrew Dawson,
Heath Gieselman, and Pavana Vennapusa

Report Authors

David J. White, Pavana K. R. Vennapusa,
Heath H. Gieselman, Alexander J. Wolfe, Alexander E. Johnson, Rachel Franz, La Zhao
Iowa State University

Sponsored by

the Federal Highway Administration (FHWA)
DTFH61-06-H-00011 Work Plan 18
FHWA Pooled Fund Study TPF-5(183): California, Iowa (lead state),
Michigan, Pennsylvania, Wisconsin

Preparation of this report was financed in part
through funds provided by the Iowa Department of Transportation
through its Research Management Agreement with the
Institute for Transportation
(InTrans Project 09-352)

National Concrete Pavement Technology Center and Center for Earthworks Engineering Research (CEER)

Iowa State University
2711 South Loop Drive, Suite 4700
Ames, IA 50010-8664
Phone: 515-294-5798
www.cptechcenter.org and www.ceer.iastate.edu

TABLE OF CONTENTS

ACKNOWLEDGMENTS	xi
LIST OF ACRONYMS AND SYMBOLS	xiii
EXECUTIVE SUMMARY	xv
CHAPTER 1. INTRODUCTION	1
CHAPTER 2. PROJECT INFORMATION	3
Project Background.....	3
Pavement Design Input Parameter Selection and Assumptions	6
Construction Details and Specifications	7
CHAPTER 3. EXPERIMENTAL TEST METHODS.....	13
Laboratory Testing Methods and Data Analysis	13
Particle-Size Analysis and Index Properties	13
Resilient Modulus and Shear Strength Testing Sample Preparation	13
Resilient Modulus and Shear Strength Triaxial Testing	17
Resilient Modulus Data Analysis.....	19
Determination of Dynamic Secant Modulus from Cyclic Stress-Strain Data	20
Laboratory Permeability Tests	21
Compressive Strength Testing	24
Wet-Dry and Freeze/Thaw Durability Tests.....	24
In Situ Testing Methods.....	25
Real-Time Kinematic Global Positioning System	27
Zorn Light Weight Deflectometer	27
Kuab Falling Weight Deflectometer	27
Dynamic Cone Penetrometer	29
Nuclear Gauge	30
Rapid Gas Permeameter Test.....	30
Static Plate Load Test	31
Determination of k_{comp} Values	31
CHAPTER 4. LABORATORY TEST RESULTS	32
Particle-Size Analysis Results	33
Moisture-Dry Unit Weight Results.....	33
M_r and UU Test Results.....	36
Compressive Strength Test and Wet-Dry and Freeze-Thaw Durability Test Results.....	44
Laboratory Permeability Test Results.....	46
CHAPTER 5. IN SITU TEST RESULTS	48
Description of Test Sections	48
Geostatistical Data Analysis	48
TS1/TS3: Subbase Layer	49
Experimental Testing.....	49
In Situ Point Test Results and Discussion–TS1 and TS3	51

Geostatistical Analysis of Dense Grid Point Testing–TS1	57
TS2: Cement Treated Base (CTB) Layer.....	62
Test Beds Construction and Experimental Testing.....	62
In Situ Test Results and Data Analysis.....	65
Comparison of Design Values, In Situ Measurements, and Laboratory Measurements	73
Base Layer Elastic Modulus (E_{SB}).....	74
Subgrade Resilient Modulus (M_r).....	74
Composite Modulus of Subgrade Reaction (k_{comp}).....	75
Drainage Coefficient (C_d)	75
CHAPTER 6. SUMMARY AND CONCLUSIONS	76
REFERENCES	79
APPENDIX A: MDOT OFFICE MEMORANDUM (MAY 4, 2009) – PAVEMENT SELECTION.....	83
APPENDIX B: SPECIAL PROVISION 03CT303(A140) – OPEN GRADED DRAINAGE COURSE, MODIFIED (PORTLAND CEMENT-TREATED PERMEABLE BASE USING CRUSHED CONCRETE)	89
APPENDIX C: AASHTO (1993) DESIGN CHARTS.....	95
APPENDIX D: STRESS-STRAIN CURVES FROM RESILIENT MODULUS TESTS	99

LIST OF FIGURES

Figure 1. Approximate project start and end and test section locations	4
Figure 2. Compacted sand subbase layer on I-96 EB lane just north of M-43 intersection	8
Figure 3. Placement of geosynthetic layer and CTB over sand subbase layer	10
Figure 4. CTB layer placement	11
Figure 5. Compaction of CTB layer	12
Figure 6. Final CTB layer about 5 days after placement on I-96 EB lane near the West Grand River Hwy and I-96 interchange	12
Figure 7. Split mold, steel platen (4 in. diameter), and vibratory hammer for compaction of subbase material samples	14
Figure 8. Compaction of subbase material samples in split mold (left) and verification of thickness of each lift using calipers (right)	14
Figure 9. Shelby tube sampling and the sample extrusion device mounted on the freightliner truck of the ISU Geotechnical Mobile Laboratory	15
Figure 10. Aluminum spacers (4 in. diameter) used during static compaction	16
Figure 11. Static compaction procedure (left) and sample extrusion procedure (right) of a compacted cohesive soil sample	16
Figure 12. Triaxial chamber, load frame, and computer equipment for resilient modulus tests	17
Figure 13. One load cycle in M_r testing	19
Figure 14. Comparison of resilient ($M_{r(T307)}$), cyclic secant ($E^*_{s(T307)}$), and dynamic secant ($E_{s(T307)}$) modulus values	21
Figure 15. Large scale aggregate compaction mold laboratory permeameter	22
Figure 16. Setup used for permeability testing of CTB samples	23
Figure 17. Application of sealing gum around the top perimeter of a CTB sample	23
Figure 18. Compaction of CTB samples in a split Proctor mold using Marshall hammer for durability testing	24
Figure 19. Trimble SPS-881 hand-held receiver, Kuab falling weight deflectometer, and Zorn light weight deflectometer (top row left to right); dynamic cone penetrometer, nuclear gauge, and gas permeameter device (middle row left to right); and static plate load test (bottom row)	26
Figure 20. FWD deflection sensor setup used for this study and an example deflection basin	28
Figure 21. E_{v1} and E_{v2} determination procedure from static PLT for subgrade and base materials	31
Figure 22. Particle-size distribution curves of subgrade, subbase, and OGDC base materials	33
Figure 23. Moisture-dry unit weight relationships of subgrade material from Proctor tests and moisture-dry unit weight of M_r samples	34
Figure 24. Moisture-dry unit weight relationships of subbase material from Proctor tests and moisture-dry unit weight of M_r samples	35
Figure 25. Moisture-dry unit weight relationships of subbase material from vibratory compaction tests and moisture-dry unit weight of M_r samples	36
Figure 26. σ_d versus M_r for laboratory compacted subgrade samples at different dry unit weights and moisture contents	39

Figure 27. σ_d versus M_r for Shelby tube samples taken at 0.4 to 1.0 m below sand subbase layer.....	40
Figure 28. σ_B versus M_r for sand subbase samples.....	41
Figure 29. σ_B versus M_r for subbase and subgrade composite sample.....	42
Figure 30. Sand + subgrade composite sample during M_r testing (left) and after shearing (right)	43
Figure 31. Sand + subgrade composite sample extruded after shearing.....	43
Figure 32. CTB samples prepared by ISU research team before (left) and after (right) compression strength testing.....	44
Figure 33. Compressive strength test results on CTB samples prepared in laboratory by ISU research team and QC samples by MDOT (between 4/19/10 and 5/6/10).....	45
Figure 34. Compacted CTB sample from split mold for wet-dry and freeze-thaw testing	45
Figure 35. Percent mass loss during wet-dry and freeze-thaw cycles on three CTB samples.....	46
Figure 36. Description and parameters of a typical experimental and spherical semivariogram.....	49
Figure 37. TS1/TS3: Plan view of in situ test locations (left), detailed plan layout (top right), and image showing test locations.....	50
Figure 38. TS1/TS3: In situ NG, LWD, and PLT test results from Sta. 458+50 to 468+50	52
Figure 39. TS1/TS3: In situ DCP test results and estimated subgrade M_r from DCP test results from Sta. 804+00 to Sta. 814+00	53
Figure 40. TS3: DCP-CBR profiles at each test location	54
Figure 41. TS1: DCP-CBR profiles along each row.....	55
Figure 42. TS1 and TS3: Histograms of in situ test measurements.....	56
Figure 43. TS1: Kriged spatial contour maps (top) and semivariograms (middle) and histogram (bottom) plots of γ_d (left), and w (right) measurements.....	58
Figure 44. TS1: Kriged spatial contour map (top), semivariogram (middle), and histogram (bottom) plots of % fines (left) and K_{sat} (right) measurements.....	59
Figure 45. TS1: Kriged spatial contour map (top), semivariogram (middle), and histogram (bottom) plots of E_{LWD-Z3} (left) and $H_{Subbase}$ (right) measurements.....	60
Figure 46. TS1: Kriged spatial contour map (top), semivariogram (middle), and histogram (bottom) plots of DCP-CBR _{Subbase} (left) and DCP-CBR _{Subgrade} (right) measurements	61
Figure 47. TS2 CTB layer (looking east near Sta. 296+25)	62
Figure 48. GPT on TS2 CTB layer	63
Figure 49. FWD testing on TS2 CTB layer	63
Figure 50. Test locations along I-96 EB right lane (looking east near Sta. 297+00).....	64
Figure 51. TS2: CTB layer at selected test locations.....	65
Figure 52. TS2 CTB: Kriged spatial contour map (top), measurements longitudinally along the test section (middle), histogram (bottom left), and semivariogram (bottom right) of E_{FWD-K3} measurements	66
Figure 53. TS2 CTB: Kriged spatial contour map (top), measurements longitudinally along the test section (middle), histogram (bottom left), and semivariogram (bottom right) of E_{SB} measurements	67
Figure 54. TS2 CTB: Kriged spatial contour map (top), measurements longitudinally along the test section (middle), histogram (bottom left), and semivariogram (bottom right) of uncorrected E_{SG} measurements	68

Figure 55. TS2 CTB: Kriged spatial contour map (top), measurements longitudinally along the test section (middle), histogram (bottom left), and semivariogram (bottom right) of Corrected E_{SG} ($0.33 \times$ Uncorrected E_{SG}) measurements	69
Figure 56. TS2 CTB: Kriged spatial contour map (top), measurements longitudinally along the test section (middle), histogram (bottom left), and semivariogram (bottom right) of γ_d	70
Figure 57. TS2 CTB: Kriged spatial contour map (top), measurements longitudinally along the test section (middle), histogram (bottom left), and semivariogram (bottom right) of w	71
Figure 58. TS2 CTB: Kriged spatial contour map (top), measurements longitudinally along the test section (middle), histogram (bottom left), and semivariogram (bottom right) of K_{sat}	72
Figure 59. Chart to estimate modulus of subbase layer (E_{SB}) from CBR (from AASHTO 1993 based on results from van Til et al. 1972)	95
Figure 60. Chart to estimate resilient modulus (M_r) of subgrade from CBR (from AASHTO 1993 Appendix FF based on results from van Til et al. 1972)	96
Figure 61. Chart for estimating composite modulus of subgrade reaction (k_{comp}) assuming a semi-infinite subgrade depth (from AASHTO 1993)	97
Figure 62. Cyclic stress-strain curves for subgrade sample # 1	99
Figure 63. Cyclic stress-strain curves for subgrade sample # 2	100
Figure 64. Cyclic stress-strain curves for subgrade sample # 3	101
Figure 65. Cyclic stress-strain curves for subgrade sample # 4	102
Figure 66. Cyclic stress-strain curves for subgrade sample # 5	103
Figure 67. Cyclic stress-strain curves for subgrade sample # 6	104
Figure 68. Cyclic stress-strain curves for subbase sample # 1	105
Figure 69. Cyclic stress-strain curves for subbase sample # 2	106
Figure 70. Cyclic stress-strain curves for subbase sample # 3	107
Figure 71. Cyclic stress-strain curves for subbase + subgrade composite sample	108

LIST OF TABLES

Table 1. Summary of pavement thickness design input parameters/assumptions	6
Table 2. Bid quantities, estimated unit costs, and bid costs.....	7
Table 3. Gradation requirements of the OGDC material used in CTB.....	8
Table 4. Mixture requirements for the CTB layer	9
Table 5. Resilient modulus test sequences and stress values for base/ subbase and subgrade materials (AASHTO T307).....	18
Table 6. PCA (1971) recommended maximum allowable percent mass loss after wet-dry and freeze-thaw cycles	25
Table 7. Department of the Army, the Navy, and the Air Force (1994) recommended maximum allowable percent mass loss after wet-dry and freeze-thaw cycles	25
Table 8. Summary of material index properties.....	32
Table 9. Summary of M_r and UU test results.....	37
Table 10. Summary of laboratory permeability test results	47
Table 11. Summary of test sections and in situ testing.....	48
Table 12. TS1, TS2 CBT, and TS3: In situ test results.....	73
Table 13. Summary of design, in situ measured, and laboratory measured values	74

ACKNOWLEDGMENTS

This research was conducted under Federal Highway Administration (FHWA) DTFH61-06-H-00011 Work Plan 18 and the FHWA Pooled Fund Study TPF-5(183), involving the following state departments of transportation:

- California
- Iowa (lead state)
- Michigan
- Pennsylvania
- Wisconsin

The authors would like to express their gratitude to the National Concrete Pavement Technology (CP Tech) Center, the FHWA, the Iowa Department of Transportation (DOT), and the other pooled fund state partners for their financial support and technical assistance.

Mark Grazioli, Soils and Materials Managing Engineer, MDOT Metro Region, provided assistance in identifying the project, providing access to the project site, and obtaining quality assurance (QA) test results and project design information. We greatly appreciate their help.

We also thank the help of Bob Steffes, Michael Eidem, and Andrew Wilcuts of Iowa State University with laboratory and field testing, and Christianna White for comments and editing support.

LIST OF ACRONYMS AND SYMBOLS

a	Area of the reservoir
A	Cross-sectional area of the sample
CBR	California bearing ratio
COV	Coefficient of variation
C_d	Coefficient of drainage
DCP-CBR _{Subgrade}	CBR of subgrade determined from DCP test
DCP-CBR _{Subbase}	CBR of subbase determined from DCP test
DPI	Dynamic penetration index
D_0	Deflection measured under the plate
D_1 to D_7	Deflections measured away from the plate at various set distances
D_{10}	Grain size diameter corresponding to 10% passing by mass
D_{60}	Grain size diameter corresponding to 60% passing by mass
E	Elastic modulus
E_c	Modulus of elasticity of concrete
E_s or $E_{s(T307)}$	Dynamic secant modulus
$E^*_{s(T307)}$	
E_{SB}	Subbase elastic modulus
E_{LWD-Z3}	Elastic modulus determined from 300 mm diameter plate Zorn light weight deflectometer
E_{FWD-K3}	Surface modulus determined using 300 mm diameter plate KUAB falling weight deflectometer
E_{v1}	Deformation modulus from static plate load test of the first loading cycle
E_{v2}	Deformation modulus from static plate load test of the second loading cycle
F	Shape factor
g	Acceleration due to gravity
G_s	Specific gravity
G_o	Geometric factor
H_1	Initial water head level
H_2	Final water head level
H_{SB}	Thickness of subbase
$H_{Subgrade}$	Thickness of subgrade
I	Intercept
K_{gas}	Gas permeability
K_{rg}	Relative permeability to gas
K_{sat}	Saturated hydraulic conductivity
k	Modulus of subgrade reaction
k_{comp}	Composite modulus of subgrade reaction
k_1, k_2, k_3	Regression coefficients in “universal” model
L	Length of the sample
LL	Liquid limit
M_r	Resilient modulus
n	Number of measurements
p	Number of parameters
P_{Total}	Total porosity in percentage

$P_{o(g)}$	Gauge pressure at the orifice outlet (mm of H ₂ O)
P_1	Absolute gas pressure on the soil surface
P_2	Atmospheric pressure
PI	Plasticity index
PL	Plastic limit
P_a	Atmospheric pressure
Q	Volumetric flow rate
R^2	Coefficient of determination
r	Radius
S	Water saturation
S_c	Modulus of rupture of concrete
S_e	Effective water saturation
S_r	Residual water saturation
s_u	Undrained shear strength
t	Time
UU	Unconsolidated undrained triaxial test
V	Volume of sample
W_1	Oven-dry weight of aggregate in air
W_2	Submerged weight of aggregate in water
w	Moisture content
w_{opt}	Optimum moisture content
ε	Axial strain
ε_p	Permanent strain
ε_r	Resilient strain
ρ_w	Unit weight of water
γ_d	Dry unit weight
γ_{dmin}	Minimum dry unit weight
γ_{dmax}	Maximum dry unit weight
$\gamma(h)$	Semivariogram function
μ	Statistical mean or average
μ_{gas}	Kinematic viscosity of the gas
μ_{water}	Absolute viscosity of water
η	Poisson's ratio
λ	Brooks-Corey pore size distribution index
σ	Statistical standard deviation
σ_B	Bulk stress
σ_d	Deviator stress
σ_0	Applied axial stress
$\sigma_1, \sigma_2, \sigma_3$	Principal stresses
τ_{oct}	Octahedral shear stress

EXECUTIVE SUMMARY

Quality foundation layers (the natural subgrade, subbase, and embankment) are essential to achieving excellent pavement performance. Unfortunately, many pavements in the United States still fail due to inadequate foundation layers. To address this problem, a research project, Improving the Foundation Layers for Pavements (FHWA DTFH 61-06-H-00011 WO #18; FHWA TPF-5(183)), was undertaken by Iowa State University (ISU) to identify, and provide guidance for implementing, best practices regarding foundation layer construction methods, material selection, in situ testing and evaluation, and performance-related designs and specifications. As part of the project, field studies were conducted on several in-service concrete pavements across the country that represented either premature failures or successful long-term pavements. A key aspect of each field study was to tie performance of the foundation layers to key engineering properties and pavement performance. In-situ foundation layer performance data, as well as original construction data and maintenance/rehabilitation history data, were collected and geospatially and statistically analyzed to determine the effects of site-specific foundation layer construction methods, site evaluation, materials selection, design, treatments, and maintenance procedures on the performance of the foundation layers and of the related pavements. A technical report was prepared for each field study.

This report presents results and analysis from a field study conducted on an interstate highway I-96 reconstruction project in Lansing, Michigan. The old section of the highway was a 4 to 6 lane divided freeway with a 230 mm (9 in.) thick jointed portland cement concrete (PCC) pavement, 104 mm (4 in.) of select subbase, and 254 mm (10 in.) of sand subbase. Field studies by the Michigan Department of Transportation (MDOT) indicated that the ride quality of the existing pavement was poor and needed replacement. MDOT decided to reconstruct the highway with a twenty-year design life jointed PCC pavement with 292 mm (11.5 in.) thick PCC at 4.3 m (14 ft) joint spacing, 127 mm (5 in.) cement treated base (CTB) layer with recycled PCC (RPCC) material and 279 mm (11 in.) existing or new sand subbase with a geotextile separator at the CTB/subbase interface. Review of construction bid documents indicated that the construction cost of the foundation layers (i.e., CTB, subbase, and geotextile separator) was about 34% (\$1,996,113) of the total cost of the project (\$5,937,041).

The ISU research team was present at the project site from May 18 to May 23, 2010, during the reconstruction process to conduct a field study on the foundation layers constructed for the new pavement. Field testing was conducted on three test sections. Two test sections involved testing the sand subbase and the underlying subgrade layers, and one test section involved testing the CTB layer. Field testing was conducted by spacing the test measurements about 50 to 100 m apart to capture the variability along the road alignment. Testing was also conducted in a dense grid pattern (spaced at about 0.9 to 3.0 m) to capture spatial variability over a small area. Geostatistical semivariogram analysis was performed to analyze the point test data from the dense grid pattern testing to characterize and quantify spatial non-uniformity of the foundation layer properties. Comparisons between the measured design input parameters from laboratory and in situ testing and the design assumed values revealed the following:

- The average CTB/sand subbase layer modulus (E_{SB}) back-calculated from FWD data was

about 362 MPa (52 ksi). On average, it was about 0.87 times the design E_{SB} value of 413.7 MPa (60 ksi), with about 81 out of the 119 measurements being lower than the design value. The in situ E_{SB} values showed a COV of about 50% with values ranging from 35.5 MPa (5.1 ksi) to 709.5 MPa (102.9 ksi).

- Subgrade layer resilient modulus (M_r) determined from laboratory measurements on Shelby tube samples at field anticipated stress conditions showed an average of 31 MPa (4.5 ksi) and was about 1.5 times higher than the design M_r of 20.7 MPa (3.0 ksi). The in situ M_r values determined from FWD measurements showed an average of about 18.9 MPa (2.7 ksi), which was slightly lower than the design value. The M_r value determined from DCP-CBR_{Subgrade} was on average about 7.7 times higher than the design value.
- Composite modulus of subgrade reaction (k_{comp}) values were determined based on E_{SB} and M_r values. A lower bound $k_{comp} = 101$ kPa/mm (370 pci) value was estimated assuming average E_{SB} and average M_r determined from FWD measurements. Similarly, an upper bound $k_{comp} = 327$ kPa/mm (1200 pci) value was estimated using average E_{SB} from FWD measurements and $M_r = 138$ MPa (20 ksi) based on DCP measurements. The lower bound and upper bound k_{comp} values were about 0.74 times and 2.4 times the design k_{comp} value.
- The C_d value assumed in design = 1.05, which represents that the quality of drainage is rated as Good. According to AASHTO (1993), if water is removed from the pavement system in one day, the quality of drainage is rated as Good. Both laboratory and field measurements indicated that the quality of the drainage layer can be rated as Excellent according to AASHTO (1993), which exceeds the Good rating assumed in the design.

Laboratory testing was conducted on foundation layer materials obtained from field to determine index properties, moisture-dry unit weight relationships from compaction tests and resilient modulus. Resilient modulus tests were conducted on single samples as well as composite samples (i.e., sand subbase over subgrade). Hydraulic conductivity tests were conducted on sand subbase, untreated RPCC base, and CTB materials. Compressive strength and durability (to freeze-thaw and wet-dry cycles) of the CTB material were also assessed as part of the laboratory testing. Some key findings from laboratory testing are as follows:

- Results indicated that the M_r of subbase material increases with increasing bulk stresses, as expected for granular materials. M_r of subgrade materials decreased with increasing deviator stress, as expected for non-granular materials. Increasing moisture content decreased M_r and increasing dry unit weight increased M_r for both subbase and subgrade materials.
- Comparing composite and single samples revealed that the average M_r of composite samples is about 1.2 times lower than the average M_r of a single layer subbase sample at a similar density. The reason for this reduction in M_r in the composite sample is attributed to the weaker subgrade layer. This is an important finding and efforts are underway in this research study to further investigate the influence of composite soil layer configurations on M_r properties.
- Compressive strength test results from ISU and MDOT indicated that with the exception of one sample, all other samples met the specified seven-day compressive strength range (i.e., 1,380 to 4,830 kPa).
- All CTB samples tested for durability (i.e., 12 wet-dry and freeze-thaw cycles) showed percent mass loss less than the PCA (1971) recommended maximum allowable percent loss

of 14%. One of the three CTB samples subjected to wet-dry cycles showed a percent loss of about 12%, which was greater than the Department of Army, the Navy, and the Air Force (1994) recommended 11% maximum allowable loss.

The findings from the field studies under the Improving the Foundation Layers for Pavements research project will be of significant interest to researchers, practitioners, and agencies dealing with design, construction, and maintenance of PCC pavements. The technical reports are included in Volume II (Appendices) of the *Final Report: Improving the Foundation Layers for Pavements*. Data from the field studies are used in analyses of performance parameters for pavement foundation layers in the *Mechanistic-Empirical Pavement Design Guide* (MEPDG) program. New knowledge gained from this project will be incorporated into the *Manual of Professional Practice for Design, Construction, Testing, and Evaluation of Concrete Pavement Foundations*, to be published in 2015.

CHAPTER 1. INTRODUCTION

This report presents laboratory and in situ test results and analysis from an experimental field study conducted on interstate highway I-96 reconstruction project between mile posts 90 and 93 in Lansing, Michigan. The existing section for I-96 is a 4 to 6 lane divided freeway with paved outside and inside shoulders. The existing pavement consisted of a 230 mm (9 in.) thick jointed portland cement concrete (PCC) pavement, 104 mm (4 in.) thick select subbase, and 254 mm (10 in.) thick sand subbase. Field studies by the Michigan Department of Transportation (MDOT) indicated that the ride quality of the existing pavement was poor and needed replacement. MDOT evaluated two reconstruction alternatives using the 1993 American Association of State Highway Transportation Officials (AASHTO) pavement design guide (AASHTO 1993). Alternative # 1 was to reconstruct the roadway with a twenty-year design life hot mix asphalt (HMA) pavement, and alternative #2 was to reconstruct with a twenty-year design life jointed PCC pavement. Based on life cost analysis of the two alternatives, MDOT selected alternative #2, which involved construction of a 292 mm (11.5 in.) thick jointed PCC pavement with 4.3 m (14 ft) joint spacing, 127 mm (5 in.) cement treated base layer (CTB), a geotextile separator, and 279 mm (11 in.) existing or new sand subbase. The CTB layer consisted of crushed recycled PCC material obtained from crushing the existing pavement on the project.

The Iowa State University (ISU) research team was present at the project site during the reconstruction process from May 18 to May 23, 2010, to conduct a field study on the foundation layers constructed for the new pavement. Field testing involved using the following in situ test methods: Kuab falling weight deflectometer (FWD) to determine elastic modulus; Zorn light weight deflectometer (LWD) to determine elastic modulus; cone penetrometer (DCP) to estimate California bearing ratio and resilient modulus; Humboldt nuclear gauge (NG) to determine moisture and dry unit weight; rapid gas permeameter test (GPT) device to measure saturated hydraulic conductivity; and static plate load test (PLT) to obtain elastic modulus and modulus of subgrade reaction. In addition, “undisturbed” Shelby tube samples were obtained from the subgrade layer for laboratory testing. The spatial northing and easting of all test measurement locations were obtained using a real-time kinematic (RTK) global positioning system (GPS). Laboratory testing was conducted on materials collected from the field to characterize the index properties (i.e., gradation, compaction, specific gravity, soil classification), and determine resilient modulus (M_r). Resilient modulus (M_r) tests were conducted on the subgrade and sand subbase materials. M_r testing was also conducted on composite subbase and subgrade materials to assess the composite behavior. Compressive strength and freeze-thaw durability tests were conducted on CTB samples prepared at the batching plant.

Field testing was conducted on three test sections. Two test sections involved testing the sand subbase layer, and one test section involved testing the CTB layer. Field point testing was conducted by spacing the test measurements about 50 to 100 m apart to capture the variability along the road alignment. Testing was also conducted in a dense grid pattern (spaced at about 0.9 to 3.0 m) to capture spatial variability over a small area. Geostatistical semivariogram analysis was performed to analyze the point test data from dense grid pattern testing to characterize and quantify spatial non-uniformity of the foundation layer properties.

This report contains six chapters. Chapter 2 provides background information of the project on the two alternatives evaluated by MDOT; life cycle cost analysis results; selection criteria for the PCC pavement structure; AASHTO (1993) pavement design input parameters; and construction methods and specifications. Chapter 3 presents an overview of the laboratory and in situ testing methods followed in this project. Chapter 4 presents results from laboratory testing. Chapter 5 presents results from in situ testing and analysis on the three test sections with discussion of comparisons of the laboratory and in situ measured values and the design assumed values. Chapter 6 presents key findings and conclusions from the field study.

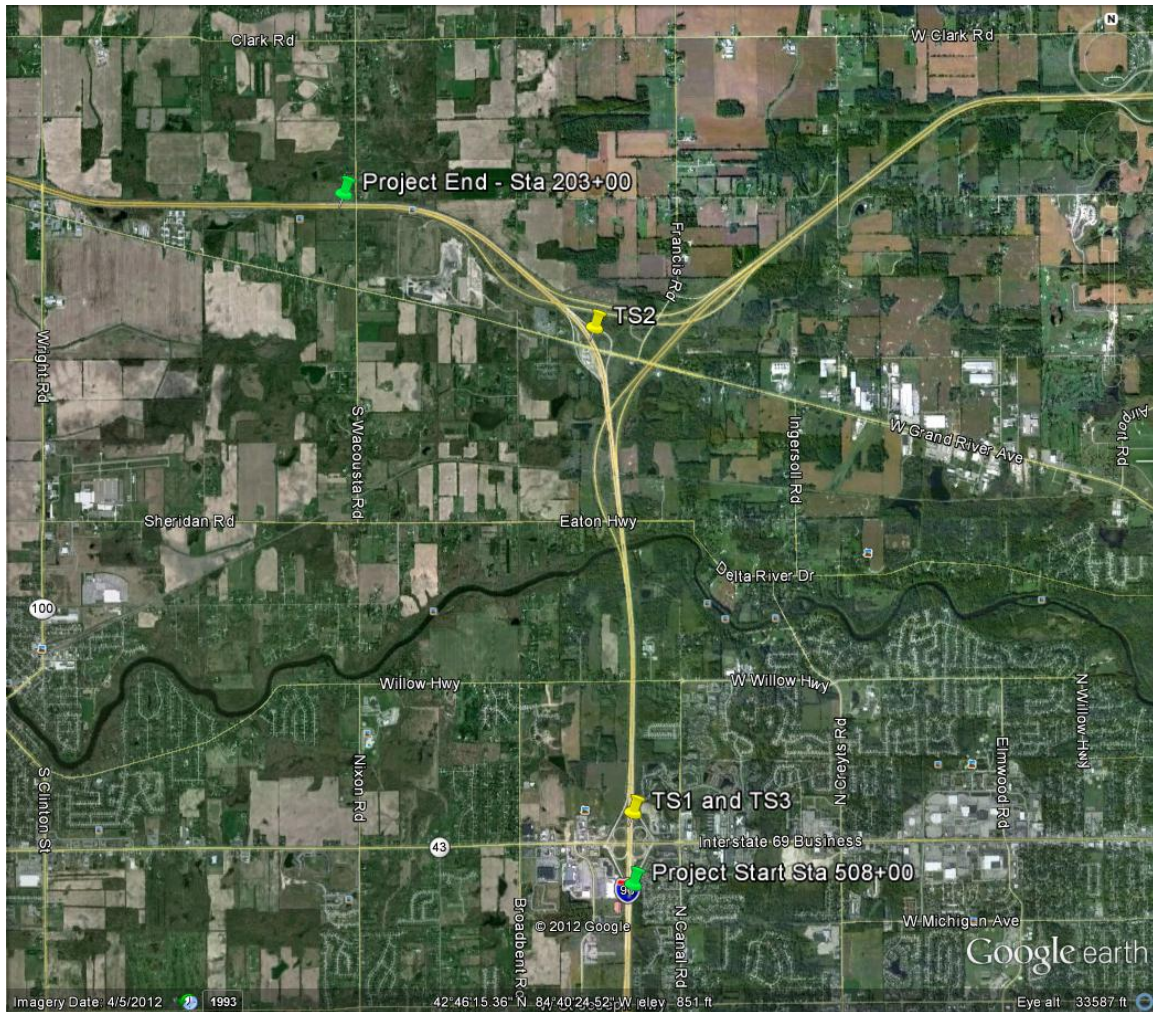
The findings from this report should be of significant interest to researchers, practitioners, and agencies who deal with design, construction, and maintenance aspects of PCC pavements. This project report is one of several field project reports developed as part of the TPF-5(183) and FHWA DTFH 61-06-H-00011:WO18 studies.

CHAPTER 2. PROJECT INFORMATION

This chapter presents brief background information on the project based on the information provided in an MDOT office memorandum dated May 4, 2009, and the authors' field observations, pavement thickness design parameter selection and assumptions during the design phase of the project, and the new pavement foundation layer construction details (see Appendix A).

Project Background

This project involved reconstruction of about 5.8 miles of I-96 from just west of Wacousta Road (mile post 90) to south of M-43 (mile post 93) and about 0.8 miles of M-43 reconstruction from east of Market place Boulevard to east of Canal Road, in Clinton and Eaton Counties near Lansing, Michigan (Figure 1). ISU testing was conducted on I-96 so only details of I-96 reconstruction are provided in this report.



Map: ©2012 Google

Figure 1. Approximate project start and end and test section locations

The old pavement section for I-96 was a 4 to 6 lane divided freeway with 3.66 m (12 ft) wide paved lanes, a 2.74 m (9 ft) paved outside shoulder, and a 1.22 m (4 ft) to 2.74 m (9 ft) paved inside shoulder in each direction. The pavement consisted of a 230 mm (9 in.) thick jointed PCC pavement, 104 mm (4 in.) of select subbase, and 254 mm (10 in.) of sand subbase. According to the MDOT memorandum, the ride quality index (RQI) of the existing pavement was about 74 on the east bound lanes and 71 on the west bound lanes. The average remaining service life (RSL) was about 2 on the east and west bound lanes. Based on the RQI and RSL data, the pavement quality was rated as poor. Two new pavement reconstruction alternatives were evaluated by MDOT: Alternative #1: Reconstruct with HMA pavement with twenty-year design life, and Alternative #2: Reconstruct with jointed plain concrete pavement (JPCP) with twenty-year design life. The two alternatives were evaluated using the 1993 AASHTO pavement design procedures and life cycle cost analysis using the Equivalent Uniform Annual Cost (EUAC) calculation method approved by the Engineering Operations Committee, MDOT, in June 1999 (MDOT 2005). The construction costs used in the estimations were reportedly

historical averages from similar projects, and user costs were reportedly calculated using MDOT's Construction Congestion Cost model developed by the University of Michigan.

Alternative #1 consisted of the following pavement and foundation layer structure:

- 51 mm (2 in.) HMA, gap-graded superpave, top course (mainline and inside shoulder)
- 64 mm (2.5 in.) HMA, 4E30, leveling course (mainline and inside shoulder)
- 159 mm (6.25 in.) HMA, 3E30, base course (mainline and inside shoulder)
- 51 mm (2 in.) HMA, 5E3, top course (outside shoulder)
- 64 mm (2.5 in.) HMA, 4E3, leveling course (outside shoulder)
- 159 mm (6.25 in.) HMA, 3E3, base course (outside shoulder)
- 127 mm (5 in.) Open-graded drainage course (OGDC), geotextile separator at subgrade/OGDC interface
- 483 mm (19 in.) Sand subbase
- 152 mm (6 in.) Underdrain system (diameter)

Life cycle analysis results for alternative #1 showed the following results:

Present value initial construction cost: \$1,984,358/directional mile
Present value initial user cost: \$397,854/directional mile
Present value maintenance cost: \$176,481/directional mile
Equivalent uniform annual cost (EUAC): **\$138,233/directional mile**

Alternative #2 consisted of the following pavement and foundation layer structure:

- 292 mm (11.5 in.) Non-reinforced concrete pavement with 14 ft joint spacing
- 127 mm (5 in.) Stabilized OGDC [CTB]
Geotextile separator at subbase/CTB interface
Existing sand subbase (65% of the project)
- 279 mm (11 in.) New sand subbase (35% of the project)
- 152 mm (6 in.) Open-graded underdrain system (diameter)

Life cycle analysis results for alternative #2 produced the following results:

Present value initial construction cost: \$1,167,170/directional mile
Present value initial user cost: \$266,047/directional mile
Present value maintenance cost: \$106,597/directional mile
Equivalent uniform annual cost (EUAC): **\$83,188/directional mile**

Based on the guidelines outlined in MDOT (2005), alternative #2, the alternative with lower EUAC, was selected.

Pavement Design Input Parameter Selection and Assumptions

A summary of pavement thickness design input parameters is provided in Table 1. A composite modulus of subgrade reaction, $k_{comp} = 135$ kPa/mm (500 pci), was determined by MDOT following the AASHTO 1993 design guidelines based on an assumed mean subbase layer elastic modulus, E_{SB} , mean subgrade resilient modulus, M_r , and target subbase layer thickness, H_{SB} , as summarized in Table 1.

Table 1. Summary of pavement thickness design input parameters/assumptions

Parameter	Value
General Assumptions	
ESALs over initial performance period	38,009,260 (18-kip)
Design period	20 years
Surface Layer Design Assumptions	
Pavement type	JPCP
Initial serviceability	4.5
Terminal serviceability	2.5
28-day mean PCC modulus of rupture, S_c	4620 kPa (670 psi)
28-day mean modulus of elasticity of concrete, E_c	29,000 MPa (4,200,000 psi)
Reliability level	95%
Overall standard deviation	0.39
Load transfer coefficient, J	2.7
Foundation Layer Design Assumptions	
Subbase layer thickness, H_{SB}	406 mm (16 in.) [137 mm (5 in.) CTB and 279 mm (11 in.) sand subbase]
Mean subbase elastic modulus, E_{SB}	410 MPa (60,000 psi)
Mean subgrade resilient modulus, M_r	20 MPa 3,000 psi [stiff clay to semi-infinite depth, i.e., > 10 ft]
Composite modulus of subgrade reaction, k_{comp}	135 kPa/mm (500 pci)
Loss of support (due to erosion), LS	0.5
Effective modulus of subgrade reaction, k_{eff}	76 kPa/mm (280 psi/in)
Overall drainage coefficient, C_d	1.05 (Quality of drainage = <i>Good</i> according to AASHTO 1993)
Saturated hydraulic conductivity, K_{sat} *	0.1 cm/s (260 ft/day)
Other	Geotextile separator at sand subbase and CTB layer interface (6 inch diameter)
Pavement Thickness Design	
Calculated design thickness	287 mm (11.29 in.) [292 mm (11.5 in.) actual]

*Estimated assuming 90% of water to be removed within 1 day and effective porosity of CTB = 0.3.

The design guide requires determining seasonal variations in the E_{SB} and M_r values and then an average value for analysis. The E_{SB} and M_r values provided in Table 1 represent average values.

Seasonal variations in the E_{SB} and M_r values were not determined by the design engineer (Email communication with Mark Grazioli, MDOT). The effective modulus of subgrade reaction, k_{eff} , was then estimated based on an assumed potential loss of support (due to erosion), $LS = 0.5$.

The assumed drainage coefficient $C_d = 1.05$ represents that the quality of drainage is good to excellent (varies as a function of time above a threshold base saturation level). These design assumptions are compared with the actual field measurements in Chapter 6.

Construction Details and Specifications

A summary of bid quantities, engineers' estimated costs, and bid costs is presented in Table 2.

Table 2. Bid quantities, estimated unit costs, and bid costs

Item Description	Bid Quantity	Unit	Estimated Unit Cost	Total Cost
Earth excavation	52,637	yd ³	\$3.07	\$161,596
Sand subbase	16,850	yd ³	\$2.79	\$47,012
Geotextile separator	163,094	yd ²	\$0.96	\$156,570
5 in. CTB	163,094	yd ²	\$10.00	\$1,630,935
11.5 in. PCC layer	163,094	yd ²	\$20.80	\$3,392,345
Contraction joint with load transfer (ML)	67,131	ft	\$7.61	\$510,869
Contraction joint with load transfer (shoulder)	37,714	ft	\$1.00	\$37,714
<i>Total Project Cost</i>				\$5,937,041
<i>Total Foundation Layer Construction Cost</i>				\$1,996,113

Based on the contractor's bid costs, the cost of the construction of foundation layers (i.e., CTB, subbase, and geotextile separator) was about 34% of the total cost of the project.

In about 65% of the project, the existing sand subbase layer was reused, and in about 35% of the project, new 279 mm (11 in.) thick sand subbase layer was placed. A picture of the sand subbase layer taken near I-96 and M-43 intersection is shown in Figure 2.



Figure 2. Compacted sand subbase layer on I-96 EB lane just north of M-43 intersection

A 127 mm (5 in.) thick CTB layer was installed over the sand subbase layer with a Geoturf[®] W270 woven geotextile at the interface of sand subbase and CTB layers. Recycled PCC material was used in the CTB layer.

A special provision (SP) 03CT303(A140) was used for the CTB layer (see Appendix B). The SP indicates that the OGDC material used in the CTB should consist of crushed PCC from this project, meeting the gradation specifications provided in Table 3, and the material should contain at least 90% of crushed material.

Table 3. Gradation requirements of the OGDC material used in CTB

Sieve Size	Percent Passing
38.1 mm (1.5 in.)	100
25.4 mm (1.0 in.)	90–100
12.7 mm (0.5 in.)	25–60
#4	0–20
#8	0–8
#200	0–5

The CTB layer mix design proportions are provided in Table 4.

Table 4. Mixture requirements for the CTB layer

Material	Proportions (lbs/yd³)	Proportions (kg/m³)
Crushed PCC aggregate	27 x dry rodded unit weight of the material (lb/ft ³)	Dry rodded unit weight of material (kg/m ³)
Cement (ASTM C150, Type I)	250	147.5
Water*	100–120	59–71

*The water content is based on the assessment of the workability of the mixture. Net water includes any surface moisture on the OGDC material plus water added at the mixer.

The design seven-day compressive strength range of the mix is 1,380 kPa (200 psi) to 4,830 kPa (700 psi). Compressive strength testing was performed on 152 mm (6 in.) wide by 304 mm (12 in.) tall sample cylinders made on-site at the batching plant. The samples were prepared in a plastic mold by placing the material in three layers and tamping each layer 25 times using a circular plate tamper by raising the tamper 102 mm (4 in.) above each layer surface. The samples were cured in field for about 24 to 48 hours and transported to the lab. Cylinders are required to be in the mold until day of compression testing.

Images of placing the geosynthetic layer over the sand subbase, placing the CTB layer, compacting the CTB layer, and the final CTB layer are shown in Figure 3 through Figure 6, respectively.



Figure 3. Placement of geosynthetic layer and CTB over sand subbase layer



Figure 4. CTB layer placement



Figure 5. Compaction of CTB layer



Figure 6. Final CTB layer about 5 days after placement on I-96 EB lane near the West Grand River Hwy and I-96 interchange

CHAPTER 3. EXPERIMENTAL TEST METHODS

This chapter presents a summary of the laboratory and in situ testing methods used in this study.

Laboratory Testing Methods and Data Analysis

Particle-Size Analysis and Index Properties

Samples from sand subbase, OGDC material used in the CTB, and subgrade layers were collected from the field and were carefully sealed and transported to the laboratory for testing. Particle-size analysis tests on the OGDC material samples were performed in accordance with ASTM C136-06 *Standard test method for sieve analysis of fine and coarse aggregates*. Particle-size analysis tests on the sand subbase and subgrade materials were conducted in accordance with ASTM D422-63 *Standard Test Method for Particle-Size Analysis of Soils*.

Atterberg limit tests (i.e., liquid limit—LL, plastic limit—PL, and plasticity index—PI) were performed in accordance with ASTM D4318-10 “*Standard test methods for liquid limit, plastic limit, and plasticity index of soils*” using the dry preparation method. Using the results from particle-size analysis and Atterberg limits tests, the samples were classified using the unified soil classification system (USCS) in accordance with ASTM D2487-10 “*Standard Practice for Classification of Soils for Engineering Purposes (Unified Soil Classification System)*” and AASHTO classification system in accordance with ASTM D3282-09 “*Standard Practice for Classification of Soils and Soil-Aggregate Mixtures for Highway Construction Purposes.*”

Two laboratory compaction tests were used to determine the relationship between dry density and moisture content for the soils obtained from the field. Subgrade soil compaction characteristics were determined using standard and modified Proctor compaction methods in accordance with ASTM D698-07 “*Standard test methods for laboratory compaction characteristics of soil using standard effort*” and ASTM D1557-07 “*Standard test methods for laboratory compaction characteristics of soil using modified effort*”, respectively. Maximum and minimum index density tests were performed using a vibratory table on the sand subbase and OGDC base materials in accordance with ASTM D4253-00 “*Standard test methods for maximum index density and unit weight of soil using a vibratory table*” and D4254-00 “*Standard test methods for minimum index density and unit weight of soils and calculation of relative density.*” In addition, moisture-unit weight relationships for the sand subbase sand were determined by performing maximum index density tests by incrementally increasing the moisture content by approximately 1.5% for each test.

Resilient Modulus and Shear Strength Testing Sample Preparation

Subgrade and subbase materials were tested for resilient modulus (M_r) and unconsolidated undrained (UU) shear strength generally following the AASHTO T-307 procedure—granular base/subbase and cohesive subgrade. In addition, composite soil samples (i.e., consisting of both

subbase and subgrade) were tested in this study. The methods used to prepare these samples are described below.

Subbase Material

Subbase material samples were prepared using the vibratory compaction method as described in AASHTO T-307 for preparation of granular base/subbase materials. Prior to compaction, materials were moisture-conditioned and allowed to mellow for at least 3 to 6 hours. A 101.6 mm (4 in.) diameter split mold was used to compact the sample (Figure 7) in five lifts of equal mass and thickness using an electric rotary hammer drill and a circular steel platen placed against the material (Figure 8).



Figure 7. Split mold, steel platen (4 in. diameter), and vibratory hammer for compaction of subbase material samples

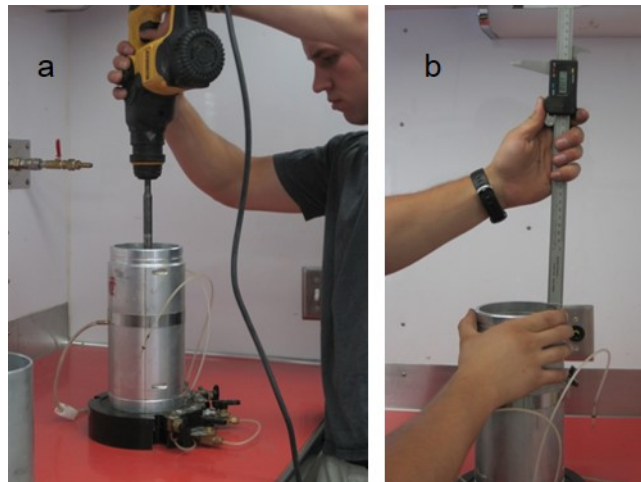


Figure 8. Compaction of subbase material samples in split mold (left) and verification of thickness of each lift using calipers (right)

Calipers were used to verify consistent compaction layer thicknesses (Figure 8).

Subgrade Material

The subgrade material samples were obtained from the field in an “undisturbed” state using Shelby tube sampling methods. Disturbed bag samples of the subgrade material were also obtained for testing by compacting the material to a target moisture and density.

Shelby tube samples of subgrade materials were obtained by hydraulically pushing a 75 mm (3 in.) diameter thin-walled Shelby tube into the subgrade (Figure 9).



Figure 9. Shelby tube sampling and the sample extrusion device mounted on the freightliner truck of the ISU Geotechnical Mobile Laboratory

Samples were obtained from depths ranging from 0.4 m (1.3 ft) to 1.0 m (3.3 ft) below the top of subbase layer. Samples were extruded on site from the Shelby tubes and were carefully trimmed and cut to about 142 mm (5.6 in.) height for M_r and UU testing. Prior to testing, the sample dimensions were measured and the samples were weighed to determine field moisture density. After testing, the entire sample was oven dried for at least 24 hours to determine the moisture content and dry density of the material.

Disturbed bag samples were used to prepare samples for testing using static compaction method as described in AASHTO T-307. Before compaction, the materials were moisture-conditioned and allowed to mellow for at least 16 hours. Static compaction involved a hydraulic press, steel mold, and six steel spacers (Figure 10) to form the soil into a 101.6 mm diameter by 203.2 mm tall (4 in. diameter by 8 in. tall) cylinder.



Figure 10. Aluminum spacers (4 in. diameter) used during static compaction

Note that AASHTO T-307 describes compaction procedure to prepare a 71 mm diameter by 142 mm tall (2.8 in. diameter by 5.6 in. tall) samples. The static compaction process is shown in Figure 11.



Figure 11. Static compaction procedure (left) and sample extrusion procedure (right) of a compacted cohesive soil sample

When making the samples, the soil was compacted in five lifts of equal mass and thickness. Each lift of soil was pressed between the steel spacers to a uniform thickness. After compaction, the soil samples were extruded (Figure 11).

Composite Subbase and Subgrade Samples

AASHTO T307 does not describe a procedure for fabricating composite samples. Composite samples tested in this study included 101.6 mm (4 in.) thick subbase over 101.6 mm (4 in.) thick subgrade. For the composite sample, the bottom subgrade layer was compacted first using the static compaction technique described above, in three lifts. The first two lifts were about 40.6 mm (1.6 in.) thick, and the third lift was about 20.3 mm (0.8 in.) thick. A pre-determined amount of material was placed in each lift keeping the unit weight constant in each lift. After compaction of the subgrade, the sample was extruded and placed on the triaxial chamber base. The split mold used for granular materials was then placed around the sample, and the base layer was compacted in three equal lifts of 33.9 mm (1.3 in.) using the vibratory compaction procedure described above.

Resilient Modulus and Shear Strength Triaxial Testing

M_r and UU tests were performed using the Geocomp automated M_r test setup (Figure 12) in accordance with AASHTO T-307.



Figure 12. Triaxial chamber, load frame, and computer equipment for resilient modulus tests

The setup consists of a Load Trac-II load frame, electrically controlled servo valve, an external signal conditioning unit, and a computer with a network card for data acquisition. The system uses a real-time adjustment of proportional-integral-derivative (PID) controller to adjust the system control parameters as the stiffness of the sample changes to apply the target loads during the test. Figure 12 shows the triaxial test chamber used in this study.

The chamber is set up to perform 71 mm (2.8 in.) or 101.6 mm (4 in.) diameter samples. Two linear voltage displacement transducers (LVDTs) are mounted to the piston rod to measure resilient strains in the sample during the test.

M_r tests were performed following the AASHTO T-307 conditioning and loading sequences suggested for base and subgrade materials (Table 5).

Table 5. Resilient modulus test sequences and stress values for base/ subbase and subgrade materials (AASHTO T307)

Base/Subbase Materials						Subgrade Materials					
Sequence No.	Confining Pressure		Max. Axial Stress		No. of cycles	Sequence No.	Confining Pressure		Max. Axial Stress		No. of cycles
	kPa	psi	kPa	psi			kPa	psi	kPa	psi	
0	103.4	15	103.4	15	500-1000	0	41.4	6	27.6	4	500-1000
1	20.7	3	20.7	3	100	1	41.4	6	13.8	2	100
2	20.7	3	41.4	6	100	2	41.4	6	27.6	4	100
3	20.7	3	62.1	9	100	3	41.4	6	41.4	6	100
4	34.5	5	34.5	5	100	4	41.4	6	55.2	8	100
5	34.5	5	68.9	10	100	5	41.4	6	68.9	10	100
6	34.5	5	103.4	15	100	6	27.6	4	13.8	2	100
7	68.9	10	68.9	10	100	7	27.6	4	27.6	4	100
8	68.9	10	137.9	20	100	8	27.6	4	41.4	6	100
9	68.9	10	206.8	30	100	9	27.6	4	55.2	8	100
10	103.4	15	68.9	10	100	10	27.6	4	68.9	10	100
11	103.4	15	103.4	15	100	11	13.8	2	13.8	2	100
12	103.4	15	206.8	30	100	12	13.8	2	27.6	4	100
13	137.9	20	103.4	15	100	13	13.8	2	41.4	6	100
14	137.9	20	137.9	20	100	14	13.8	2	55.2	8	100
15	137.9	20	275.8	40	100	15	13.8	2	68.9	10	100

Each load cycle consisted of a 0.1 second haversine-shaped load pulse followed by a 0.9 second rest period. M_r is calculated as the ratio of the applied cyclic deviator stress (σ_d) and resilient strain (ϵ_r). The σ_d and ϵ_r values from a typical stress-strain cycle during the test are shown in Figure 13.

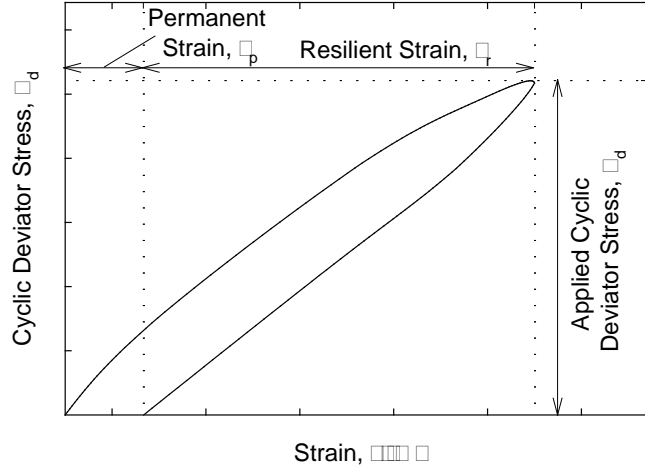


Figure 13. One load cycle in M_r testing

The average σ_d and ϵ_r of the last five cycles of a loading sequence are used in M_r calculations. After M_r testing, UU shear strength testing was performed on each sample by applying a confining pressure of 34.5 kPa (5 psi) to the base and subbase samples and 27.6 kPa (4 psi) to the subgrade samples.

Resilient Modulus Data Analysis

M_r values are used in pavement design as a measure of stiffness of unbound materials in the pavement structure. The M_r parameter is a highly stress-dependent parameter. Many non-linear constitutive models have been proposed that incorporate the effects of stress levels and predict M_r values. Most soils exhibit the effects of increasing stiffness with increasing bulk stress and decreasing stiffness with increasing shear stress (Andrei et al. 2004). A non-linear constitutive model (also called as “universal” model) proposed by Witczak and Uzan (1988) (Equation 1) was used in this study:

$$M_r = k_1 P_a \left(\frac{\sigma_B}{P_a} \right)^{k_2} \left(\frac{\tau_{oct}}{P_a} + 1 \right)^{k_3} \quad (1)$$

where

P_a = atmospheric pressure (MPa);

σ_B = bulk stress (MPa) = $\sigma_1 + \sigma_2 + \sigma_3$;

τ_{oct} = octahedral shear stress (MPa) = $\frac{\sqrt{(\sigma_1 - \sigma_2)^2 + (\sigma_2 - \sigma_3)^2 + (\sigma_3 - \sigma_1)^2}}{3}$;

$\sigma_1, \sigma_2, \sigma_3$ = principal stresses; and

k_1, k_2, k_3 = regression coefficients.

Equation 1 combines the effects of bulk and shear stresses into a single constitutive model. Bulk stress, octahedral shear stress, and measured resilient modulus values from the last five load cycles in each loading sequence were input into the statistical analysis program, JMP, to determine the regression coefficients k_1 , k_2 , and k_3 . The k_1 coefficient is proportional to M_r and therefore is always > 0 . The k_2 coefficient explains the behavior of the material with changes in the bulk stresses. Increasing bulk stresses increases the M_r value and therefore the k_2 coefficient should be ≥ 0 . The k_3 coefficient explains the behavior of the material with changes in shear stresses. Increasing shear stress softens the material and decreases the M_r value. Therefore the k_3 coefficient should be ≤ 0 .

The R^2 values determined from were adjusted for the number of regression parameters using Equation 2.

$$R^2 (\text{Adjusted}) = 1 - \left[\frac{(1 - R^2)(n - 1)}{n - p - 1} \right] \quad (2)$$

where

n = the number of data points and

p = the number of regression parameters.

Determination of Dynamic Secant Modulus from Cyclic Stress-Strain Data

The cyclic stress-strain data obtained from the resilient modulus test was used to estimate dynamic secant modulus (E_s) to compare with dynamic elastic modulus measurements from the field. Secant modulus was determined from the slope of the line connecting the origin to a selected point on the stress-strain curve of a material, as illustrated in Figure 14.

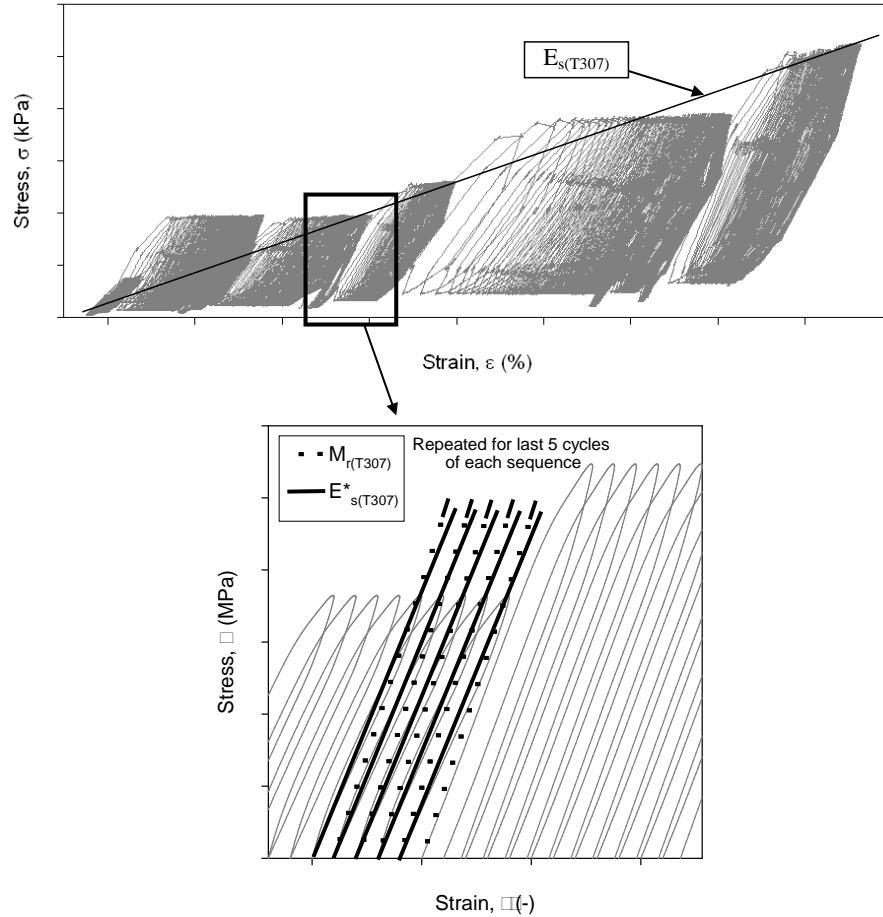


Figure 14. Comparison of resilient ($M_{r(T307)}$), cyclic secant ($E^*_{s(T307)}$), and dynamic secant ($E_{s(T307)}$) modulus values

The difference between secant moduli and resilient moduli is the use of permanent strain instead of resilient strain in the calculations.

Laboratory Permeability Tests

A specially fabricated 0.3 m diameter by 0.3 m high aggregate compaction mold large scale laboratory permeameter (LSLP) was used to perform falling head permeability tests on sand subbase and OGDC material used in CTB (Figure 15).



Figure 15. Large scale aggregate compaction mold laboratory permeameter

The details of the LSLP test equipment is described in White et al. (2004). Preparation of the test samples for the LSLP tests involved uniform mixing and compaction of the material in six lifts of equal thickness. The samples were compacted using a Marshall hammer. Falling head permeability tests were conducted by recording the time taken for the water head in the reservoir to drop from H_1 to H_2 to determine K_{sat} using Equation 3.

$$K_{sat} = \left(\frac{aL}{At} \right) \ln \left(\frac{H_1}{H_2} \right) \quad (3)$$

where

K_{sat} = saturated hydraulic conductivity (cm/s);

a = area of the reservoir (cm²);

L = length of the sample (cm);

A = cross-sectional area of the sample (cm²);

t = time (sec) taken for the water head to drop from H_1 to H_2 ;

and H_1 and H_2 = water height above the exit (which is at the bottom of the sample).

CTB samples with 150 mm (5.9 in.) diameters were cored out of a slab prepared with the mix proportions in the specifications to conduct falling head permeability tests. The setup used for permeability testing of CTB samples is shown in Figure 16.



Figure 16. Setup used for permeability testing of CTB samples

The core samples were confined in a rubber membrane with adjustable hose clamps and were directly attached to the pipe. A flexible sealing gum was used around the top perimeter of the sample to prevent water leakage around the edges (see Figure 17).



Figure 17. Application of sealing gum around the top perimeter of a CTB sample

A falling head test was conducted by filling the standpipe and recording the time for change in head. Equation 3 was used to determine K_{sat} . Porosity of the CTB samples (P_{total} in percentage) was determined by obtaining oven-dry weight in air (W_1) and weight in water when submerged (W_2) and using Equation 4.

$$P_{total} = \left[1 - \frac{W_1 - W_2}{\rho_w V} \right] \times 100 \quad (4)$$

where

ρ_w = unit weight of water and
 V = volume of CTB sample.

Compressive Strength Testing

CTB sample cylinders of size 152 mm x 304 mm were prepared in accordance with the procedure described previously in the Construction Details and Specifications subsection of Chapter 2 of this report, to determine compressive strength of the material. Compression testing was conducted in accordance with ASTM C39 “*Standard test method for compressive strength of cylindrical concrete specimens.*”

Wet-Dry and Freeze/Thaw Durability Tests

The CTB material was tested for resistance to wetting/drying cycles and freezing/thawing cycles. The samples were prepared and tested in general accordance to ASTM D559-03 “*Wetting and Drying Compacted Soil-Cement Mixtures*” and ASTM D560-03 “*Freezing and Thawing Compacted Soil-Cement Mixtures.*” Instead of using standard Proctor hammer during compaction of sample as described in the ASTM standards, the samples were compacted using a Marshall hammer (Figure 18).



Figure 18. Compaction of CTB samples in a split Proctor mold using Marshall hammer for durability testing

However, the compaction energy used to compact the samples was similar to the standard Proctor energy. The Marshall hammer was chosen over a standard Proctor hammer to reduce damage caused to the aggregate during compaction. Three samples for wetting/drying tests and three samples for freezing/thawing tests were prepared at the batching plant. All samples were subjected to 12 wetting/drying and freezing/thawing cycles.

Table 6 presents the Portland Cement Association (PCA) recommended maximum allowable percent mass loss after the after wet-dry and freeze-thaw cycles (PCA 1971).

Table 6. PCA (1971) recommended maximum allowable percent mass loss after wet-dry and freeze-thaw cycles

AASHTO Soil Group	Maximum allowable loss (%)
A-1, A-2-4, A-2-5, and A-3	14
A-2-6, A-2-7, A-4, and A-5	10
A-6 and A-7	7

Similarly, Table 7 presents the Department of the Army, the Navy, and the Air Force recommended maximum allowable percent mass loss values (Dept. of Army, the Navy, and the Air Force 1994).

Table 7. Department of the Army, the Navy, and the Air Force (1994) recommended maximum allowable percent mass loss after wet-dry and freeze-thaw cycles

Type of stabilized soil	Maximum allowable loss (%) after 12 cycles
Granular, PI < 10	11
Granular, PI > 10	8
Silts	8
Clays	6

In Situ Testing Methods

The following in situ testing methods and procedures were used in this study: real-time kinematic (RTK) global positioning system (GPS); Kuab falling weight deflectometer (FWD) setup with 300 mm diameter plate; Zorn light weight deflectometer (LWD) setup with 300 mm diameter plate; dynamic cone penetrometer (DCP); calibrated Humboldt nuclear gauge (NG); rapid gas permeameter test (GPT) device; and static plate load test (PLT) setup with 300 mm diameter plate. Pictures of these test devices are shown in Figure 19.



Figure 19. Trimble SPS-881 hand-held receiver, Kuab falling weight deflectometer, and Zorn light weight deflectometer (top row left to right); dynamic cone penetrometer, nuclear gauge, and gas permeameter device (middle row left to right); and static plate load test (bottom row)

Real-Time Kinematic Global Positioning System

RTK-GPS system was used to obtain spatial coordinates (x, y, and z) of in situ test locations and tested pavement slabs. A Trimble SPS 881 receiver was used with base station correction provided from a Trimble SPS851 established on site. According to the manufacturer, this survey system is capable of horizontal accuracies of < 10 mm and vertical accuracies < 20 mm.

Zorn Light Weight Deflectometer

Zorn LWD tests were performed on base and subbase layers to determine elastic modulus. The LWD was setup with 300 mm diameter plate and 71 cm drop height. The tests were performed following manufacturer recommendations (Zorn 2003) and the elastic modulus values were determined using Equation 5,

$$E = \frac{(1 - \eta^2) \sigma_0 r}{D_0} \times F \quad (5)$$

where

E = elastic modulus (MPa);

D_0 = measured deflection under the plate (mm);

η = Poisson's ratio (0.4);

σ_0 = applied stress (MPa);

r = radius of the plate (mm); and

F = shape factor depending on stress distribution (assumed as 8/3) (see Vennapusa and White 2009).

The results are reported as E_{LWD-Z3} where Z represents Zorn LWD and 3 represents 300 mm diameter plate.

Kuab Falling Weight Deflectometer

Kuab FWD tests on this project were conducted on the CTB base layer. Tests were conducted by applying one seating drop using a nominal force of about 24.5 kN (5500 lb) followed by two test drops, each at a nominal force of about 24.5 kN (5500 lb) and 36.9 kN (8300 lb). The actual applied force was recorded using a load cell. Deflections were recorded using seismometers mounted on the device, per ASTM D4694-09 *Standard Test Method for Deflections with a Falling-Weight-Type Impulse Load Device*. The FWD plate and deflection sensor setup and a typical deflection basin are shown in Figure 20.

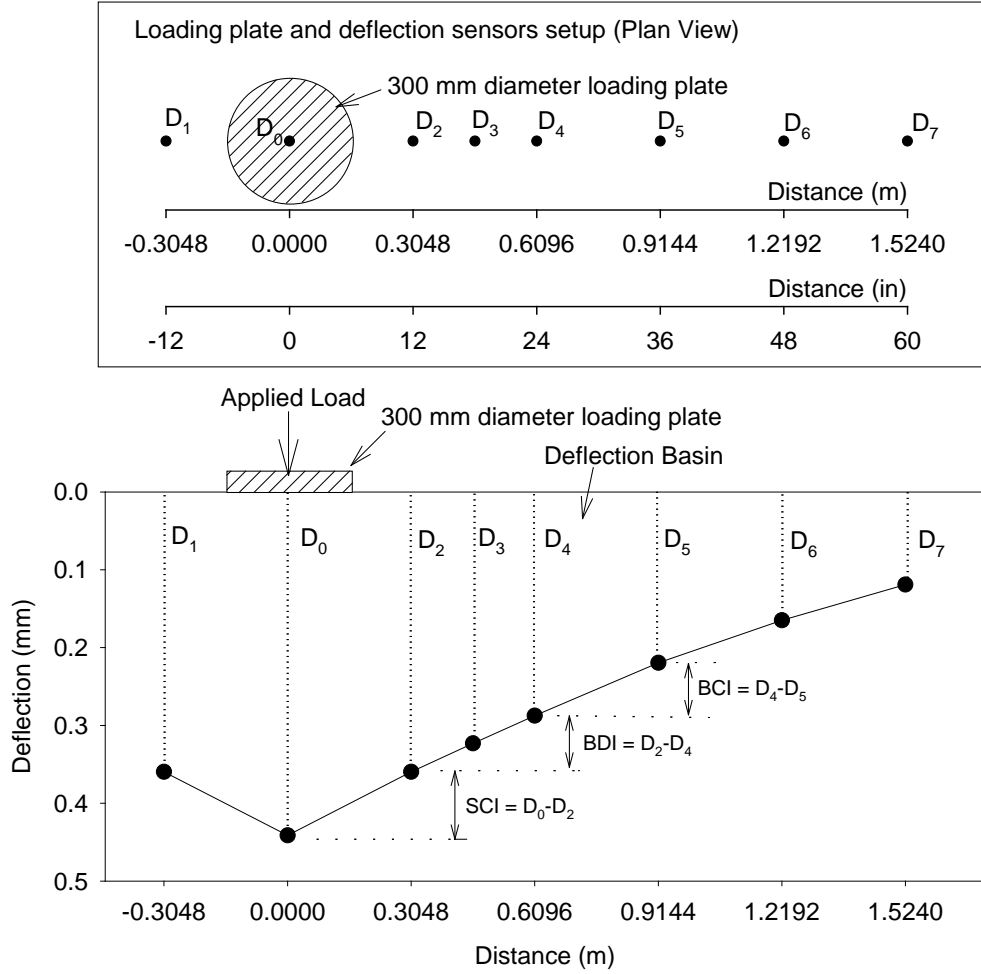


Figure 20. FWD deflection sensor setup used for this study and an example deflection basin

A composite modulus value (E_{FWD-K3}) was calculated using the measured deflection at the center of the plate (D_0), corresponding applied contact force, and Equation 5. The plate that used the Kuab FWD is a four-segmented plate, and therefore, shape factor $F = 2$ was used in the calculations assuming a uniform stress distribution (see Vennapusa and White 2009).

The subgrade layer modulus (E_{SG}) was determined using Equation 6, per AASHTO (1993):

$$E_{SG} = \frac{(1 - \eta^2) \sigma_0 r^2}{d_i D_i} \quad (6)$$

where

D_i = measured deflection at distance d_i (mm); and

d_i = radial distance of the sensor away from the center of the loading plate.

According to AASHTO (1993), the modulus values estimated from FWD tests exceed the laboratory measured resilient modulus values by a factor of three or more. Therefore, an adjustment factor $C \leq 0.33$ is recommended to correct E_{SG} determined from Equation 7. In this study, corrected E_{SG} values are calculated using $C = 0.33$:

$$\text{Corrected } E_{SG} = 0.33 \times E_{SG} \quad (7)$$

AASHTO (1993) suggests that the d_i must be far enough away that it provides a good estimate of the subgrade modulus, independent of the effects of any layers above, but also close enough that it does not result in a too small value. A graphical solution is provided in AASHTO (1993) to estimate the minimum radial distance based on an assumed effective modulus of all layers above the subgrade and the d_0 value. Salt (1998) indicated that if E_{SG} values are plotted against radial distance, in linear elastic materials such as sands and gravels, the modulus values decrease with increasing distance and then level off after a certain distance. The deformations at the distance at which the modulus values level off can be used to represent E_{SG} . In some cases, the modulus values decrease and then increase with distance. Such conditions represent either soils with moderate to high moduli with poor drainage at the top of the subgrade or soft soils with low moduli. In those cases, the distance where the modulus is low is represented as E_{SG} .

Ullidtz (1987) described the Odemark's method of equivalent thickness (MET) concept and is used in AASHTO (1993). According to the MET concept, a two-layered system with the top layer modulus higher than the bottom layer, can be transformed into a single layer of equivalent thickness with properties of the bottom layer. Using this concept and the modulus of the bottom layer (E_{SG}), the top layer modulus (E_{SB}) can be back-calculated.

In this study, tests conducted on the CTB layer were used to calculate E_{SG} and back-calculate E_{SB} values and compare with the design assumptions.

Dynamic Cone Penetrometer

DCP tests were performed in accordance with ASTM D6951-03 "*Standard Test Method for Use of the Dynamic Cone Penetrometer in Shallow Pavement Applications*" to determine dynamic penetration index (DPI) and calculate California bearing ratio (CBR) using Equation 8.

$$CBR = \frac{292}{DPI^{1.12}} \quad (8)$$

The DCP test results are presented in this report as CBR with depth profiles at a test location and as point values of DCP-CBR_{Subbase} or DCP-CBR_{Subgrade}. The point data values represent the weighted average CBR within each layer. The depths of each layer were identified using the DCP-CBR profiles.

Nuclear Gauge

A calibrated nuclear moisture-density gauge (NG) device was used to provide rapid measurements of soil dry unit weight (γ_d) and moisture content (w) in the base materials. Tests were performed following ASTM D6938-10 “*Standard Test Method for In-Place Density and Water Content of Soil and Soil-Aggregate by Nuclear Methods (Shallow Depth)*.” Measurements of w and γ_d were obtained at each test location, and the average value is reported.

Rapid Gas Permeameter Test

A rapid gas permeameter test (GPT) device (White et al. 2010a) was used to determine the saturated hydraulic conductivity of the CTB and the existing subbase layers. Air was used as the permeating gas in this field study. The GPT consists of a self-contained pressurized gas system with a self-sealing base plate and a theoretical algorithm to rapidly determine the K_{sat} . The gas flow is controlled using a regulator and a precision orifice. The inlet pressure and flow rate values are recorded in the device and are used in K_{sat} calculations using Equation 9.

$$K_{sat} = \left[\frac{2\mu_{gas} Q P_1}{r G_o (P_1^2 - P_2^2)} \right] \times \frac{\rho g}{\mu_{water} (1 - S_e)^2 (1 - S_e^{((2+\lambda)/\lambda)})} \quad (9)$$

where

K_{sat} = saturated hydraulic conductivity (cm/s);

K_{gas} = gas permeability;

K_{rg} = relative permeability to gas;

μ_{gas} = kinematic viscosity of the gas (PaS);

Q = volumetric flow rate (cm³/s);

P_1 = absolute gas pressure on the soil surface (Pa) $P_{o(g)} \times 9.81 + 101325$;

$P_{o(g)}$ = gauge pressure at the orifice outlet (mm of H₂O);

P_2 = atmospheric pressure (Pa);

r = radius at the outlet (4.45 cm);

G_o = Geometric factor (constant based on geometry of the device and test area; White et al. 2007);

S_e = effective water saturation [$S_e = (S - S_r)/(1 - S_r)$];

λ = Brooks-Corey pore size distribution index;

S_r = residual water saturation;

S = water saturation;

ρ = density of water (g/sm³);

g = acceleration due to gravity (cm/s²); and

μ_{water} = absolute viscosity of water (gm/cm-s).

More details on the test device and K_{sat} calculation procedure are provided in White et al. (2007, 2010a). The degree of saturation (S) values were obtained from in situ dry unit weight and moisture content measurements. The S_r and λ parameters can be obtained by determining the

soil-water retention properties (also known as soil water characteristic curves (SWCC) of the materials). Tests to determine SWCC parameters can be time-consuming and require precise calibration of test equipment. As an alternative, empirical relationships from material gradation properties can be used (Zapata and Houston 2008). A summary of these relationships and the procedure to estimate S_r and λ parameters are summarized in White et al. (2010a). For the results presented in this report, $\lambda = 3.7$ and $S_r = 10\%$ were used for the sand subbase material, and $\lambda = 0.2$ and $S_r = 0\%$ were used for the CTB material.

Static Plate Load Test

Static PLTs were conducted on the sand subbase layer by applying a static load on 300 mm diameter plate against a 62-kN capacity reaction force. The applied load was measured using a 90-kN load cell, and deformations were measured using three 50-mm linear voltage displacement transducers (LVDT). The load and deformation readings were continuously recorded during the test using a data logger. The E_{V1} and E_{V2} values were determined from Equation 5 using deflection values at 0.2 and 0.4 MPa contact stresses, as shown in Figure 21.

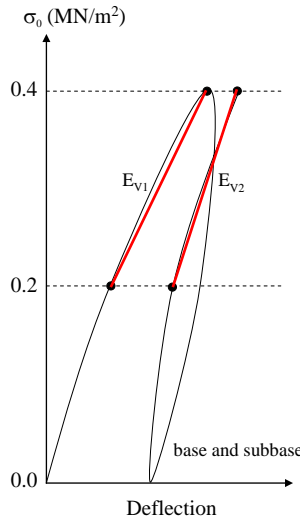


Figure 21. E_{V1} and E_{V2} determination procedure from static PLT for subgrade and base materials

Determination of k_{comp} Values

For the pavement reconstruction project described in this study, k_{comp} values were used in the design based on E_{SB} , H_{SB} , and subgrade M_r values. The E_{SB} values were directly measured using back-calculation analysis of FWD data. M_r was directly measured using laboratory testing, back-calculated from FWD (i.e., corrected E_{SG}), and empirically estimated based on DCP- $CBR_{Subgrade}$ values using correlations provided in AASHTO (1993) between CBR and M_r (see Appendix C). These results were converted to k_{comp} in accordance with AASHTO (1993) for comparison with the design assumptions.

CHAPTER 4. LABORATORY TEST RESULTS

Laboratory test results of subgrade, subbase, and OGDC base layer (unstabilized RPCC) samples collected from the field are presented in this chapter. A summary of the material index properties (i.e., laboratory compaction test, grain-size analysis, Atterberg limits test, soil classification, and specific gravity results) is provided in Table 8.

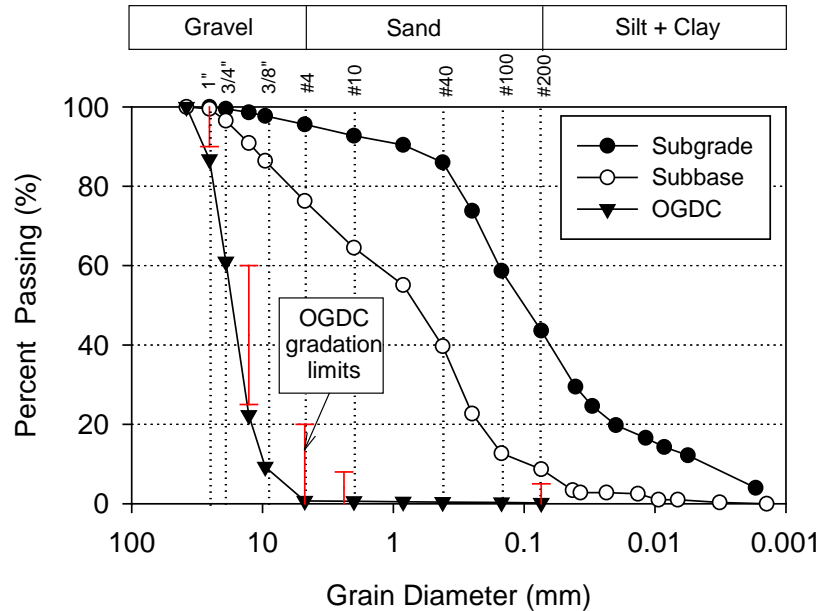
Table 8. Summary of material index properties

Parameter	RPCC base material used in CTB	Sand Subbase	Subgrade
Standard Proctor Test Results (ASTM D698-07)			
γ_{dmax} (kN/m ³)	*	19.96	20.10
W_{opt}		7.9	9.5
Modified Proctor Test Results (ASTM D1557-07)			
γ_{dmax} (kN/m ³)	*	20.57	20.67
W_{opt}		7.2	8.1
Maximum and Minimum Relative Density Test Results (ASTM D4253-00 and D4254-00)			
γ_{dmax} (kN/m ³)	13.61	20.06	*
γ_{dmin} (kN/m ³)	12.26	14.98	
Particle-Size Analysis Results (ASTM D 422-63 and ASTM C136-06)			
Gravel Content (%) (> 4.75mm)	99	24	4
Sand Content (%) (4.75mm – 75 μ m)	1	68	52
Silt Content (%) (75 μ m – 2 μ m)			38
Clay Content (%) (< 2 μ m)	0	8	6
D ₁₀ (mm)	9.7501	0.0956	0.0038
D ₃₀ (mm)	14.0043	0.3163	0.0415
D ₆₀ (mm)	18.8631	1.2746	0.1575
Coefficient of Uniformity, c_u	1.93	13.33	41.04
Coefficient of Curvature, c_c	1.07	0.82	2.85
Atterberg Limits Test Results (ASTM D4318-05)			
Liquid Limit, LL (%)			20
Plastic Limit, PL (%)	Non Plastic	Non Plastic	12
Plasticity Index, PI (%)			8
AASHTO Classification (ASTM D3282-09)	A-1-a	A-1-b	A-4
USCS Classification (ASTM D2487-00)	GP	SP-SM	SC

*Test not performed

Particle-Size Analysis Results

Grain-size distribution curves from particle-size analysis tests for OGDC base material used in CTB, subbase, and subgrade materials are provided in Figure 22.



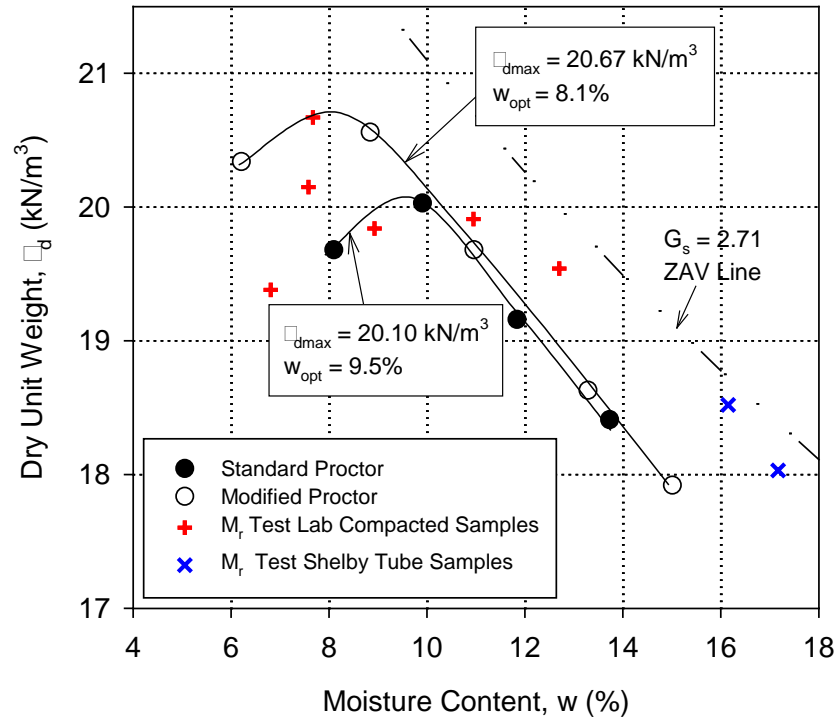


Figure 23. Moisture-dry unit weight relationships of subgrade material from Proctor tests and moisture-dry unit weight of M_r samples

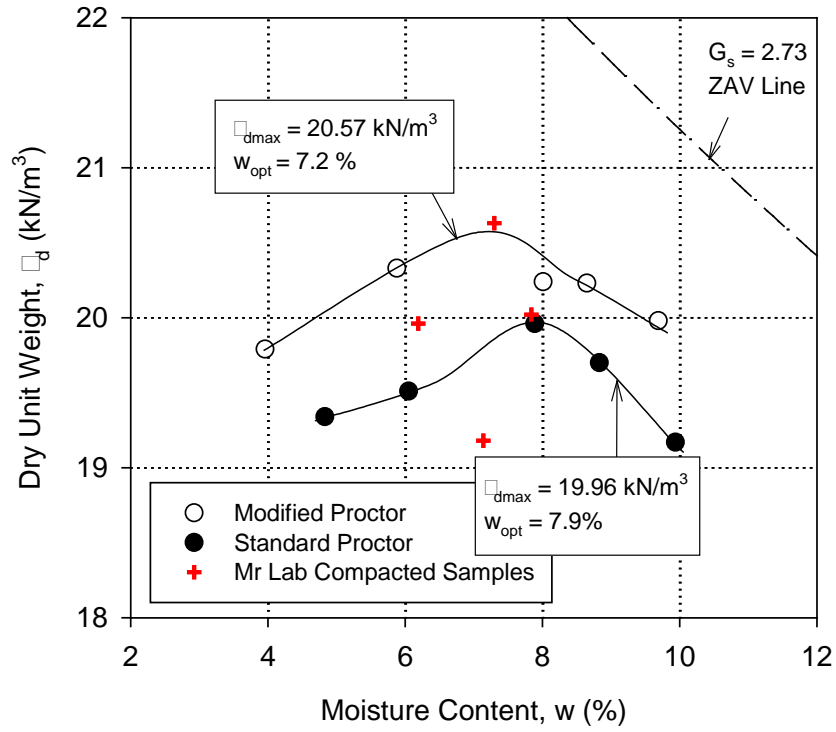


Figure 24. Moisture-dry unit weight relationships of subbase material from Proctor tests and moisture-dry unit weight of Mr samples

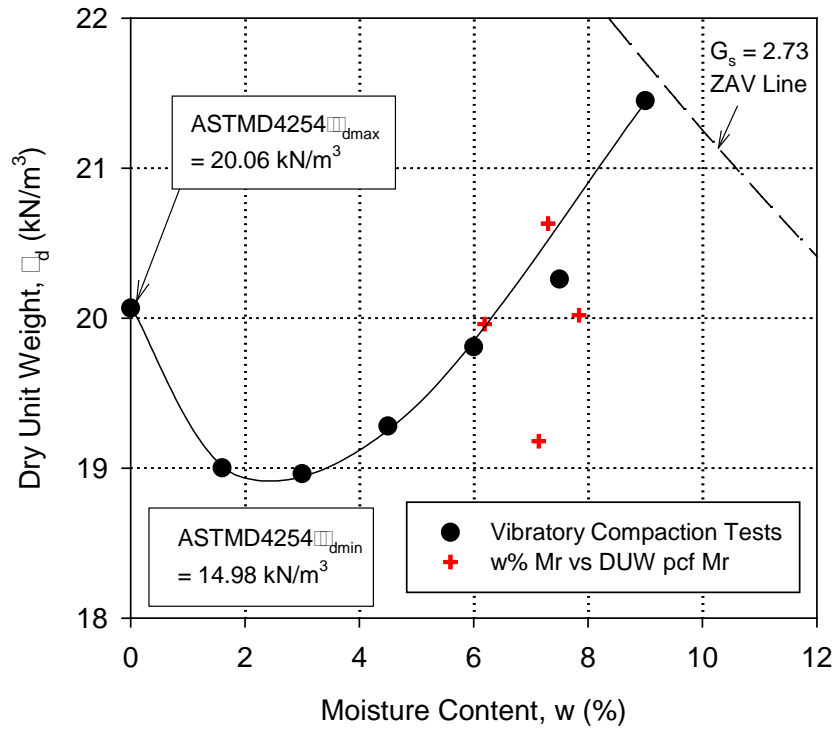


Figure 25. Moisture-dry unit weight relationships of subbase material from vibratory compaction tests and moisture-dry unit weight of M_r samples

M_r and UU Test Results

Table 9 summarizes the test results for the three materials and shows the γ_d , $w\%$, average M_r of the 15 AASHTO T-307 loading sequences; M_r at specific stress states; dynamic secant modulus (E_s); permanent strain (ϵ_p) at the end of the M_r test; universal model regression coefficients; undrained shear strength (s_u) at failure or at 5% axial strain; and s_u at 1% strain.

Table 9. Summary of M_r and UU test results

Sample	M_r Test										UU Test	
	γ_d (kN/m ³)	w (%)	Ave. M_r (MPa)	M_r at Selected Stress States (MPa) [#]	E_s (MPa)	ϵ_p (%)	k_1	k_2	k_3	R^2 (adj.)	s_u (kPa) [§]	s_u @ $\epsilon = 1\%$ (kPa)
Subgrade*	20.67	7.7	140.0	56.8	139.8	0.6	613.0	0.64	0.22	0.95	233.1	206.3
Subgrade*	19.91	11.0	36.6	37.0	36.2	4.4	251.9	0.09	2.23	0.76	104.5	55.2
Subgrade*	20.15	7.6	101.2	92.2	101.2	0.2	1206.9	0.26	-1.32	0.30	231.7	160.0
Subgrade*	19.38	6.8	91.2	79.0	90.7	0.2	1194.8	0.40	-1.99	0.21	173.2	141.6
Subgrade*	19.45	9.7	54.9	46.2	54.9	0.8	543.8	0.49	-0.45	0.71	98.9	83.0
Subgrade*	19.84	8.9	75.0	59.9	75.1	0.4	1001.8	0.57	-2.37	0.77	140.4	106.4
Subgrade**	18.03	17.2	29.1	22.3	28.8	2.2	633.5	0.33	-5.69	0.75	77.2	42.8
Subgrade**	18.52	16.2	33.1	28.4	33.0	1.4	734.0	-0.01	-5.54	0.77	89.8	39.4
Subbase*	19.18	7.1	141.9	108.4	141.3	0.9	607.9	0.65	0.25	0.96	105.0	101.4
Subbase*	20.92	4.4	232.6	164.2	232.5	0.2	990.0	0.87	-0.34	0.93	210.3	208.5
Subbase*	20.02	7.8	143.3	89.8	142.2	3.6	554.5	1.11	-0.84	0.92	99.1	97.3
Subbase*	20.63	7.3	146.9	94.4	146.8	1.0	532.2	1.04	-0.48	0.98	125.2	125.7
Subbase*	19.96	6.2	200.5	159.8	200.3	0.3	827.4	0.51	0.71	0.92	138.3	137.4
Composite subgrade* + subbase*	19.98 19.78	6.1 9.0	163.5	114.5	163.2	0.9	690.3	0.86	-0.32	0.89	129.6	126.0

* = laboratory compacted sample, ** Shelby tube sample, # subgrade: $\sigma_3 = 14$ kPa (2 psi) and $\sigma_{cyclic} = 41$ kPa (6 psi), and for subbase $\sigma_3 = 35$ kPa (5 psi), $\sigma_{cyclic} = 103$ kPa (15 psi); § at axial strain $\epsilon = 5\%$ or at failure

Stress states for granular and cohesive materials were those recommended in the NCHRP 1-28A report (NCHRP 2004) as $\sigma_3 = 35$ kPa (5 psi) and $\sigma_{\text{cyclic}} = 103$ kPa (15 psi) for base or subbase materials and $\sigma_3 = 14$ kPa (2 psi) and $\sigma_{\text{cyclic}} = 41$ kPa (6 psi) for subgrade materials. Equation 2 and the k_1 , k_2 , and k_3 regression coefficients were used to calculate the M_r at those stress states.

Deviator stress (σ_d) versus M_r for laboratory compacted subgrade samples and Shelby tube subgrade samples obtained from the field along with the universal model prediction curves are presented in Figure 26 and Figure 27, respectively.

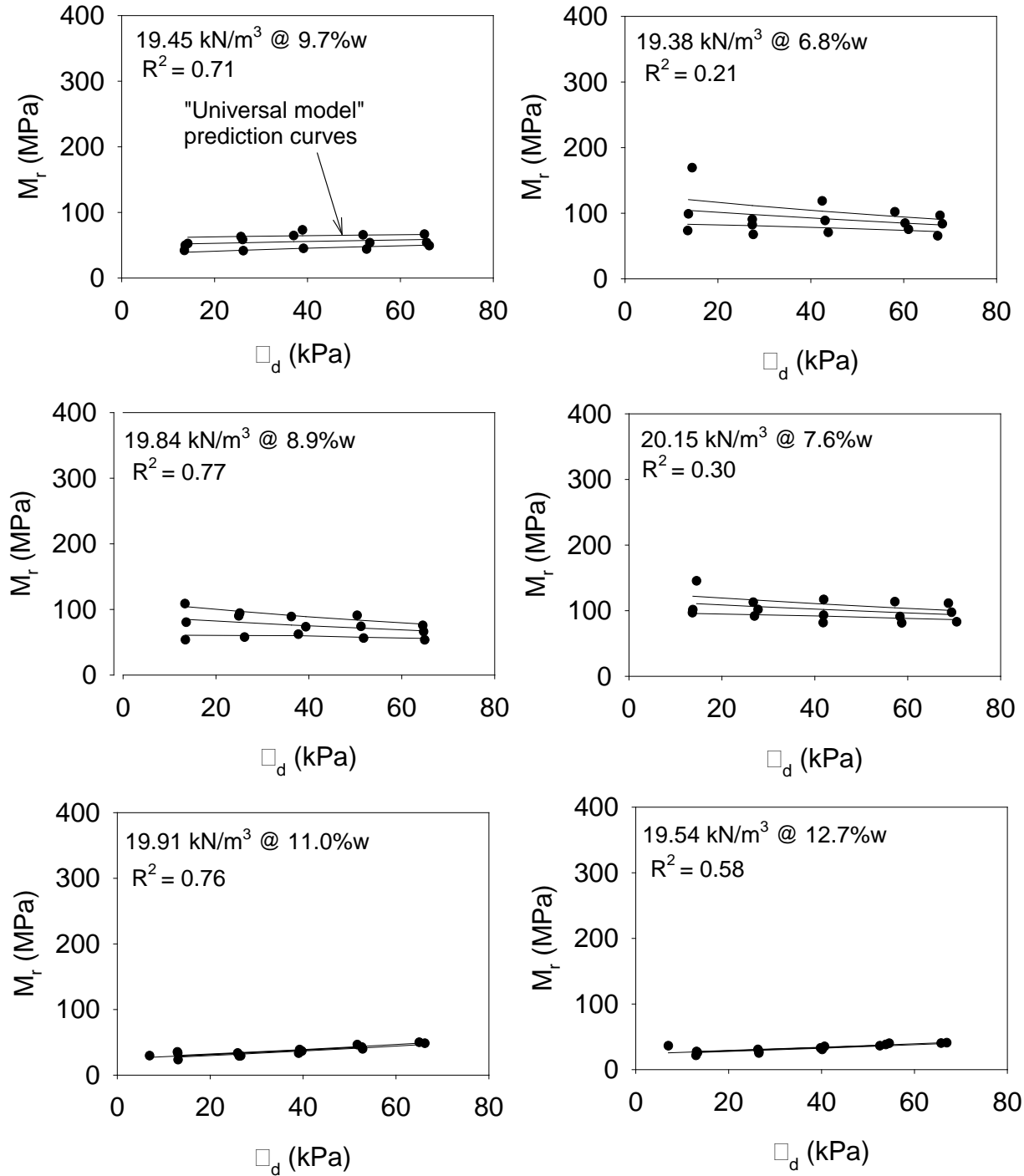


Figure 26. σ_d versus M_r for laboratory compacted subgrade samples at different dry unit weights and moisture contents

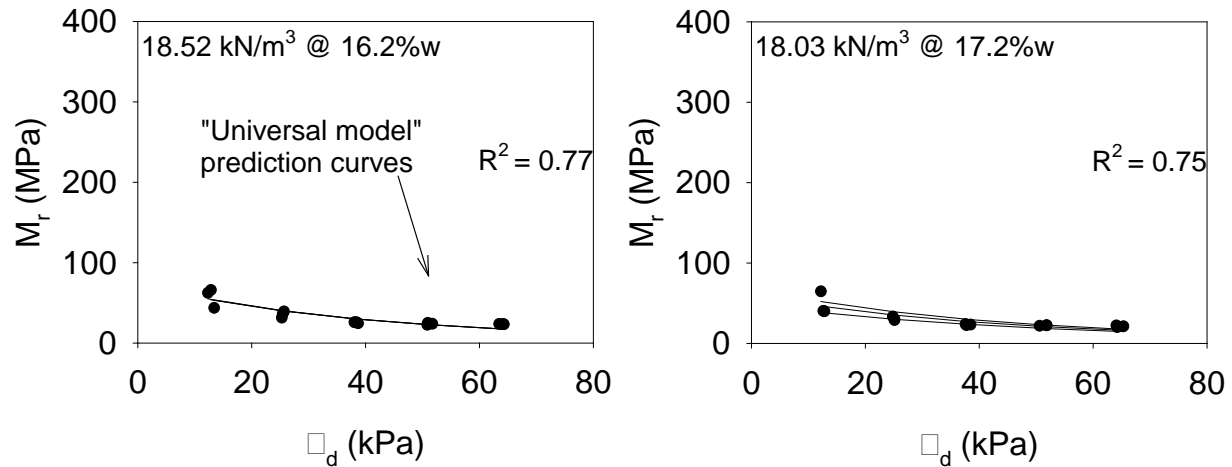


Figure 27. σ_d versus M_r for Shelby tube samples taken at 0.4 to 1.0 m below sand subbase layer

As expected, for subgrade materials these figures illustrate that the M_r generally decreases with increasing σ_d . The laboratory samples had high dry unit weights and low moisture contents, while the Shelby tube samples had low dry unit weights and high moisture contents. Therefore, as expected, the laboratory compacted samples showed higher M_r compared to the field samples.

Bulk stress (σ_B) versus M_r for sand subbase samples along with the corresponding universal model prediction curves are presented in Figure 28.

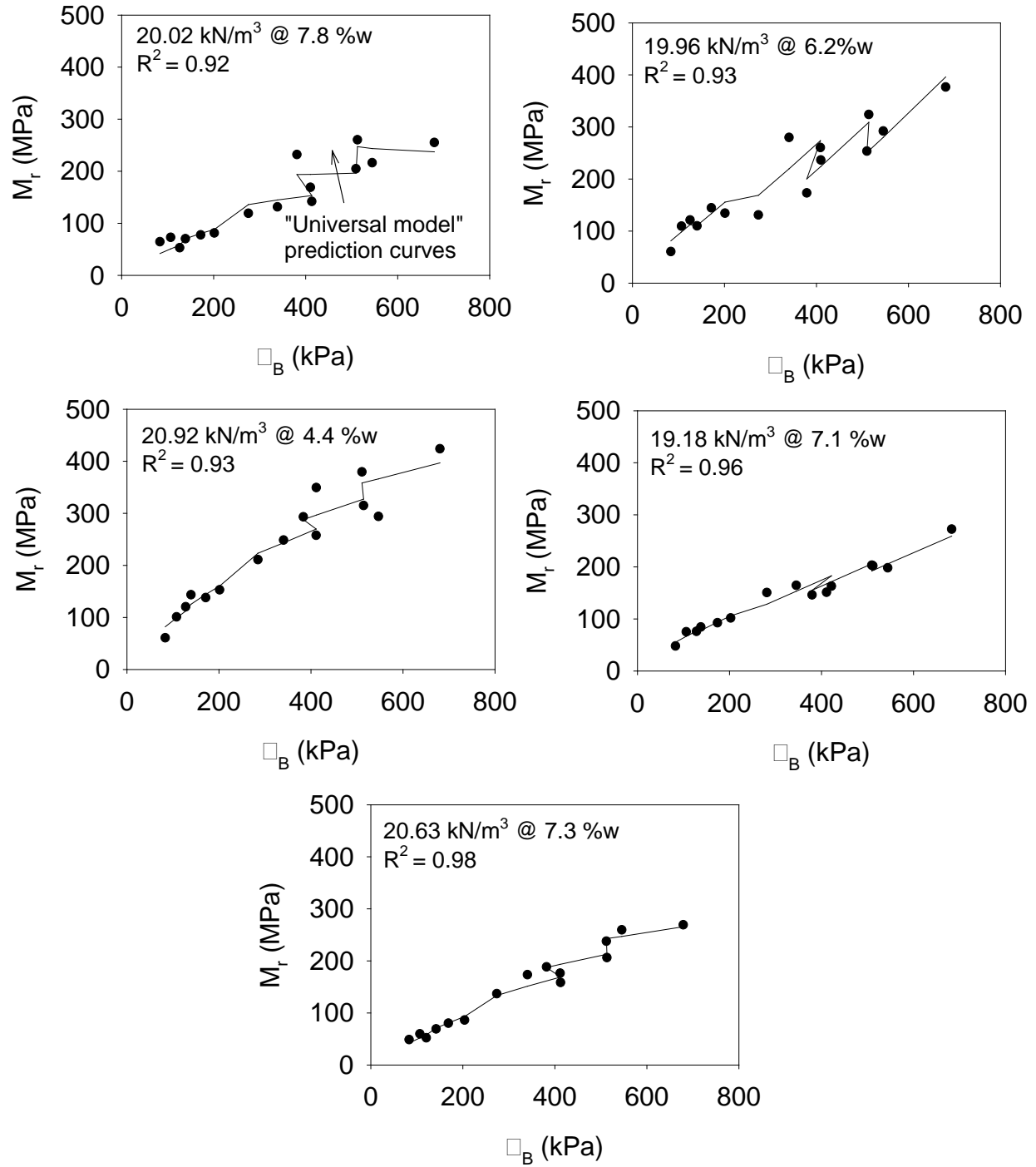


Figure 28. σ_B versus M_r for sand subbase samples

Results indicated that the M_r of subbase material increase with increasing bulk stresses, as expected. Increasing moisture content decreased M_r and increasing dry unit weight increased M_r for both subbase and subgrade materials.

σ_B versus M_r along with corresponding universal model prediction curves for the composite sample are compared with the subbase and subgrade single sample measurements in Figure 29.

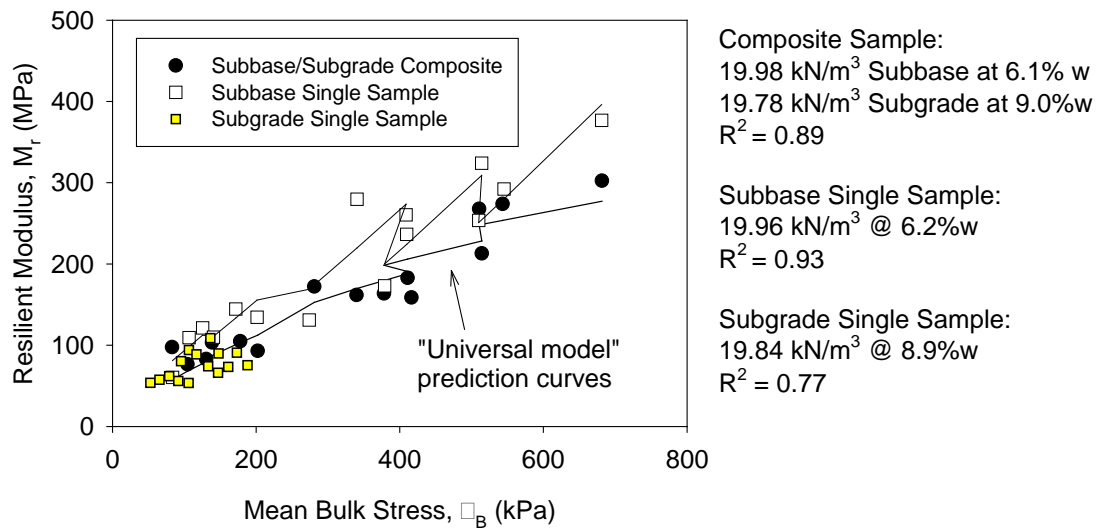


Figure 29. σ_B versus M_r for subbase and subgrade composite sample

Pictures of a composite sample (subbase over subgrade) during and after testing are shown in Figure 30 and Figure 31.

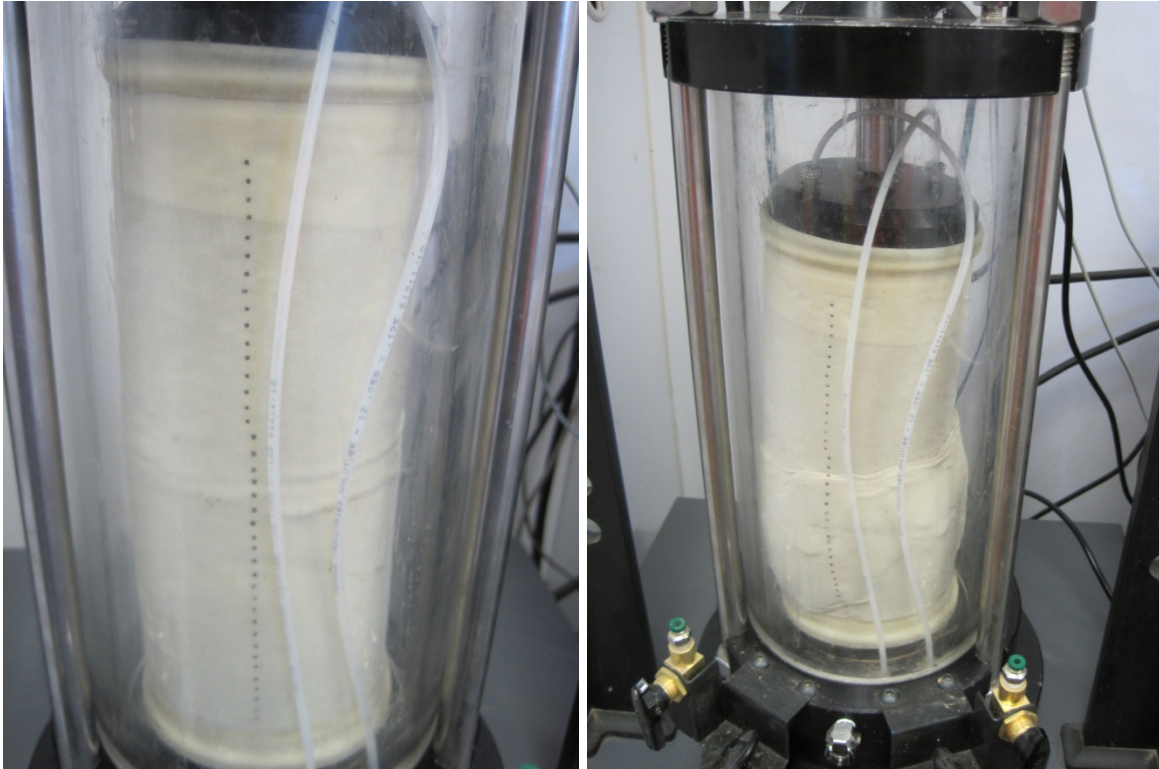


Figure 30. Sand + subgrade composite sample during Mr testing (left) and after shearing (right)

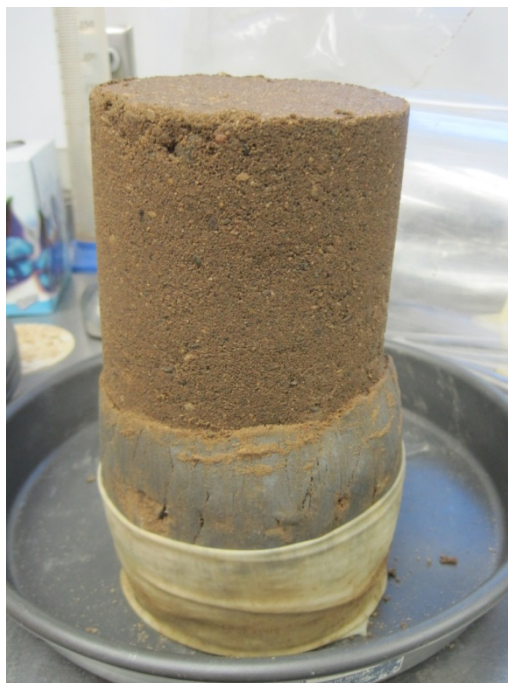


Figure 31. Sand + subgrade composite sample extruded after shearing

Comparing composite and single samples reveals that the average M_r of composite samples is about 1.2 times lower than the average M_r of a single layer subbase sample at a similar density. This reduction in M_r in the composite sample is attributed to the weaker subgrade layer. This is an important finding and must be further studied with adequate testing in various combinations of composite sample configurations. Other studies that are part of the larger Improving the Foundation Layers for Pavements (TPF-5(183)) are underway to further investigate the influence of composite soil layer configurations on M_r properties.

Compressive Strength Test and Wet-Dry and Freeze-Thaw Durability Test Results

Compressive strength testing was conducted on three CTB samples each after 7 days and 14 days of curing, and on two samples after 21 days of curing. Pictures of a sample before and after testing are shown in Figure 32.



Figure 32. CTB samples prepared by ISU research team before (left) and after (right) compression strength testing

Results from this test are provided in Figure 33.

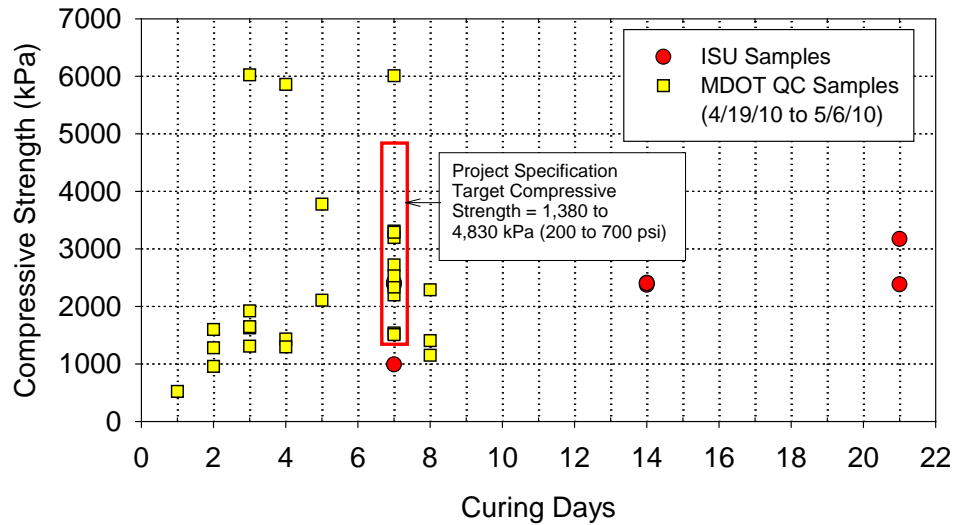


Figure 33. Compressive strength test results on CTB samples prepared in laboratory by ISU research team and QC samples by MDOT (between 4/19/10 and 5/6/10)

Also included in Figure 33 are compression test results on CTB from MDOT QC records between 19 April 2010 and 6 May 2010, after 1 to 8 days of curing. With the exception of one ISU sample, all other samples met the specified seven-day compressive strength range (i.e., 1,380 to 4,830 kPa).

Three samples each for wet-dry and freeze-thaw durability testing were compacted in a split mold. An image of an extracted sample is shown in Figure 34.

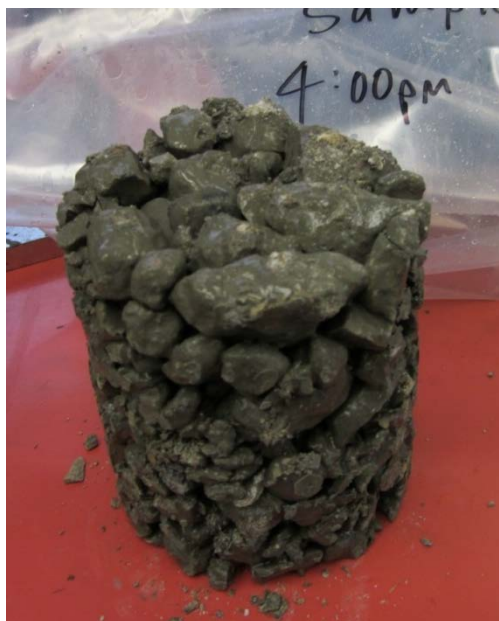


Figure 34. Compacted CTB sample from split mold for wet-dry and freeze-thaw testing

Percent mass loss results during each wet-dry cycle and after 12 freeze-thaw cycles are presented in Figure 35.

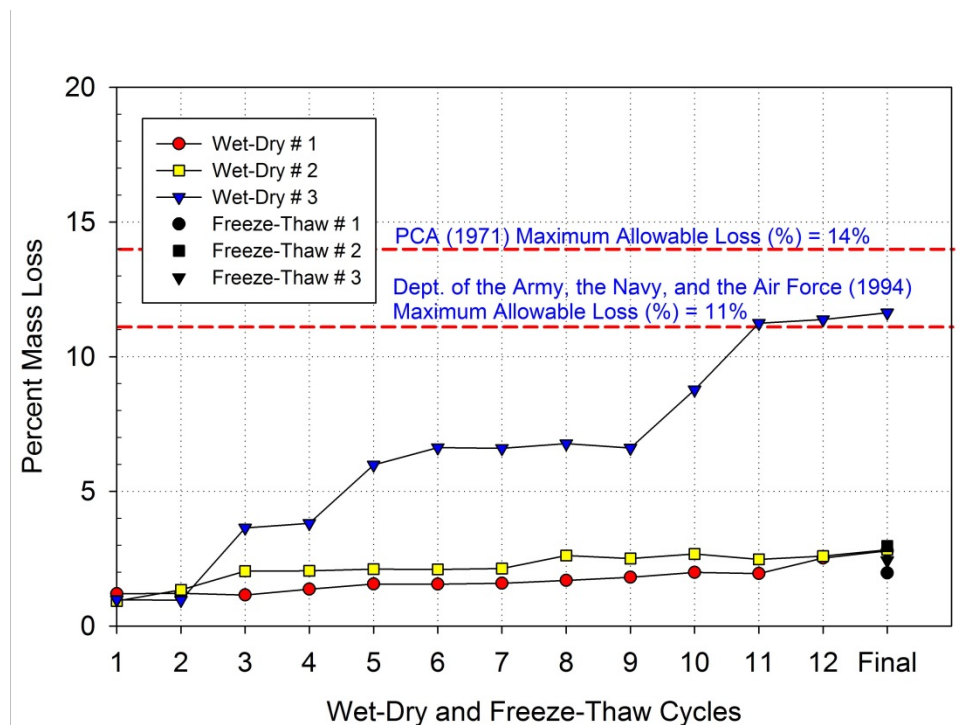


Figure 35. Percent mass loss during wet-dry and freeze-thaw cycles on three CTB samples

One of the three samples tested showed a total percent mass loss of about 11.5% after 12 wet-dry cycles. The total percent mass loss on the other two samples was < 3%. Similarly, the three samples subjected to freeze-thaw cycles also showed a percent mass loss < 3%. For reference, the maximum allowable percent loss limits recommended by PCA (1971) and the Dept. of the Army, the Navy, and the Air Force (1994) are also shown in Figure 35. All samples were below the PCA (1971) recommended maximum allowable percent loss of 14%.

Laboratory Permeability Test Results

Laboratory permeability tests on sand subbase and OGDC material used in CTB were performed using aggregate compaction mold LSLP test equipment. The materials were oven-dried prior to permeability testing. A summary of sample size, dry unit weight, water head conditions, and K_{sat} values of sand subbase and OGDC base material is provided in Table 10. Five CTB core samples with varying sample heights (from about 78 mm to 134 mm) were tested. A summary of the CTB test results are shown in Table 10.

Table 10. Summary of laboratory permeability test results

Material	Sample Size [Dia. x Ht.]	Dry Unit Weight (kN/m³)	Porosity (%)	Head (cm)	K_{sat} (cm/s)
Sand Subbase	304 mm x 304 mm	19.40	27.5	45	0.001
OGDC Base (untreated)	304 mm x 304 mm	15.09	43.0	55	3.9
CTB # 1	150 mm x 134 mm	15.41	35.0	152	1.9
CTB # 2	150 mm x 83 mm	17.64	20.6	152	1.7
CTB # 3	150 mm x 78 mm	16.41	29.7	152	0.9
CTB # 4	150 mm x 60 mm	15.22	36.0	152	0.4
CTB # 5	150 mm x 101 mm	16.13	31.3	140	0.7

The permeability of the CTB samples was about 2 to 10 times lower than the untreated OGDC base layer sample.

CHAPTER 5. IN SITU TEST RESULTS

Description of Test Sections

Three test sections (TS) were tested as part of this project. TS1 and TS2 consisted of areas with sand subbase layer, and TS3 consisted of a CTB layer. Various in situ testing methods were used in characterizing the foundation layer properties, and a summary of each TS is provided in Table 11.

Table 11. Summary of test sections and in situ testing

TS	Date	Location	Material	In Situ Test Measurements	Comments
1	5/18/10	Between Hwy M-43 exit ramp and Hwy M-43 overpass on I-96 east/south bound lane (near Sta. 464+40)	Sand subbase layer underlain by subgrade	NG, DCP, LWD, GPT	In situ testing at 73 points in a dense grid pattern
2	5/19/10 and 5/23/10	West of W Grand River Avenue overpass on I-96 east/south bound lane (between Sta. 296+00 and 299+00)	CTB underlain by sand subbase and subgrade	FWD, NG, GPT	CTB placed on 5/15/10; FWD and NG tests at 119 points and APT tests at 67 points.
3	5/20/10	Along centerline from Sta. 468+50 to 458+00 near Hwy M-43 on I-96 east/south bound lane	Sand subbase layer underlain by subgrade	NG, DCP, LWD, PLT, Shelby tube sampling of subgrade	Additional tests across the width of the pavement base at Sta. 461+50.

Note: TS—test section, NG—nuclear gauge, DCP—dynamic cone penetrometer (DCP) test, LWD—Zorn light weight deflectometer with a 300 millimeter plate, GPT—gas permeameter test device, FWD—Kuab falling weight deflectometer, PLT—static plate load test.

Geostatistical Data Analysis

Spatially referenced in situ point measurements in a dense grid pattern were obtained in TS1 and TS2. These data sets provide an opportunity to quantify “non-uniformity” of compacted fill materials. Non-uniformity can be assessed using conventional univariate statistical methods (i.e., by statistical standard deviation (σ) and coefficient of variation (COV)), but they do not address the spatial aspect of non-uniformity. Vennapusa et al. (2010) demonstrated the use of semivariogram analysis in combination with conventional statistical analysis to evaluate non-uniformity in QC/QA during earthwork construction. A semivariogram is a plot of the average squared differences between data values as a function of separation distance, and is a common tool used in geostatistical studies to describe spatial variation. A typical semivariogram plot is presented in Figure 36. The semivariogram $\gamma(h)$ is defined as one-half of the average squared

differences between data values that are separated at a distance h (Isaaks and Srivastava 1989). If this calculation is repeated for many different values of h (as the sample data will support) the result can be graphically presented as experimental semivariogram, shown as circles in Figure 36. More details on experimental semivariogram calculation procedure are available elsewhere in the literature (e.g., Clark and Harper 2002, Isaaks and Srivastava 1989).

To obtain an algebraic expression for the relationship between separation distance and experimental semivariogram, a theoretical model is fit to the data. Some commonly used models include linear, spherical, exponential, and Gaussian models. A spherical model was used for data analysis in this report. Arithmetic expression of the spherical model and the spherical variogram are shown in Figure 36. Three parameters are used to construct a theoretical semivariogram: sill ($C+C_0$), range (R), and nugget (C_0). These parameters are briefly described in Figure 36.

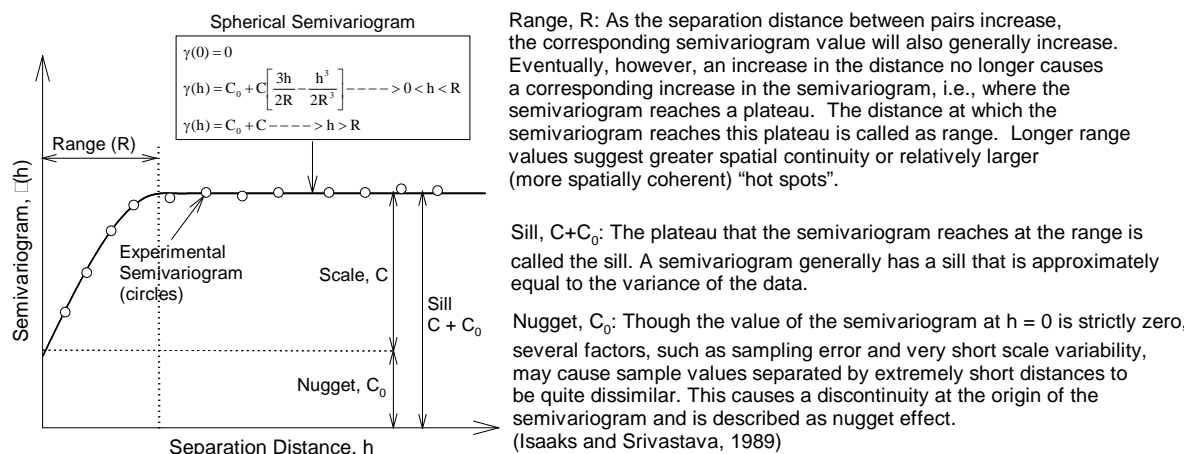


Figure 36. Description and parameters of a typical experimental and spherical semivariogram

Additional discussion on the theoretical models can be found elsewhere in the literature (e.g., Clark and Harper 2002, Isaaks and Srivastava 1989). For the results presented in this report, the sill, range, and nugget values during theoretical model fitting were determined by checking the models for "goodness" using the modified Cressie goodness fit method (see Clark and Harper 2002) and cross-validation process (see Isaaks and Srivastava 1989). From a theoretical semivariogram model, a low sill and longer range of influence values represent the best conditions for uniformity, while the opposite represents an increasingly non-uniform condition.

TS1/TS3: Subbase Layer

Experimental Testing

TS1 and TS3 consisted of testing the final compacted and trimmed sand subbase layer along I-96 EB lane alignment with NG, LWD, GPT, PLT, and DCP. Shelby tube samples of subgrade were obtained from TS1. TS3 involved testing between Sta. 458+00 and 468+50 at every +50 station along the centerline of the alignment. In addition, tests were conducted at five test locations

across the pavement width at Sta. 461+50. TS1 involved testing a 9 m x 9 m area near Sta. 464+40 in a dense grid pattern with 73 test points. A plan layout with GPS coordinates of the test locations on TS1 and TS3 are shown in Figure 37.

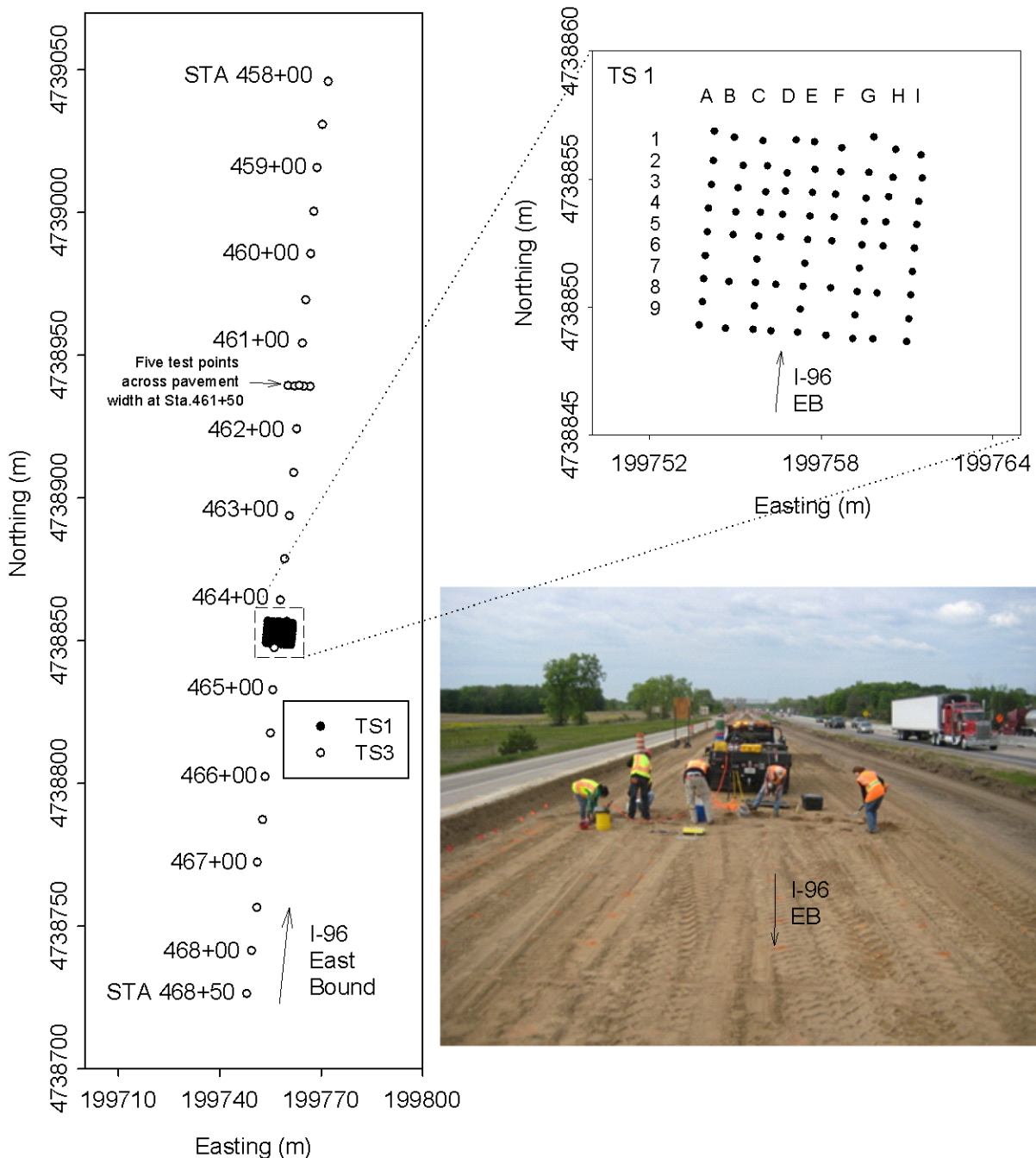


Figure 37. TS1/TS3: Plan view of in situ test locations (left), detailed plan layout (top right), and image showing test locations

In Situ Point Test Results and Discussion—TS1 and TS3

In situ test results from TS3 are presented in Figure 38 through Figure 40. Figure 38 presents γ_d and w measurements obtained from NG test, modulus measurements from LWD (E_{LWD-Z3}) and static PLTs (E_{V1} and E_{V2}) as point measurements with distance (note that each +100 station is about 30 m (100 ft) apart).

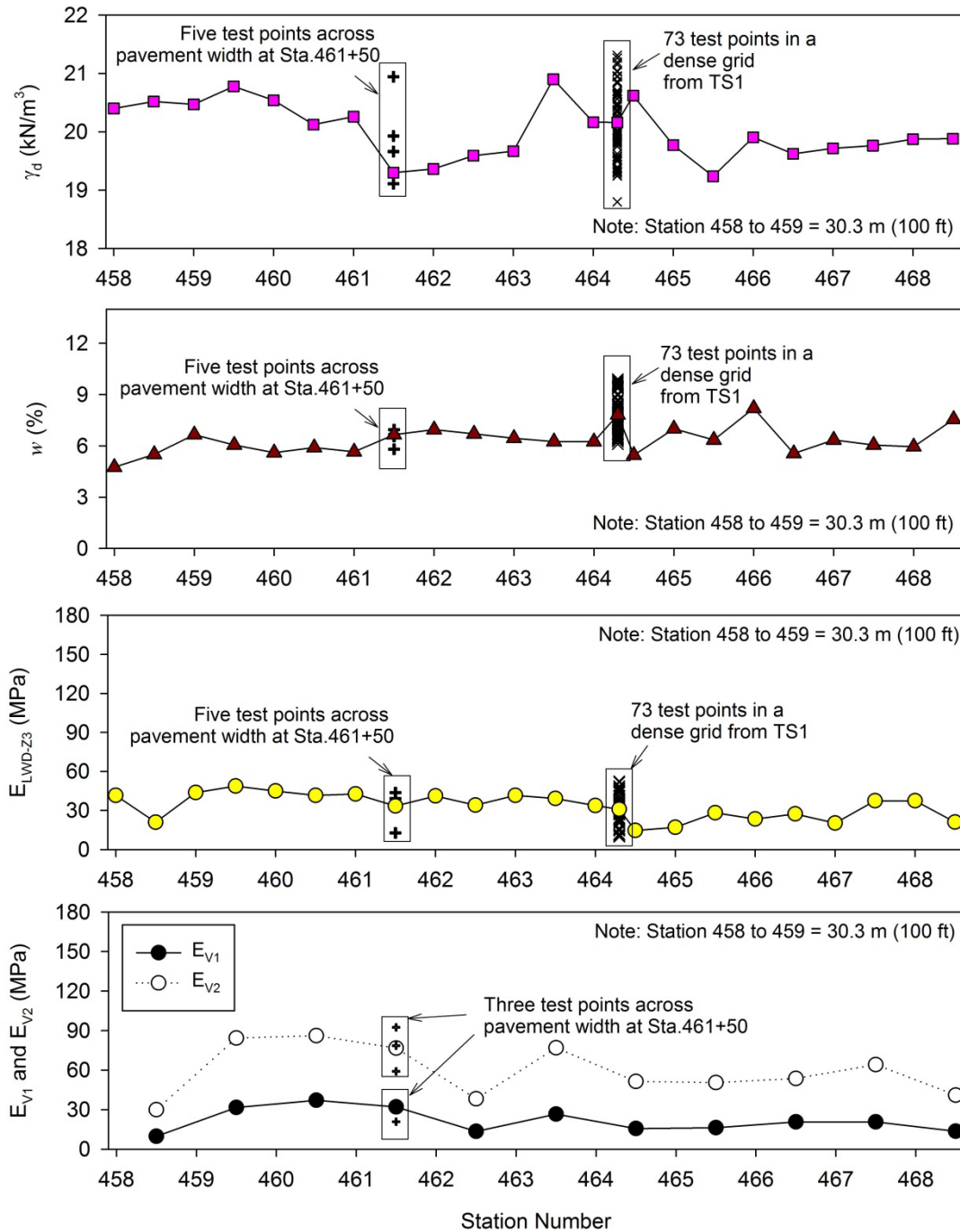


Figure 38. TS1/TS3: In situ NG, LWD, and PLT test results from Sta. 458+50 to 468+50

Figure 39 presents DCP-CBR_{Subbase}, thickness of subbase ($H_{subbase}$) determined from DCP profiles, and estimated M_r from DCP-CBR_{Subgrade} measurements. The estimated M_r values are based on correlations from AASHTO (1993).

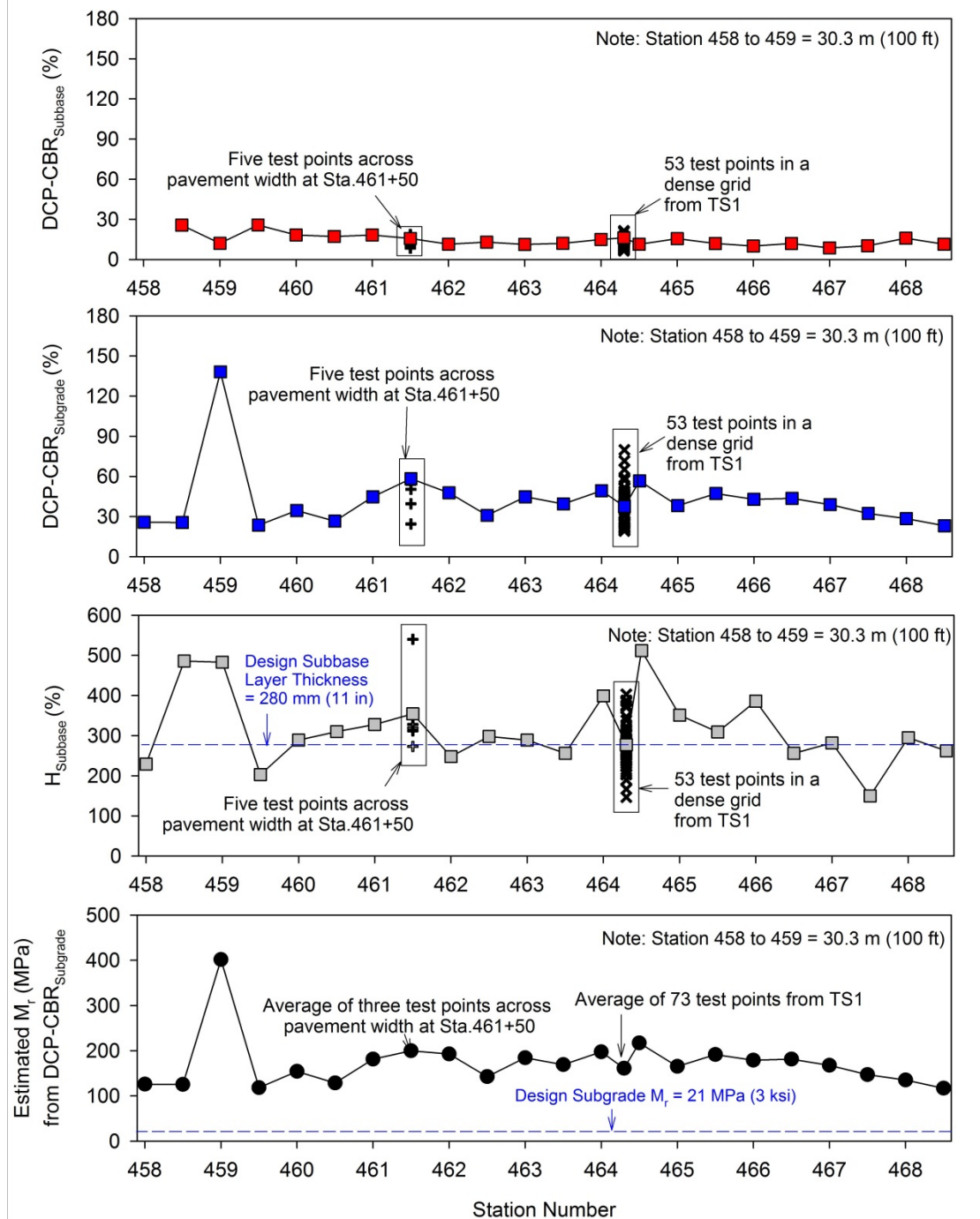


Figure 39. TS1/TS3: In situ DCP test results and estimated subgrade M_r from DCP test results from Sta. 804+00 to Sta. 814+00

Figure 40 presents DCP-CBR profiles at each station on TS3 and Figure 41 presents DCP-CBR profiles at each test location on TS1.

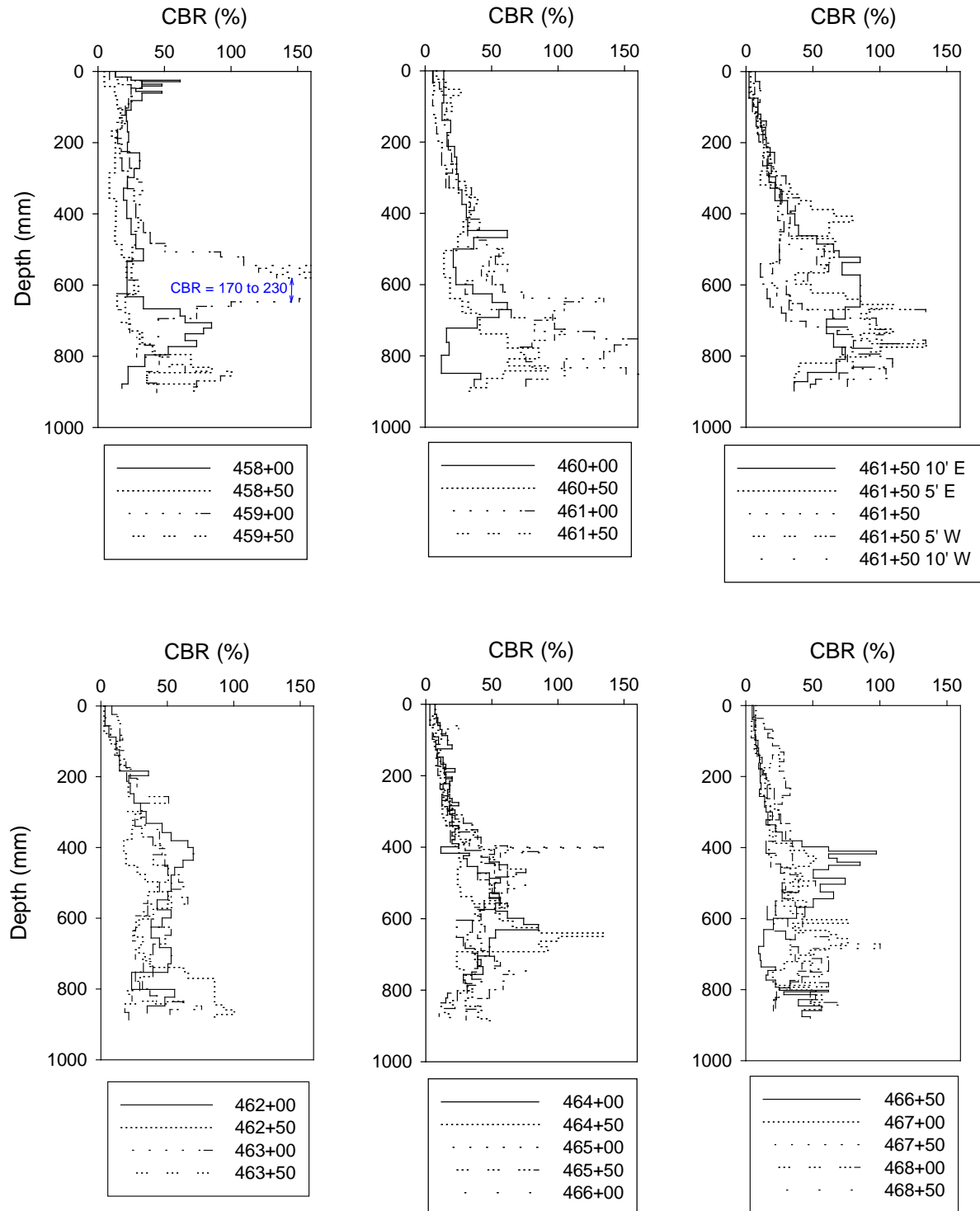


Figure 40. TS3: DCP-CBR profiles at each test location

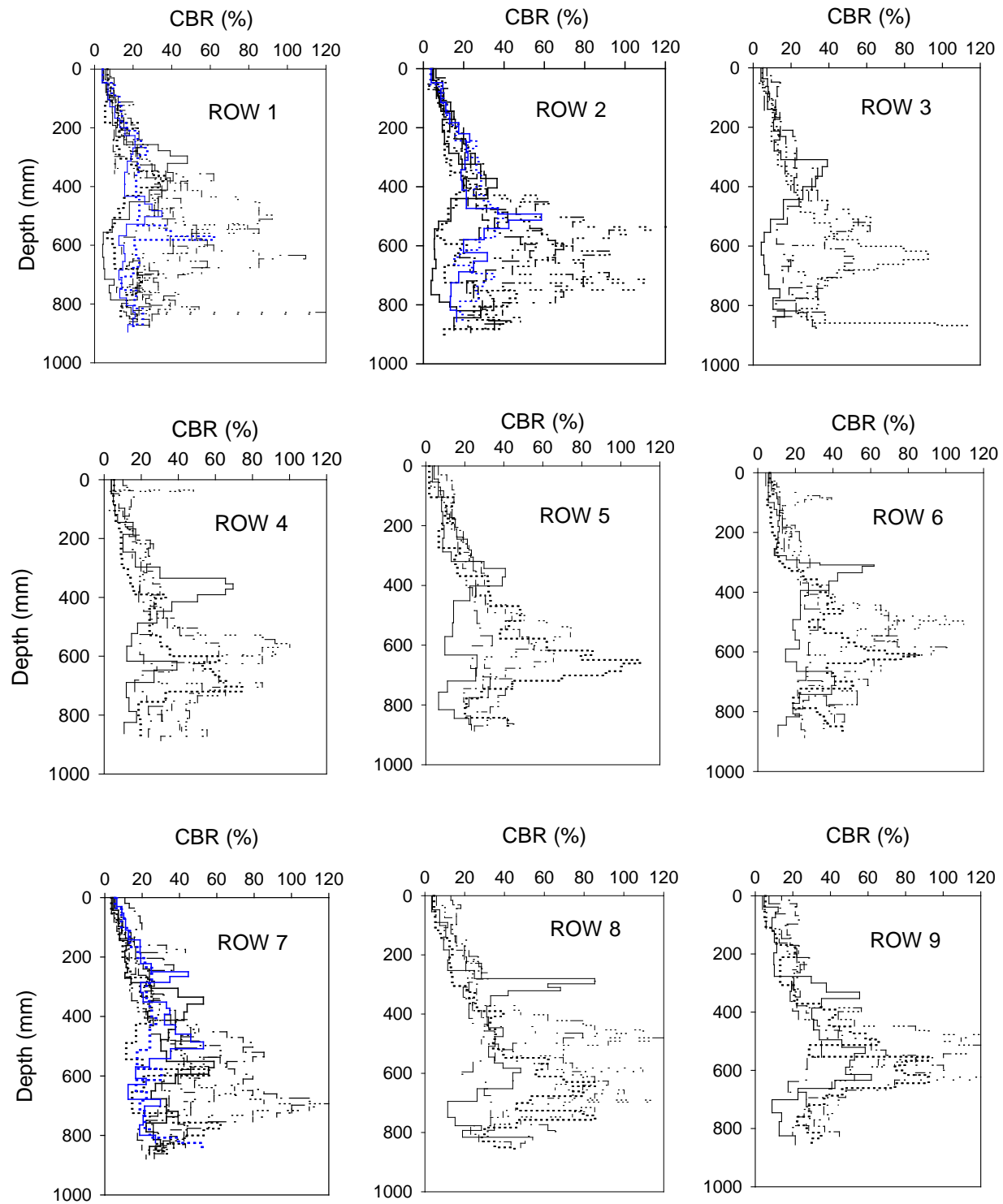


Figure 41. TS1: DCP-CBR profiles along each row

Histograms of all in situ test measurements with a summary of univariate statistics (i.e., mean μ , standard deviation σ , coefficient of variation COV) from TS1 and TS3 are shown in Figure 42.

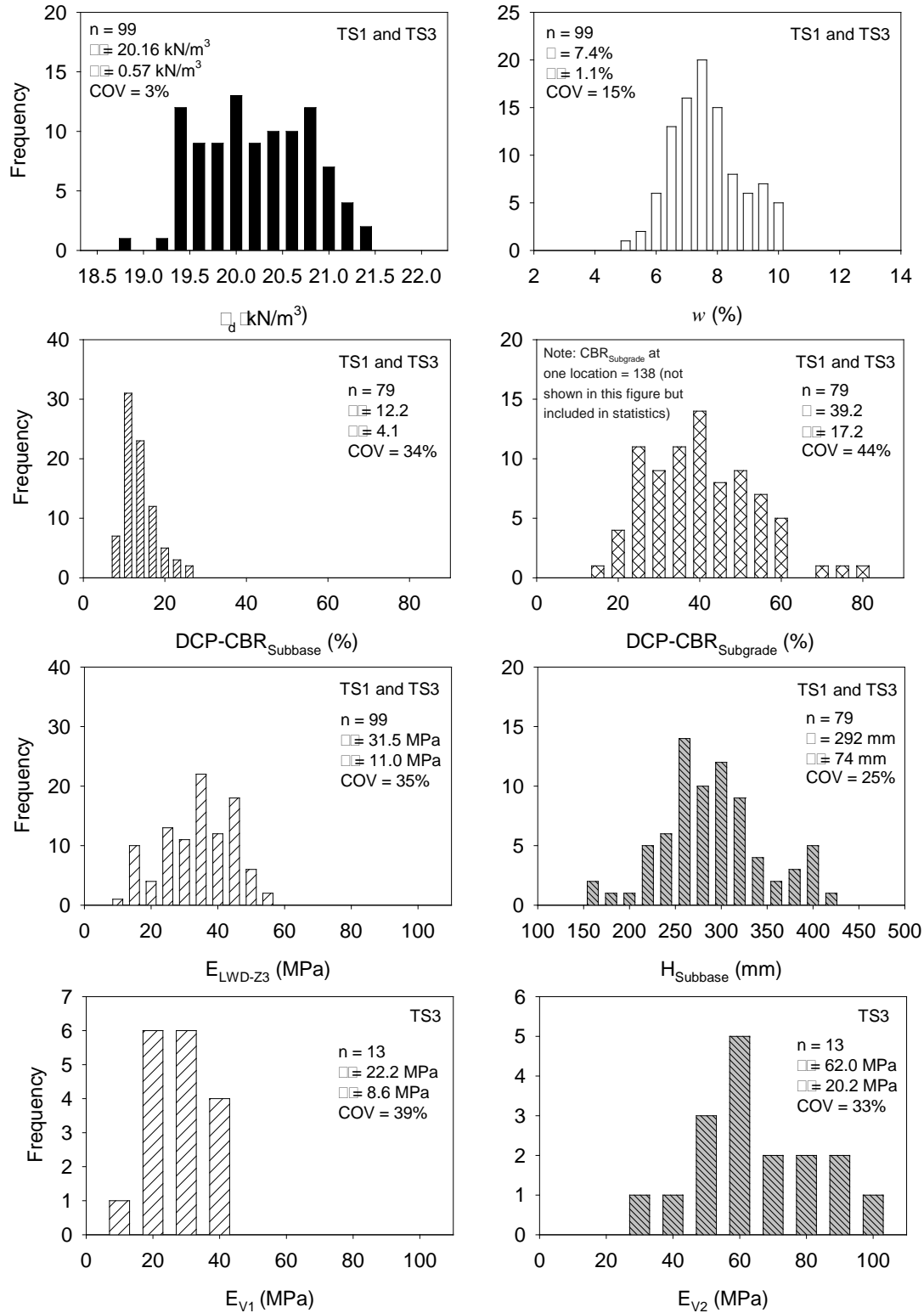


Figure 42. TS1 and TS3: Histograms of in situ test measurements

Geostatistical Analysis of Dense Grid Point Testing–TS1

Test measurements obtained from TS1 in a dense grid pattern with 73 tests over a plan area of about 9 m x 9 m provided a robust dataset to characterize the spatial characteristics of the measurements using geostatistical analysis. Kriged spatial contour maps, semivariograms, and histograms of each in situ point measurement are presented in Figure 43 through Figure 46.

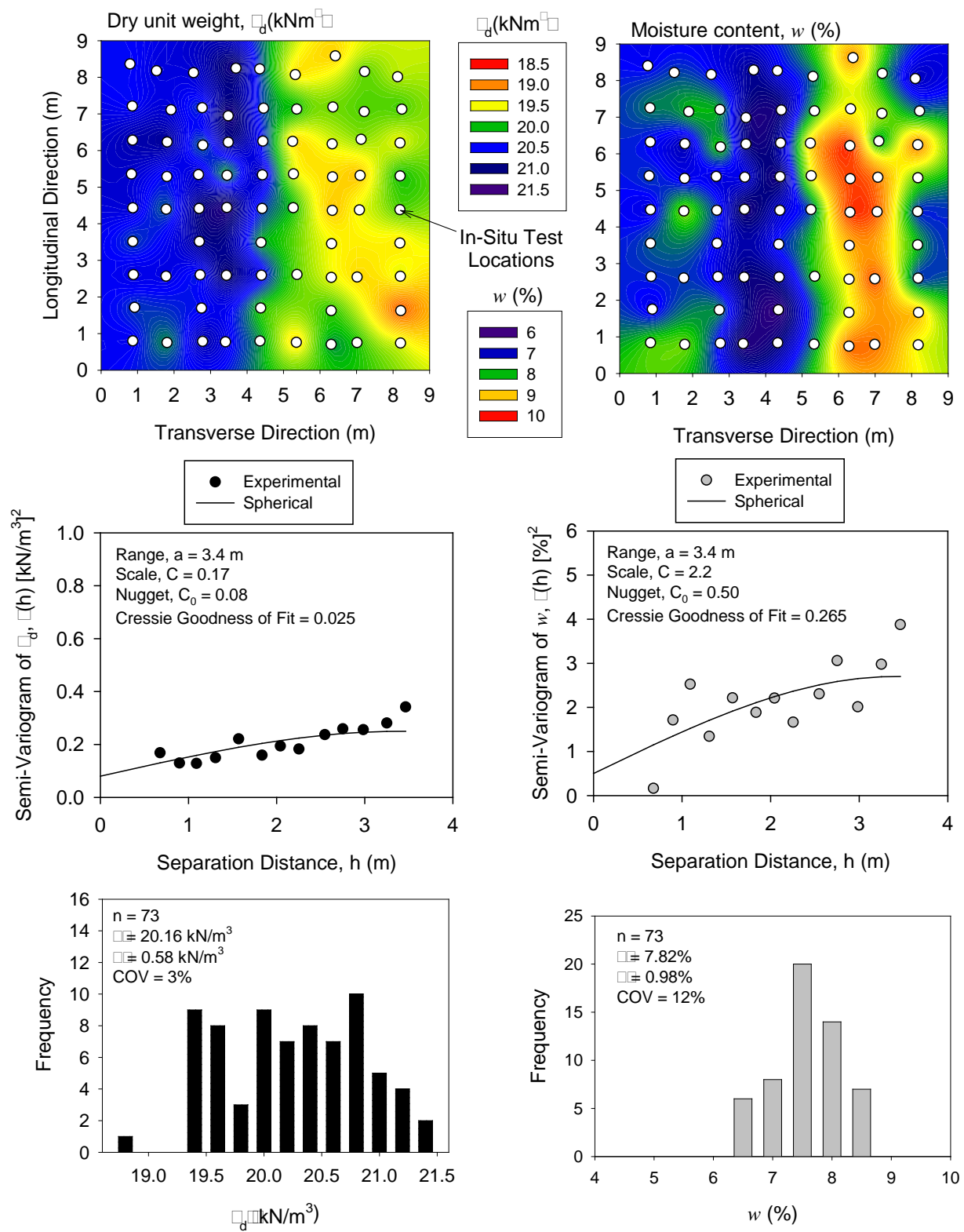


Figure 43. TS1: Kriged spatial contour maps (top) and semivariograms (middle) and histogram (bottom) plots of γ_d (left), and w (right) measurements

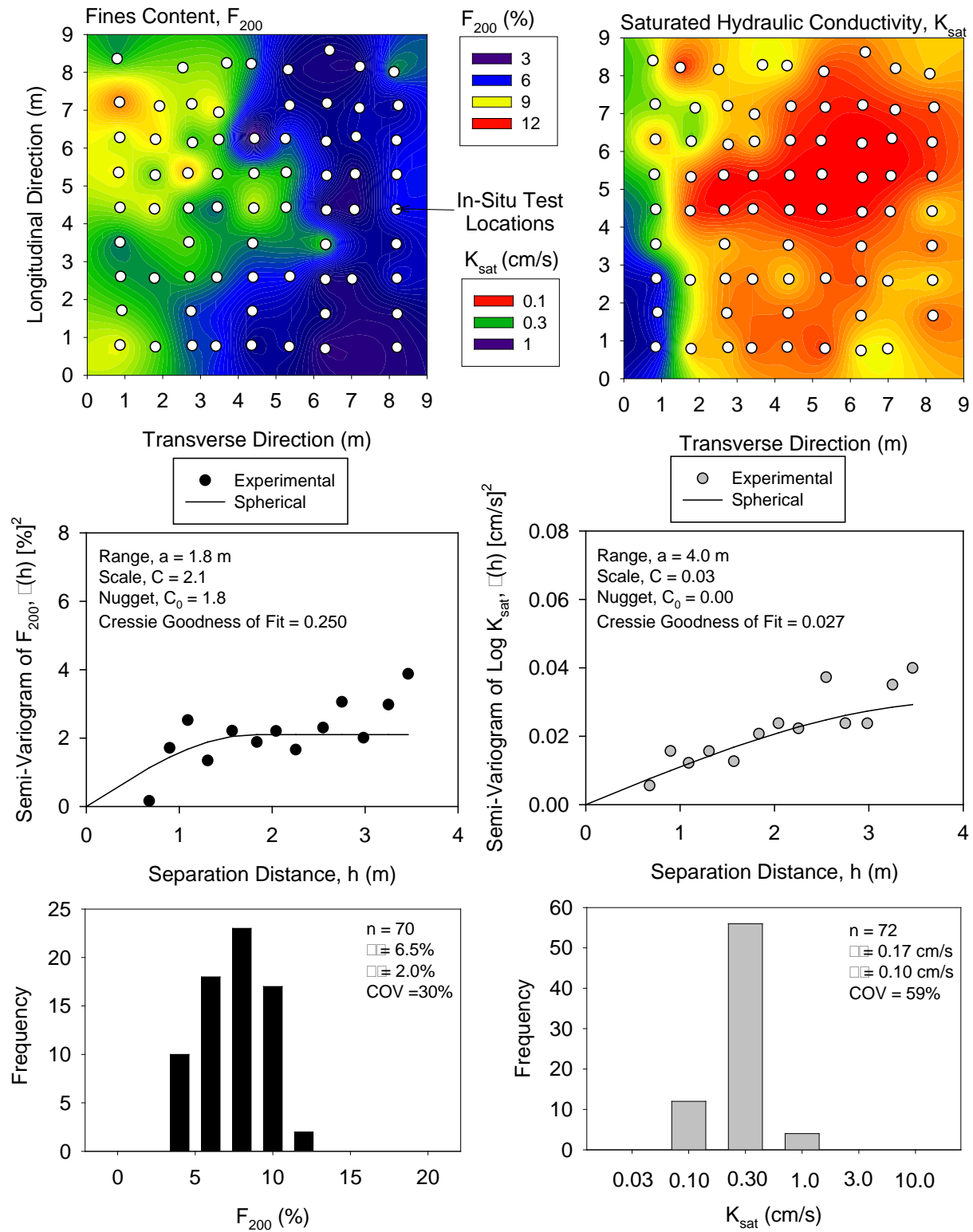


Figure 44. TS1: Kriged spatial contour map (top), semivariogram (middle), and histogram (bottom) plots of %fines (left) and K_{sat} (right) measurements

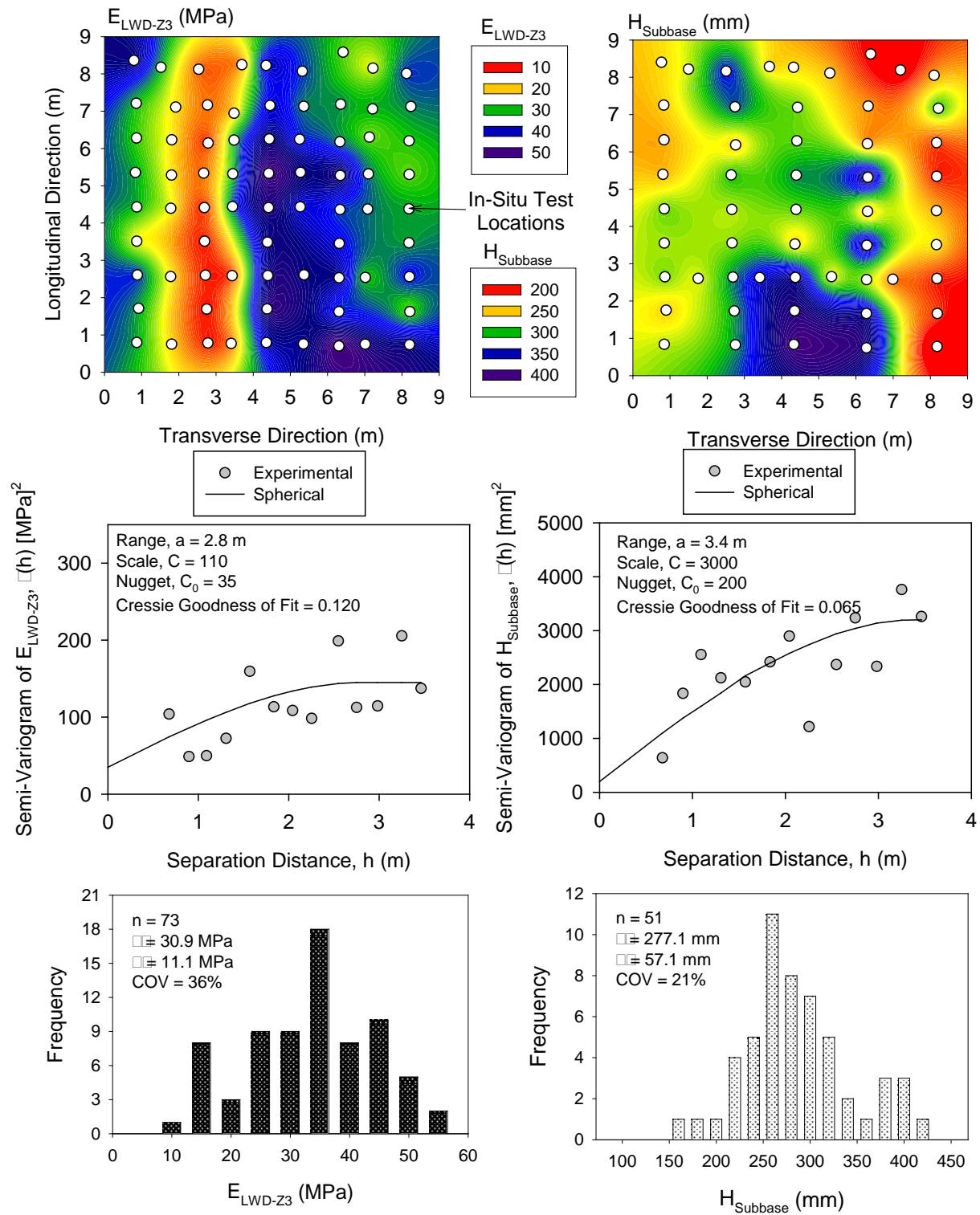


Figure 45. TS1: Kriged spatial contour map (top), semivariogram (middle), and histogram (bottom) plots of E_{LWD-Z3} (left) and $H_{Subbase}$ (right) measurements

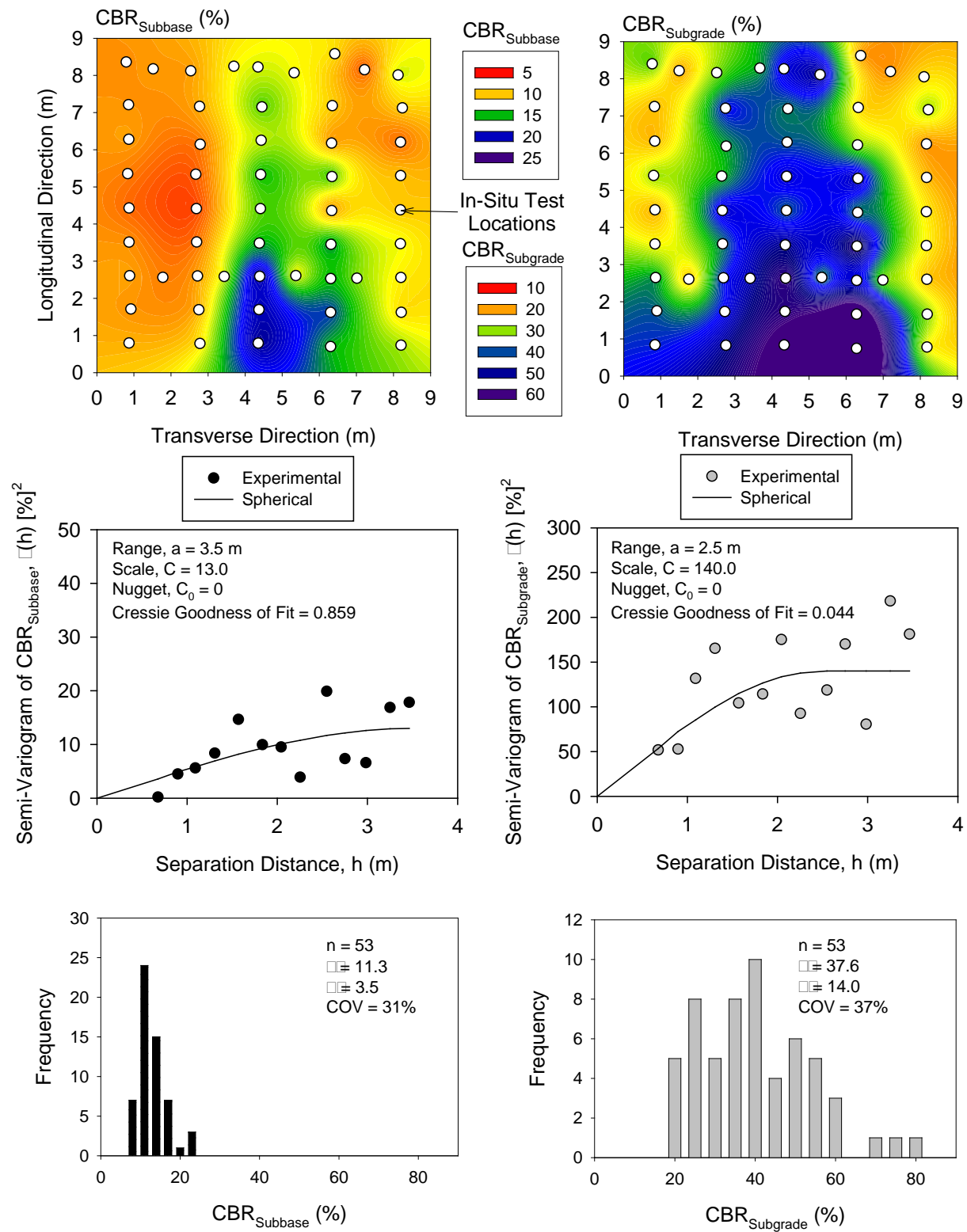


Figure 46. TS1: Kriged spatial contour map (top), semivariogram (middle), and histogram (bottom) plots of DCP-CBR_{Subbase} (left) and DCP-CBR_{Subgrade} (right) measurements

The spatial statistical parameters (i.e., scale (sill minus nugget), range, and nugget) are provided in the semivariogram plot of each figure. K_{sat} measurements showed a log-normal distribution, therefore, the data was transformed to $\log(K)$ to develop a semivariogram (Figure 44). A spherical semivariogram model showed best fit for all the measurements.

TS2: Cement Treated Base (CTB) Layer

Test Beds Construction and Experimental Testing

TS2 consisted of testing the CTB layer along I-96 EB right lane just west of West Grand River Avenue overpass between Sta. 296+00 and 299+00 (Figure 47).



Figure 47. TS2 CTB layer (looking east near Sta. 296+25)

NG, FWD, and GPT tests were conducted in this section. Tests were conducted in a grid pattern with five tests across the lane and at every 3 m along the alignment over a 90 m long section. NG and FWD tests were conducted at 119 test points and GPT tests were conducted at 62 test points. Pictures of GPT and FWD testing on CTB layer are shown in Figure 48 and Figure 49, respectively.



Figure 48. GPT on TS2 CTB layer



Figure 49. FWD testing on TS2 CTB layer

Figure 50 shows an image of test locations along TS2.



Figure 50. Test locations along I-96 EB right lane (looking east near Sta. 297+00)

Figure 51 shows close-up images of the CTB layer at different test locations showing evidence of segregation on the CTB layer.



Figure 51. TS2: CTB layer at selected test locations

In Situ Test Results and Data Analysis

Test measurements obtained from TS2 in a grid pattern with 119 tests over a plan area of about 90 m x 5.5 m provided a robust dataset to characterize the spatial characteristics of the measurements using geostatistical analysis. Kriged spatial contour maps, semivariograms, and histograms of each in situ point measurement are presented in Figure 52 through Figure 58.

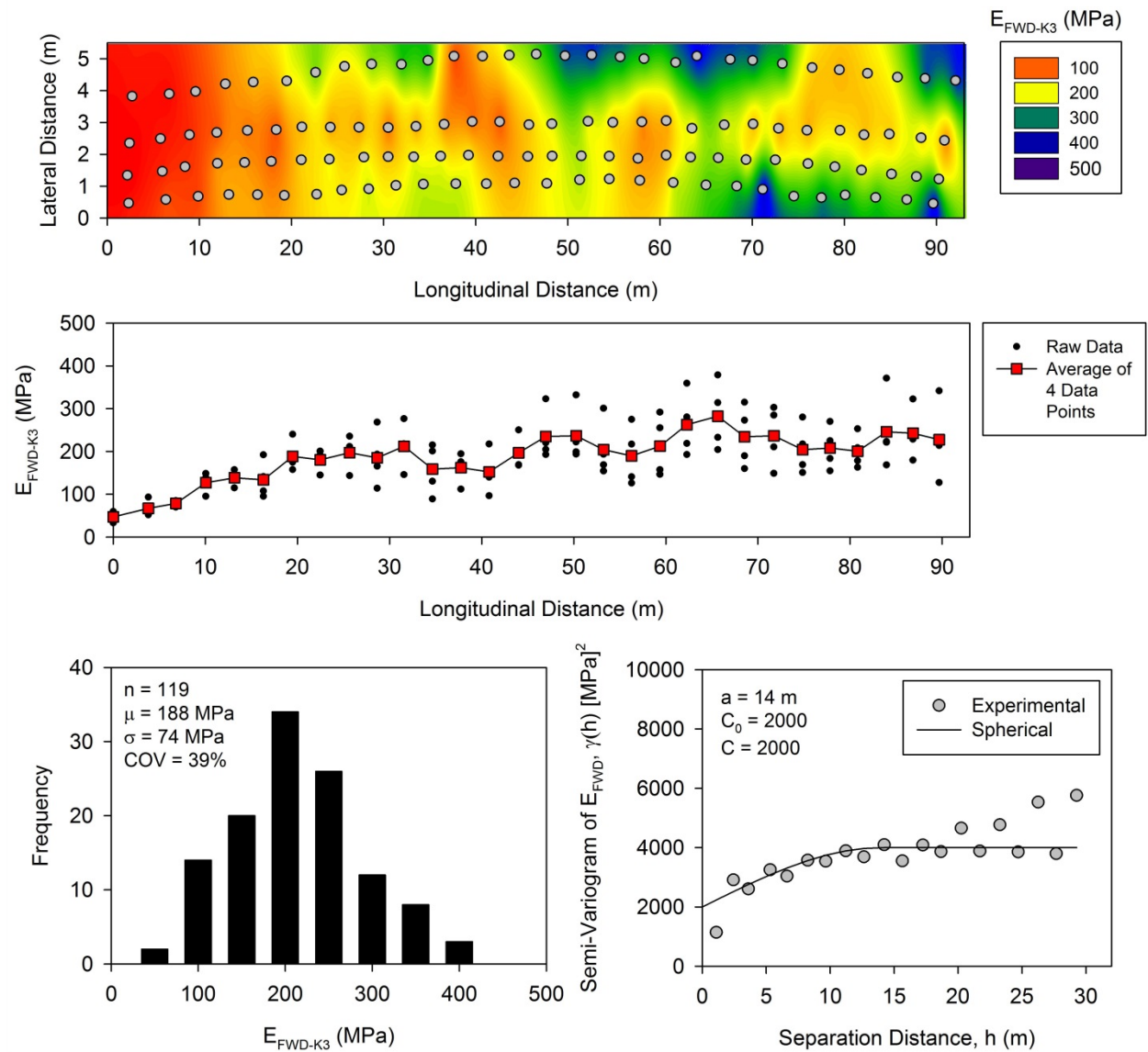


Figure 52. TS2 CTB: Kriged spatial contour map (top), measurements longitudinally along the test section (middle), histogram (bottom left), and semivariogram (bottom right) of E_{FWD-K3} measurements

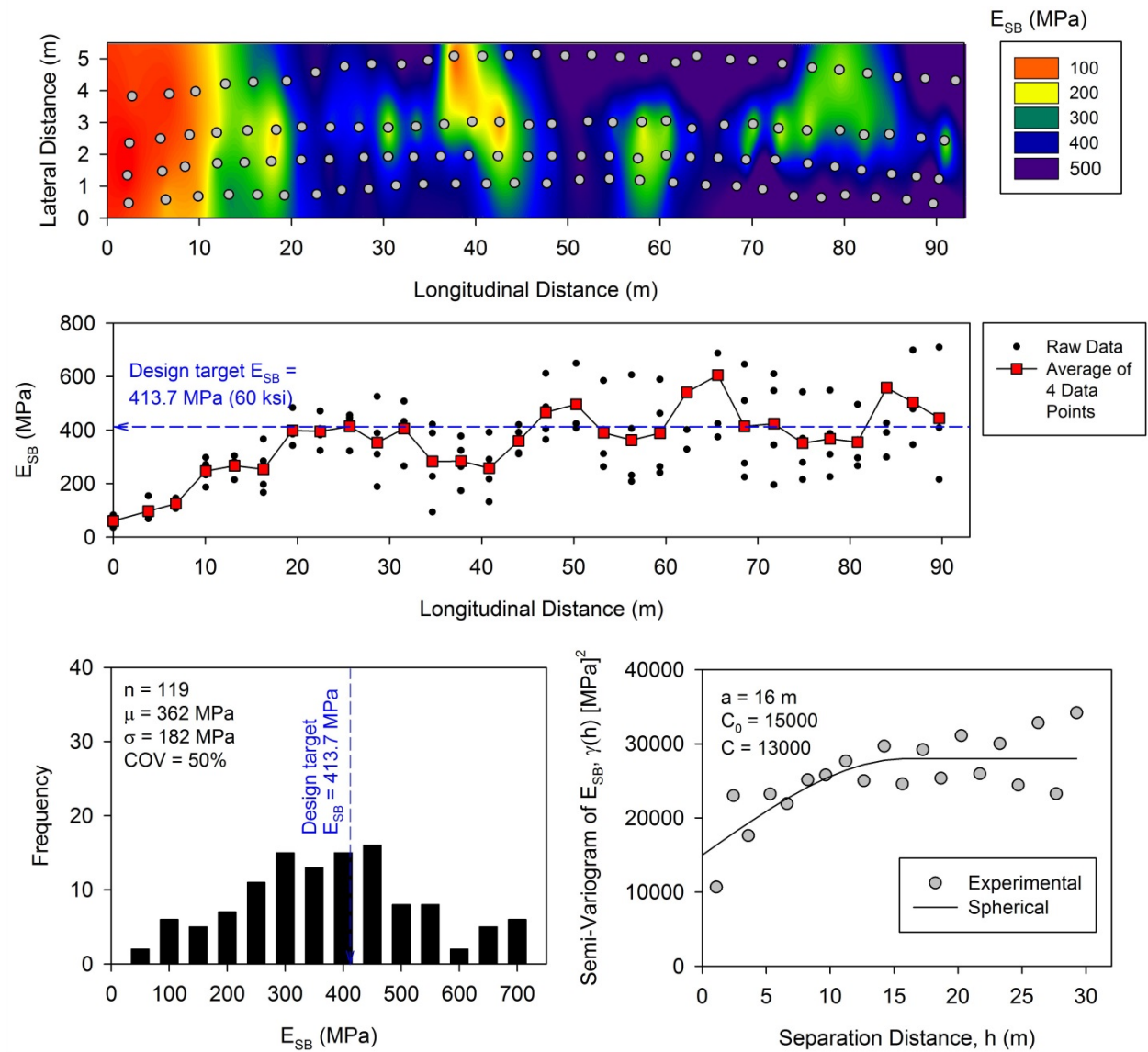


Figure 53. TS2 CTB: Kriged spatial contour map (top), measurements longitudinally along the test section (middle), histogram (bottom left), and semivariogram (bottom right) of E_{SB} measurements

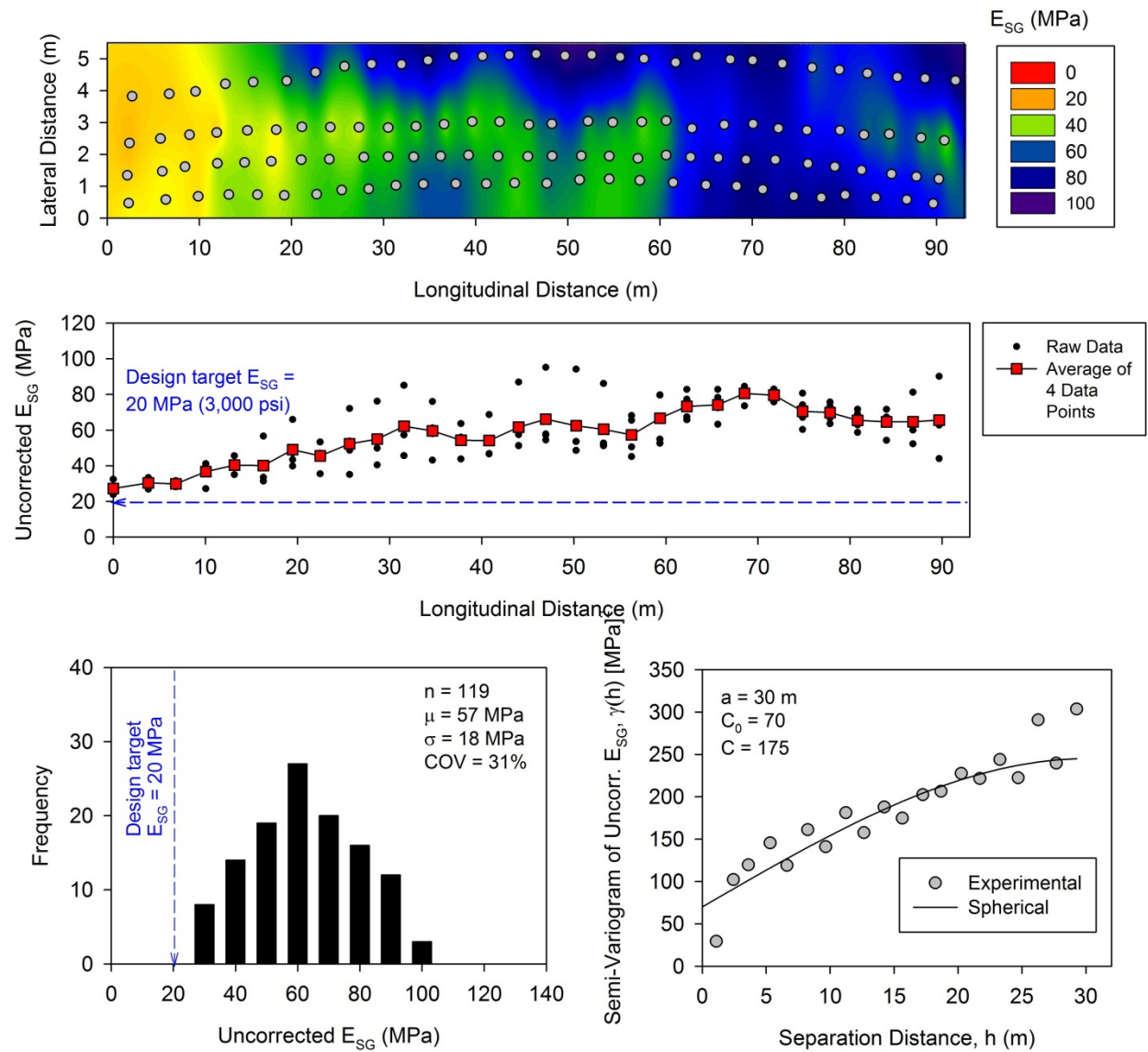


Figure 54. TS2 CTB: Kriged spatial contour map (top), measurements longitudinally along the test section (middle), histogram (bottom left), and semivariogram (bottom right) of uncorrected E_{SG} measurements

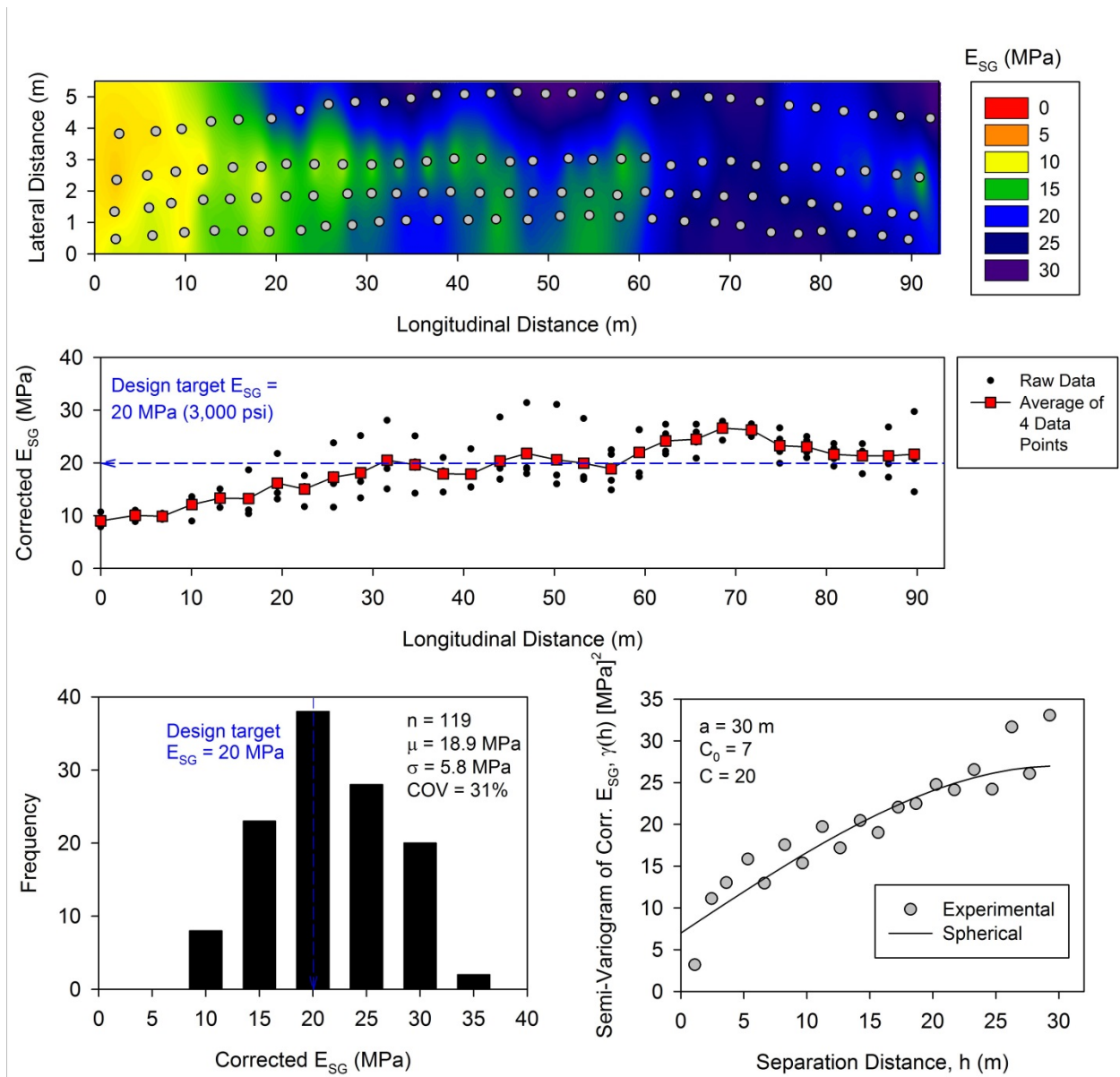


Figure 55. TS2 CTB: Kriged spatial contour map (top), measurements longitudinally along the test section (middle), histogram (bottom left), and semivariogram (bottom right) of Corrected E_{SG} ($0.33 \times$ Uncorrected E_{SG}) measurements

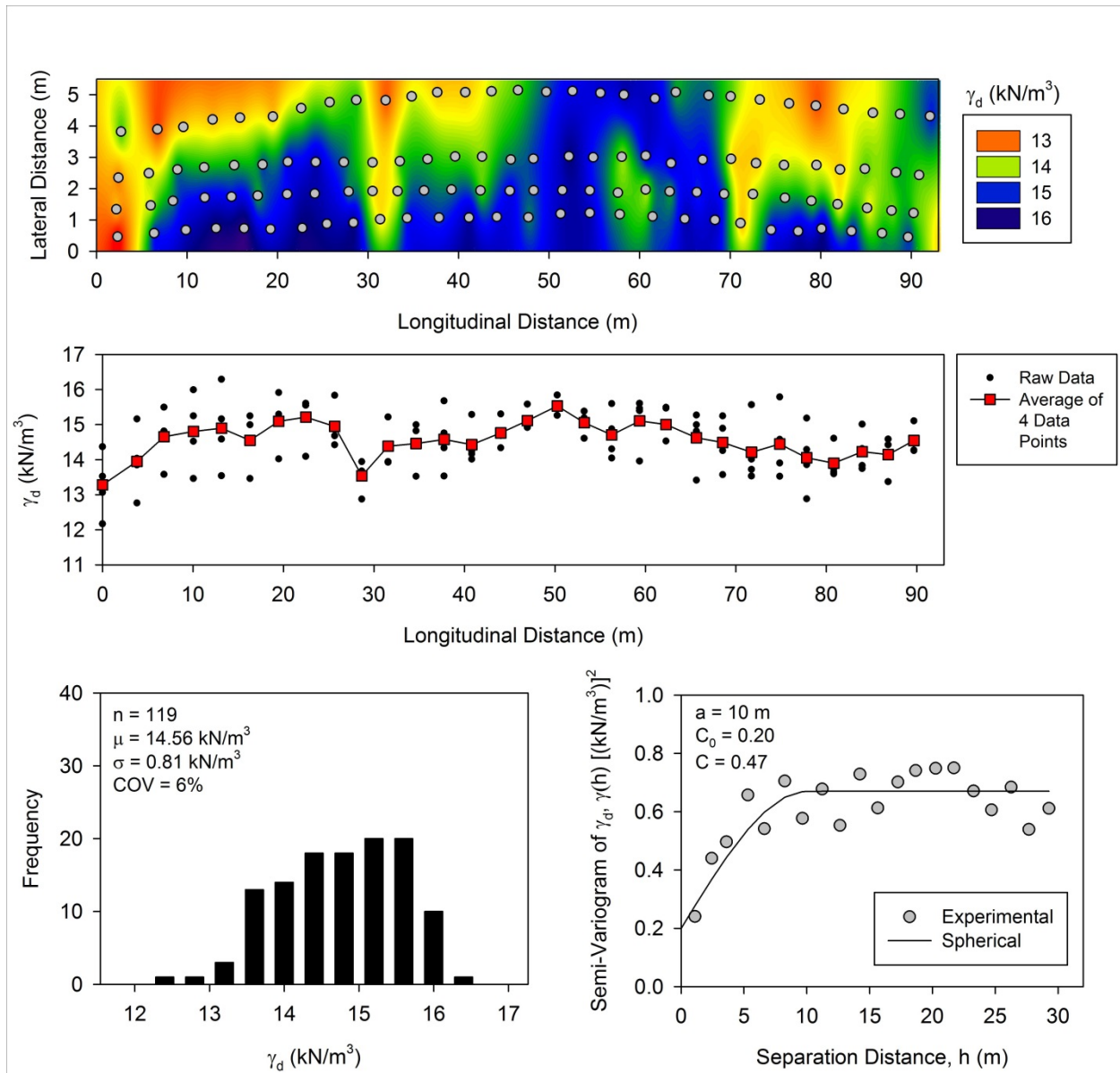


Figure 56. TS2 CTB: Kriged spatial contour map (top), measurements longitudinally along the test section (middle), histogram (bottom left), and semivariogram (bottom right) of γ_d

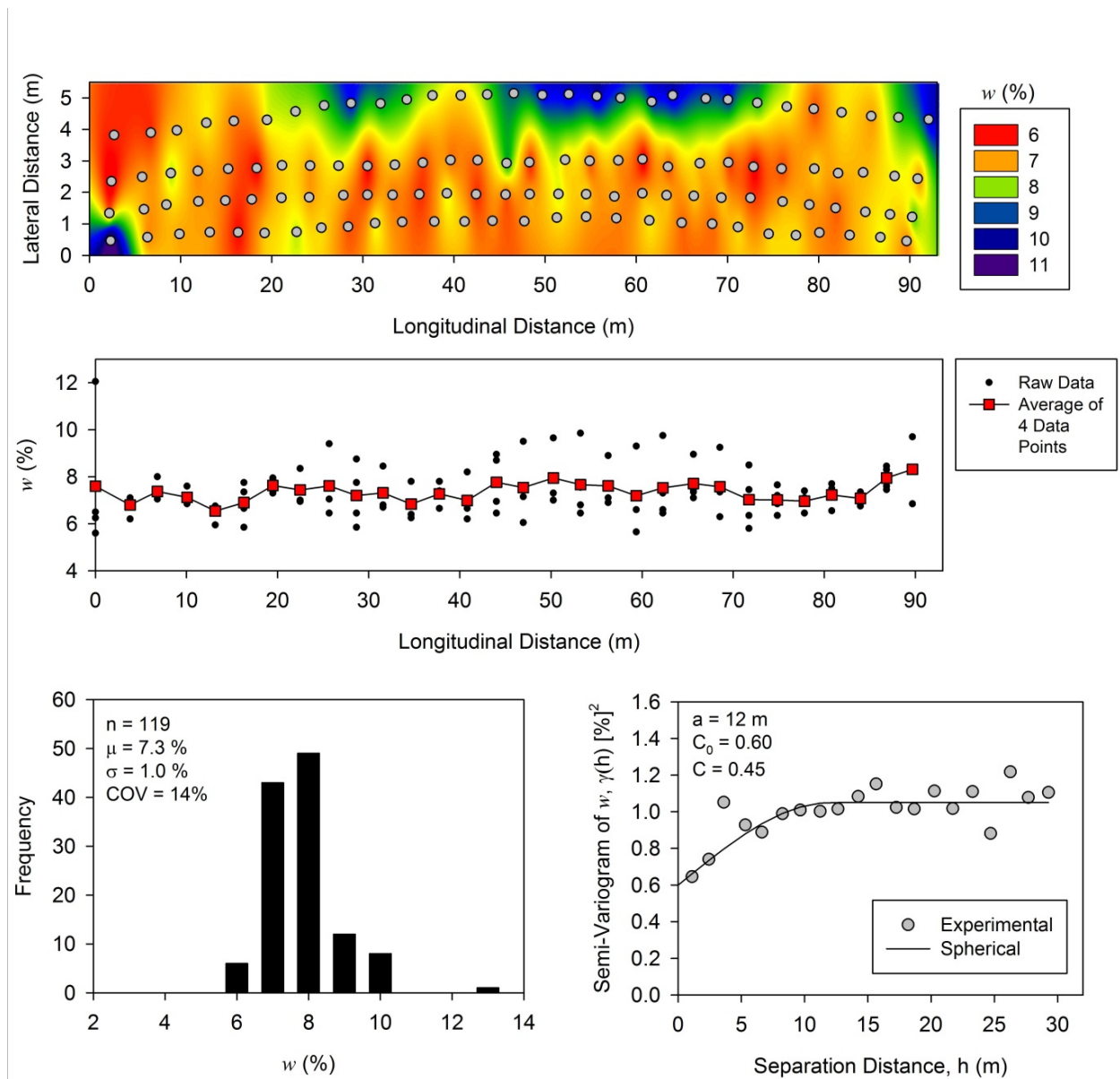


Figure 57. TS2 CTB: Kriged spatial contour map (top), measurements longitudinally along the test section (middle), histogram (bottom left), and semivariogram (bottom right) of w

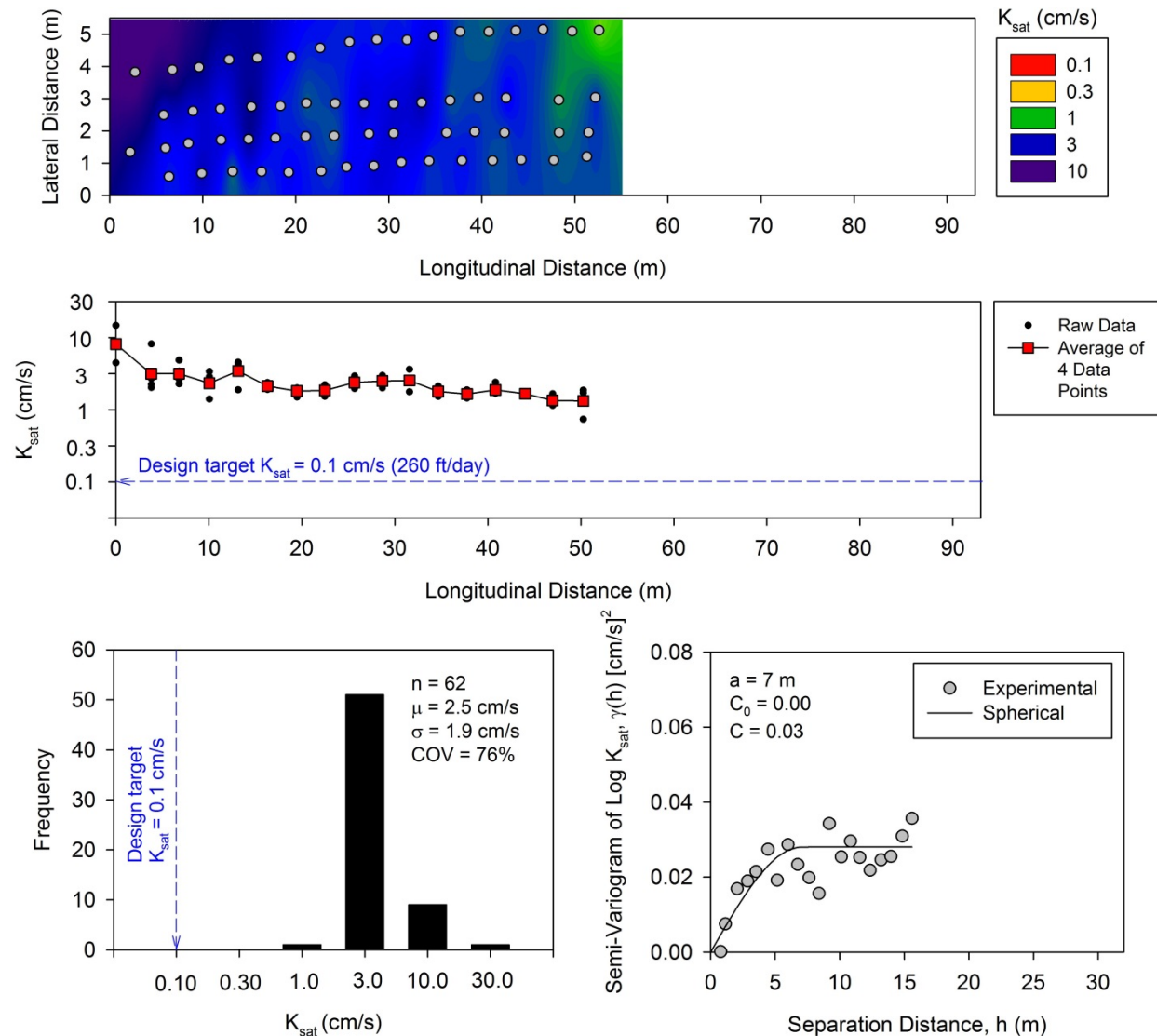


Figure 58. TS2 CTB: Kriged spatial contour map (top), measurements longitudinally along the test section (middle), histogram (bottom left), and semivariogram (bottom right) of K_{sat}

The spatial statistical parameters (i.e., scale (sill minus nugget), range, and nugget) are provided in the semivariogram plot of each figure. FWD and NG measurements showed good spatial structure without any data transformation. K_{sat} measurements showed a log-normal distribution, therefore, the data was transformed to $\log(K)$ to develop a semivariogram (Figure 58).

Similar to TS1 data, a spherical semivariogram model showed best fit for all the measurements. Also presented in these figures are raw measurements and averages of four measurements (transversely across the lane) along the 90 m long TS2.

Comparison of Design Values, In Situ Measurements, and Laboratory Measurements

Comparisons between the measured and design assumed values on the subgrade and subbase/CTB layers are shown in Figure 39, Figure 53, Figure 55, and Figure 58. A summary of the in situ measurement value statistics (i.e., μ , σ , and COV) is provided in Table 12.

Table 12. TS1, TS2 CBT, and TS3: In situ test results

Measurement	n	μ	σ	COV (%)
TS1 and TS3 Sand Subbase/Subgrade				
Subbase γ_d (kN/m ³)	99	20.16	0.57	3
Subbase w (%)	99	7.4	1.1	15
Subgrade γ_d (kN/m ³) [Shelby tube sample]	2	18.28	0.35	2
Subgrade w (%) [Shelby tube sample]	2	16.7	0.7	4
DCP-CBR _{Subbase} (%)	79	12.2	4.1	34
DCP-CBR _{Subgrade} (%)	79	39.2	17.2	44
K_{sat} (cm/s)	72	0.17	0.10	59
Fines (%)	70	6.5	2.0	30
E_{LWD-Z3} (MPa)	99	31.5	11.0	35
Estimated Subgrade M_r (MPa) [AASHTO 1993]	98	174.6	54.2	31
TS2 CTB				
γ_d (kN/m ³)	119	14.56	0.81	6
w (%)	119	7.3	1.0	14
E_{FWD-K3} (MPa)	119	187.9	74.0	39
E_{SB} (MPa)	119	361.5	182.1	50
Corrected E_{SG} (MPa)	119	18.9	5.8	31
K_{sat} (cm/s)	62	2.50	1.90	76

A summary of the average values of in situ and laboratory measured values in comparison with the design assumed values is provided in Table 13.

Table 13. Summary of design, in situ measured, and laboratory measured values

Design Parameter	Design Value	In Situ Measurements (Average)*	Laboratory Measurements (Average)
Subgrade M_r	20.7 MPa (3.0 ksi)	<i>DCP</i> : 174.6 MPa (25.3 ksi) ¹ <i>FWD</i> : 18.9 MPa (2.7 ksi) ²	31.1 MPa (4.5 ksi) ³
Subbase elastic modulus (E_{SB})	413.7 MPa (60 ksi)	<i>FWD</i> : 361.5 MPa (52.4 ksi) ⁴	— ⁵
Composite modulus of subgrade reaction (k_{comp})	135 kPa/mm (500 pci)	<i>E_{SB} and Lab M_r</i> : 133 kPa/mm (490 pci) ⁶ <i>E_{SB} and E_{SG}</i> : 100.9 kPa/mm (370pci) ⁷ <i>E_{SB} and M_r from DCP-CBR_{Subgrade}</i> : 327 kPa/mm (1200 pci) ⁸	— ⁵
C_d	1.05 (<i>Good</i>)	Excellent for the full range of K_{sat} measurements in situ on CTB layer	Excellent for the full range of lab K_{sat} values on CTB samples

These comparisons reveal some important aspects that are of high significance to this research project and are summarized below.

Base Layer Elastic Modulus (E_{SB})

The average E_{SB} back-calculated from FWD data was about 362 MPa (52 ksi). On average, it was about 0.87 times the design E_{SB} value, with about 81 out of the 119 measurements being lower than the design target value of 413.7 MPa (60 ksi). The in situ E_{SB} values showed a COV of about 50% with values ranging from 35.5 MPa (5.1 ksi) to 709.5 MPa (102.9 ksi).

Subgrade Resilient Modulus (M_r)

M_r was determined through a direct laboratory measurement on two Shelby tube samples from the subgrade on TS1. The results were summarized in Table 9 earlier in Chapter 4. Using the stress states recommended by NCHRP 1-28A (2002) for subgrade materials ($\sigma_3 = 14$ kPa (2 psi) and $\sigma_{cyclic} = 41$ kPa (6 psi)), an average $M_r = 31.1$ MPa (4.5 ksi) was determined from the laboratory tests, which exceeds the design target $M_r = 20.7$ MPa (3.0 ksi).

The in situ M_r values determined from FWD measurements (corrected E_{SG}) showed an average of about 18.9 MPa (2.7 ksi), which was slightly lower than the design M_r . The in situ M_r values determined from DCP-CBR_{Subgrade} measurements showed an average of about 174.6 MPa (25.3 psi), which was on average about 7.7 times higher than the design M_r .

Composite Modulus of Subgrade Reaction (k_{comp})

A lower bound $k_{comp} = 101$ kPa/mm (370 pci) value was estimated assuming average E_{SB} and average corrected E_{SG} . Similarly, an upper bound $k_{comp} = 327$ kPa/mm (1200 pci) value was estimated using average E_{SB} of 361.5 MPa (52.4 ksi) and $M_r = 138$ MPa (20 ksi). The estimated average subgrade M_r from DCP measurements was 175 MPa (25 ksi), as shown in Table 13, but the AASHTO nomograms are only shown up to subgrade $M_r = 138$ MPa (20 ksi). Therefore, $M_r = 138$ MPa (20ksi) was used for upper bound k_{comp} estimations. The lower bound and upper bound k_{comp} values were about 0.74 times and 2.4 times the design k_{comp} value.

Drainage Coefficient (C_d)

The C_d value assumed in design = 1.05, which represents that the quality of drainage is rated as Good. According to AASHTO (1993), if water is removed from the pavement system in one day, the quality of drainage is rated as Good. Based on the pavement geometry (i.e., cross slope, width of the pavement, thickness of the base layer), the measured K_{sat} values from the field, and an average effective porosity = 0.3 (based on porosity measurements on CTB samples), the time for a target 90% of drainage was calculated using a Visual Basic program developed by Vennapusa (2004) called Pavement Drainage Estimator (PDE version 1.0). The time for 90% drainage was estimated as 3.1 hours for $K_{sat} = 0.7$ cm/s (lower bound) to 0.2 hours for $K_{sat} = 14.7$ cm/s (upper bound). For an average $K_{sat} = 2.5$ cm/s, time for 90% drainage was estimated at about 0.9 hours. The laboratory permeability test measurements on CTB samples showed an average $K_{sat} = 1.1$ cm/s, which is within the range of the field measurements. Both laboratory and field measurements indicated that the quality of the drainage layer can be rated as Excellent according to AASHTO (1993), which exceeds the Good rating assumed in the design.

*Average of all measurements obtained from in situ testing; ¹Empirically estimated from DCP-CBR_{Subgrade} measurements using correlations from AASHTO (1993); ²Corrected E_{SG} values; ³Based on lab M_r on two Shelby tube samples; ⁴Back-calculated E_{SB} from FWD measurements; ⁵Not measured; ⁶Estimated using laboratory M_r on Shelby tube samples and E_{SB} from FWD; ⁷Estimated using corrected E_{SG} and E_{SB} from FWD; ⁸Estimated using $M_r = 138$ MPa (20 ksi) [upper limit in AASHTO 1993] based on DCP-CBR_{Subgrade} measurements and E_{SB}

CHAPTER 6. SUMMARY AND CONCLUSIONS

This report presents results and analysis of field and laboratory tests from a field study conducted on the I-96 interstate highway reconstruction project near Lansing, Michigan. The project involved removal of the existing PCC pavement and reconstruction of a new jointed PCC pavement with a cement treated base (CTB) layer and sand subbase with a geotextile separator at the CTB/subbase interface. Review of construction bid documents indicated that the construction cost of the foundation layers (i.e., CTB, subbase, and geotextile separator) was about 34% (\$1,996,113) of the total cost of the project (\$5,937,041).

Laboratory testing was conducted on foundation layer materials obtained from field to determine index properties, moisture-dry unit weight relationships from compaction tests, and resilient modulus values. M_r tests were conducted on homogenous samples and on layered composite samples (i.e., sand subbase over subgrade) to assess its influence on the M_r values. Hydraulic conductivity tests were conducted on sand subbase, untreated RPCC base, and CTB materials. Compressive strength and durability related to freeze-thaw and wet-dry cycles of the CTB material were also assessed as part of the laboratory testing. Some key findings from laboratory testing are as follows:

- Results indicated that the M_r of subbase material increased with increasing bulk stresses, as expected for granular materials. M_r of subgrade materials decreased with increasing deviator stress, as expected for non-granular materials. Increasing moisture content decreased M_r and increasing dry unit weight increased M_r for both subbase and subgrade materials.
- The comparison of composite and single samples revealed that the average M_r of composite samples is about 1.2 times lower than the average M_r of a single layer subbase sample at a similar density. The reason for this reduction in M_r in the composite sample is attributed to the weaker subgrade layer. This is an important finding and efforts are underway in this research study to further investigate the influence of composite soil layer configurations on M_r properties.
- Compressive strength test results from ISU and MDOT indicated that with the exception of one sample, all other samples met the specified seven-day compressive strength range (i.e., 1,380 to 4,830 kPa).
- All CTB samples tested for durability (i.e., 12 wet-dry and freeze-thaw cycles) showed percent mass loss less than the PCA (1971) recommended maximum allowable percent loss of 14%. One of the three CTB samples subjected to wet-dry cycles showed a percent loss of about 12%, which was greater than the Dept. of Army, the Navy, and the Air Force (1994) recommended maximum allowable loss = 11%.

Field testing was conducted on three test sections. Two test sections involved testing the sand subbase layer, and one test section involved testing the CTB layer. Field point testing was conducted by spacing the test measurements about 50 to 100 m apart to capture the variability along the road alignment. Testing was also conducted in a dense grid pattern (spaced at about 0.9 to 3.0 m) to capture spatial variability over a small area. Geostatistical semivariogram analysis was performed using the point test data from dense grid pattern testing to characterize and quantify spatial non-uniformity of the PCC surface and foundation layer properties.

Comparing the results from laboratory and in situ testing with design assumed values revealed the following:

- The average E_{SB} back-calculated from FWD data was about 362 MPa (52 ksi). On average, the E_{SB} was about 0.87 times the design E_{SB} value of 413.7 MPa (60 ksi), with 81 of the 119 measurements being lower than the design value. The in situ E_{SB} values showed a COV of about 50% with values ranging from 35.5 MPa (5.1 ksi) to 709.5 MPa (102.9 ksi).
- Subgrade M_r determined from laboratory measurements on Shelby tube samples at field-anticipated stress conditions showed an average of 31 MPa (4.5 ksi) and was about 1.5 times higher than the design M_r of 20.7 MPa (3.0 ksi). The in situ M_r values determined from FWD measurements showed an average of about 18.9 MPa (2.7 ksi), which was slightly lower than the design value. The M_r value determined from DCP-CBR_{Subgrade} was on average about 7.7 times higher than the design value.
- A lower bound $k_{comp} = 101$ kPa/mm (370 pci) value was estimated assuming average E_{SB} and average corrected E_{SG} determined from FWD measurements. Similarly, an upper bound $k_{comp} = 327$ kPa/mm (1200 pci) value was estimated using average E_{SB} from FWD measurements and $M_r = 138$ MPa (20 ksi) based on DCP measurements. The lower bound and upper bound k_{comp} values were about 0.74 times and 2.4 times the design k_{comp} value.
- The C_d value assumed in design = 1.05, which represents that the quality of drainage is rated as Good. According to AASHTO (1993), if water is removed from the pavement system in one day, the quality of the drainage layer is rated as Good. Both laboratory and field measurements indicated that the quality of the drainage layer can be rated as Excellent according to AASHTO (1993), which exceeds the Good rating assumed in the design.

REFERENCES

- AASHTO T-307. 1999. *Standard method of test for determining the resilient modulus of soils and aggregate materials*, American Association of State Highway and Transportation Officials AASHTO, Washington, DC.
- AASHTO. 1993. *AASHTO Design Guide for Design of Pavement Structures*. American Association of State Highway and Transportation Officials, Washington D.C.
- Andrei, D., M. W. Witzak, C. W. Schwartz, and J. Uzan. 2004. Harmonized resilient modulus test method for unbound pavement materials. *Transportation Research Record: Journal of the Transportation Research Board No. 1874*. Transportation Research Board, Washington, DC, 29-37.
- ASTM C39/C39M-12. 2012. *Standard test method of compressive strength of cylindrical concrete specimens*. ASTM International, West Conshohocken, PA.
- ASTM C136-06. 2010. *Standard test method for sieve analysis of fine and coarse aggregates*. ASTM International, West Conshohocken, PA.
- ASTM D422-63. 2010. *Standard test method for particle-size analysis of soils*. ASTM International, West Conshohocken, PA.
- ASTM D559-03. 2010. *Wetting and drying compacted soil-cement mixtures*. ASTM International, West Conshohocken, PA.
- ASTM D560-03. 2010. *Freezing and thawing compacted soil-cement mixtures*. ASTM International, West Conshohocken, PA.
- ASTM D698-07e1. 2010. *Standard test method for laboratory compaction characteristics of soil using standard effort 12,400 ft-lbf/ft³ 600 kN-m/m³*. ASTM International, West Conshohocken, PA.
- ASTM D1557-07. 2010. *Standard test method for laboratory compaction characteristics of soil using modified effort 56,000 ft-lbf/ft³ 2,700 kN-m/m³*. ASTM International, West Conshohocken, PA.
- ASTM D2487-10. 2010. *Standard test method for classification of soil for engineering purposes unified soil classification system*. ASTM International, West Conshohocken, PA.
- ASTM D3282-09. 2010. *Standard test method for classification of soils and soil-aggregate mixtures for highway construction purposes*. ASTM International, West Conshohocken, PA.
- ASTM D4253-00. 2010. *Standard test methods for maximum index density and unit weight of soils using a vibratory table*. ASTM International, West Conshohocken, PA.
- ASTM D4254-00. 2010. *Standard test methods for minimum index density and unit weight of soils and calculation of relative density*. ASTM International, West Conshohocken, PA.
- ASTM D4318-10. 2010. *Standard test methods for liquid limit, plastic limit, and plasticity index of soils*. ASTM International, West Conshohocken, PA.
- ASTM D6951-03. 2010. *Standard test method for use of the dynamic cone penetrometer in shallow pavement applications*. ASTM International, West Conshohocken, PA.
- ASTM D6938-10. *Standard test method for in-place density and water content of soil and soil-aggregate by nuclear methods shallow depth*. ASTM International, West Conshohocken, PA.
- Clark, I. and W. Harper. 2002. *Practical Geostatistics 2000*. 3rd reprint, Ecosse North America LLC, Columbus, OH.

- Dept. of the Army, the Air Force, and the Navy. 1004. *Soil Stabilization for Pavements*, Army TM 5-822-14/Air Force AFJMAN 32-1019, Washington, DC.
- Isaaks, E. H. and R. M. Srivastava. 1989. *An Introduction to Applied Geostatistics*. Oxford University Press, New York.
- MDOT 2005. *Pavement Design and Selection Manual*. Prepared by Pavement Management Unit and Construction & Technology Division, Michigan Department of Transportation. www.michigan.gov/documents/mdot/MDOT_Pavement_Design_and_Selection_Manual_257723_7.pdf. Accessed, February 2011.
- NCHRP 1-28A. 2002. *Recommended standard method for routine resilient modulus testing of unbound granular base/subgrade materials and subgrade soils–NCHRP protocol 1-28A*, National Cooperative Highway Research Program.
- Mohammad, L. N., A. Herath, R. Gudishala, M. Y. Abu-Farsakh, and K. Alshibli. 2008. *Development of Models to Estimate the Subgrade and Subbase Layers' Resilient Modulus from In Situ Devices Test Results for Construction Control*. Final report submitted to Louisiana Department of Transportation and Development, Louisiana Transportation Research Center, Baton Rouge, LA.
- Powell, W. D., J. F. Potter, H. C. Mayhew, and M. E. Nunn. 1984. *The structural design of bituminous roads*. Report LR1132. Transport and Road Research Laboratory, UK.
- PCA. 1971. *Soil-Cement Laboratory Handbook*, Portland Cement Association, Skokie, IL.
- Terzaghi, K., and R. B. Peck. 1967. *Soil mechanics in engineering practice*, 2nd Ed., John Wiley & Sons, Inc., New York.
- van Til, C. J., B. A. McCullough, Vallergera, B. A., and R. G. Hicks. 1972. *Evaluation of AASHTO Interim Guides for Design of Pavement Structures*. NCHRP 128, Highway Research Board.
- Vennapusa, P. 2004. *Determination of the Optimum Base Characteristics for Pavements*. Master's Thesis, Department of Civil Construction and Environmental Engineering, Iowa State University, Ames, IA.
- Vennapusa, P., and D. J. White. 2009. Comparison of light weight deflectometer measurements for pavement foundation materials. *Geotechnical Testing Journal*, ASTM, 323, 239-251.
- Vennapusa, P., D. J. White, and M. Morris. 2010. Geostatistical analysis of spatial referenced roller-integrated compaction measurements. *Journal of Geotechnical and Geoenvironmental Engineering*, ASCE, 1366, 813–822
- White, D. J., P. Vennapusa, and C. T. Jähren. 2004. *Determination of the Optimum Base Characteristics for Pavements*. Center for Transportation Research and Education, Iowa State University, Ames, IA.
- White, D. J., E. Jaselskis, V. Schaefer, and T. Cackler. 2005. Real-time compaction monitoring in cohesive soils from machine response. *Transportation Research Record: Journal of the Transportation Research Board No. 1936*, Washington DC, 173–180.
- White, D. J., P. Vennapusa, M. T. Suleiman, and C. T. Jähren. 2007. An in-situ device for rapid determination of permeability for granular bases. *Geotechnical Testing Journal*, 304, 282–291.
- White, D. J., P. Vennapusa, D. Eichner, H. Gieselman, L. Zhao, and C. T. Jähren. 2010. *Rapid, self-contained in-situ permeameter for field QA/QC of pavement base/subbase materials*. NCHRP 1-130 IDEA Project, Transportation Research Board, Washington, DC.

- Witczak, M. W. and J. Uzan. 1988. *The universal airport design system—Report I of IV: Granular material characterization*. Department of Civil Engineering, University of Maryland, College Park, MD.
- Zapata and W. N. Houston 2008. *Calibration and Validation of the Enhanced Integrated Climatic Model for Pavement Design*. NCHRP Report 602, Transportation Research Board, Washington, DC.
- Zorn, G. 2003. *Operating Manual: Light Drop-weight Tester ZFG2000*, Zorn Stendal, Germany.

**APPENDIX A: MDOT OFFICE MEMORANDUM (MAY 4, 2009) – PAVEMENT
SELECTION**

EOC Approved 7/2/2009



OFFICE MEMORANDUM

DATE: May 4, 2009

TO: Brenda J. O'Brien
Engineer of Construction and Technology

FROM: Benjamin F. Krom
Pavement Selection Engineer

SUBJECT: Pavement Selection for CS 19022, 23152 & 23042, JN 45639
Reconstruct Jointed Plain Concrete Pavement:
I-96: From W of Wacousta Road to S of M-43
CS 19022: BMP 7.032 to MP 10.179
CS 23152: MP 0.000 to EMP 2.658
Reconstruct Hot Mix Asphalt Pavement:
M-43: From E of Marketplace Boulevard to E of Canal Road
CS 23042: BMP 3.347 to EMP 4.169

I am requesting that the referenced project be placed on the agenda for the next Engineering Operations Committee (EOC) meeting. The subject project is a proposed American Recovery and Reinvestment Act of 2009 project. This is expected to be a design-build project, with a September 2009 letting.

The reconstruction alternatives being considered are a Hot Mix Asphalt Pavement (HMA Alt #1) and a Jointed Plain Concrete Pavement (JPCP Alt #2). The pavement designs being considered are as follows:

I-96 Alternative #1: Reconstruct with Hot Mix Asphalt Pavement

2"	Gap-Graded Superpave, Top Course (mainline)
2.5"	HMA, 4E30, Leveling Course (mainline)
6.25"	HMA, 3E30, Base Course (mainline)
2"	HMA, 5E3, Top Course (shoulders)
2.5"	HMA, 4E3, Leveling Course (shoulders)
6.25"	HMA, 3E3, Base Course (shoulders)
5"	Stabilized Open-Graded Drainage Course
	Geotextile Separator
19"	Sand Subbase
6" dia.	Underdrain System
34.75"	Total Section Thickness

Present Value Initial Construction Cost	\$1,984,358/directional mile
Present Value Initial User Cost	\$397,854/directional mile
Present Value Maintenance Cost	\$176,481/directional mile

Equivalent Uniform Annual Cost (EUAC)\$138,233/directional mile

I-96 Alternative #2: Reconstruct with Jointed Plain Concrete Pavement

11.5"	Non-Reinforced Concrete Pavement, P1 Modified, w/ 14' joint spacing
5"	Stabilized Open-Graded Drainage Course
	Geotextile Separator
	Existing Sand Subbase (65% of project)
11"	New Sand Subbase (35% of project)
6" dia.	Open-Graded Underdrain System
16.5"	Total Thickness

Present Value Initial Construction Cost	\$1,167,170/directional mile
Present Value Initial User Cost	\$266,047/directional mile
Present Value Maintenance Cost	\$106,597/directional mile

Equivalent Uniform Annual Cost (EUAC)\$83,188/directional mile

M-43 Alternative #1: Reconstruct with Hot Mix Asphalt Pavement

1.5"	HMA, 5E3, Top Course (mainline)
2"	HMA, 4E3, Leveling Course (mainline)
3.5"	HMA, 3E3, Base Course (mainline)
6"	Aggregate Base
18"	Sand Subbase
6" dia.	Underdrain System
31.0"	Total Section Thickness

Present Value Initial Construction Cost	\$1,060,645/mile
Present Value Initial User Cost	\$279,332/mile
Present Value Maintenance Cost	\$234,046/mile

Equivalent Uniform Annual Cost (EUAC)\$77,223/mile

M-43 Alternative #2:Reconstruct with Jointed Plain Concrete Pavement

8.5"	Non-Reinforced Concrete Pavement, P1 Modified, w/ 12' joint spacing
6"	Open Graded Drainage Course
	Geotextile Separator
10"	Sand Subbase
6" dia.	Open-Graded Underdrain System
24.5"	Total Thickness

Present Value Initial Construction Cost	\$1,196,746/mile
Present Value Initial User Cost	\$465,000/mile
Present Value Maintenance Cost	\$270,189/mile

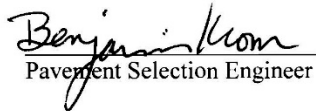
Equivalent Uniform Annual Cost (EUAC)\$94,782/mile

The pavement designs for both alternatives are based on the 1993 AASHTO "Guide for Design of Pavement Structures" and use the AASHTO pavement software DARWin Version 3.1, 2004. The Equivalent Uniform Annual Cost calculation is based on the revised pavement selection process as approved by the EOC on June 3, 1999.

The estimated construction costs are based on historical averages from similar projects. User costs are calculated using MDOT's Construction Congestion Cost model, which was developed by the University of Michigan.

Conclusion

Pavement selection was determined using the procedures outlined in the MDOT Pavement Design and Selection Manual. Department policy requires that the pavement alternative with the lowest EUAC, be selected. For I-96, **Alternative #2: Reconstruct with Jointed Plain Concrete Pavement**, and for M-43, **Alternative #1: Reconstruct with Hot Mix Asphalt Pavement**, were selected. Final pavement selection requires approval by the Engineering Operations Committee.


Pavement Selection Engineer

cc: C. Bleech
K. Kennedy
P. Schafer
M. Eacker
R. Leppala
M. Melchiori
L. Doyle
R. VanDeventer

PROJECT SUMMARY

Project Location

This project includes 5.805 miles of I-96 reconstruction from west of Wacousta Road to south of M-43, and 0.822 miles of M-43 reconstruction from east of Marketplace Boulevard to east of Canal Road. The existing section for I-96 is a 4 to 6 lane divided freeway consisting of 12' paved lanes, a 9' paved outside shoulder and a 4'-9' paved inside shoulder in each direction. The proposed section maintains the 12' lanes, but widens the shoulders to 12'. M-43 currently consists of 5-12' lanes, with curb & gutter. The proposed section matches the existing.

Existing Pavement and Condition Data

The existing typical cross section for I-96 consists of, on average, 9" of jointed reinforced concrete pavement, 4" of select subbase and 10" of sand subbase. The existing subbase meets Class IIA specifications and for Alt #2 will be left in place for 65% of the project. 35% will need to be removed and replaced due to grade changes. For Alt #1, the existing subbase thickness is insufficient, and thus requires complete removal and replacement.

The existing typical cross section for M-43 consists of, on average, 3" of HMA over 9" of jointed reinforced concrete pavement, 3" of select subbase and 9" of sand subbase. New sand subbase will be placed for both alternatives.

Average Ride Quality (2007)

RQI \geq 70 Poor

74 EB I-96

71 WB I-96

60 M-43

Average Remaining Service Life (2008)

RSL $<$ 3 Poor

3 EB I-96

3 WB I-96

8 M-43

I-96 Traffic

57,300 ADT (2011 two-way)

9,740 Commercial ADT (2011 two-way)

Growth Rate: 1.25% compound

38.0 million Rigid Design ESAL's-20 yrs

24.36 million Flexible Design ESAL's-20 yrs

Directional Distribution Factor – 50%

M-43 Traffic

36,500 ADT (2011 two-way)

730 CADT (2011 two-way)

Growth Rate: 1.25% compound

2.32 million Rigid Design ESAL's-20 yrs

1.63 million Flexible Design ESAL's-20 yrs

Directional Distribution Factor – 50%

Different 18 Kip axle equivalency factors (ESAL's) are used for the designs of Flexible and Rigid pavements because each pavement type experiences a different loss of serviceability from the passage of identical vehicles. Work done at the AASHO test road resulted in the creation of pavement design formulas that account for these differences. Proper use of these formulas requires that different ESAL's be used for Flexible and Rigid pavements, although the anticipated traffic is identical. The Engineering Operations Committee has approved the use of different ESAL factors for Flexible and Rigid pavement designs.

Hourly volumes for 24 hour periods, shown in the appendix, are based on distributions appearing in Table 3.2 of FHWA publication "Life Cycle Cost Analysis in Pavement Design". User costs for succeeding maintenance activities are based on the values shown in Table A, page 60, of the appendix.

Soils

The Regional Soils Specialist recommends a subgrade soil resilient modulus of 3,000 psi be used for design purposes. This is based on an analysis of the soil borings. For more information, refer to page 61 of the appendix.

Construction Staging and Maintaining Traffic

For information refer to the maintaining traffic memo in the appendix.

APPENDIX B: SPECIAL PROVISION 03CT303(A140) – OPEN GRADED DRAINAGE COURSE, MODIFIED (PORTLAND CEMENT-TREATED PERMEABLE BASE USING CRUSHED CONCRETE)

Reviewed for Contract Documents	
Reviewed by:	Reviewed by:
Date: 06/01/2011	Date: 06/01/2011
Signature: [Signature]	Signature: [Signature]
Accepted:	Accepted:
Date: 06/01/2011	Date: 06/01/2011
Signature: [Signature]	Signature: [Signature]

03CT303(A140)

MICHIGAN
DEPARTMENT OF TRANSPORTATION

SPECIAL PROVISION
FOR
**OPEN-GRADED DRAINAGE COURSE, MODIFIED (PORTLAND CEMENT-TREATED
PERMEABLE BASE USING CRUSHED CONCRETE)**

C&T:JFS

1 of 4

C&T:APPR:ARB:CJB:06-12-09

a. Description. Furnish, place, and compact a Portland cement-treated permeable base (CTPB) for mainline pavements, shoulders and ramps using crushed Portland cement concrete pavement from this project on a prepared pavement subbase according to the contract documents, or as directed by the Engineer.

b. Materials. Provide open-graded drainage course (OGDC) aggregate for CTPB meeting the requirements in Table 1.

TABLE 1 OPEN-GRADED DRAINAGE COURSE FOR CTPB

Gradation Requirements						
Sieve Analysis (a) (MTM 109)						Loss by Washing (MTM 108) % Passing No. 200 (a)
Sieve Size	1-1/2 inch	1 inch	1/2 inch	#4	#8	
Percent Passing	100	90 - 100	25 - 60	0 - 20	0 - 8	5.0 max
Physical Requirements						
Crushed Material, % Min (MTM 110,117)					90 (b)	
Loss, % Max, Los Angeles Abrasion (MTM 102)					45	
a. Based on dry weights.						
b. The percentage of crushed material will be determined on that portion of the sample retained on all sieves down to and including the 3/8 inch.						

Obtain OGDC aggregate only from crushed Portland cement concrete pavement from this project. If there is not a sufficient pavement quantity to complete the project, another aggregate source that meets the grading and physical requirements of this special provision may be used to produce OGDC, as approved by the Engineer.

All surplus materials resulting from the salvaging and crushing of the concrete will become the property of the Contractor and will be removed from the project. Such materials include, but are not limited to bituminous overlays, bituminous patches, steel reinforcement, joint materials, and the material from the scalping operation. Provide a written proposal to the Engineer for consideration to use the excess crushed concrete aggregates at other locations within the project limits. Approval will be based on its ability to meet the requirements for the intended use in accordance with the contract documents. Do not place excess crushed concrete aggregate within the top 3 feet below the proposed pavement surface. Blend excess surplus crushed concrete with comparable virgin material at a 50/50 proportion by volume prior to its use at other locations within the project limits.

Revised for Construction Amendments	
Reviewed by Engineer:	<i>[Signature]</i>
Date:	03/02/2018
Approved:	<i>[Signature]</i>
Date:	03/02/2018

C&T:JFS

2 of 4

03CT303(A140)
06-12-09

1. Mixture Requirements. Proportion and mix the CTPB using a dedicated batch plant or pugmill that will accurately batch and thoroughly mix CTPB, as approved by the Engineer.

Mixture proportions, lbs/yd³:

Aggregate (Table 1):	27 x (dry rodded unit weight of aggregate, lb/cu.ft.)
Cement (ASTM C150, Type I):	250
Water: *	100 - 120

* The water content is based on the assessment of the workability of the mixture. Net water includes any surface moisture on the OGDC aggregate (total moisture less absorbed moisture) plus water added at the mixer.

Adjust the amount of water depending on the characteristics of the aggregate resulting from the crushing operation, to provide a homogeneous mixture that will be stable and drainable after hardening in place.

Daily yield tests will be conducted on the CTPB mixture by belt samples or other means to verify mixture proportions, as determined by the Engineer.

Compressive Strength Requirements, psi:

Class Design Strength (CDS):	200
7-Day:	200 - 700
Construction Traffic, min:	200

c. **Construction.** Prepare the subbase according to section 301 of the Standard Specifications for Construction and the contract documents prior to placing the CTPB. Delivery vehicles will not be permitted on the prepared sand subbase.

Construct a control strip with a minimum length of 600 feet at the start of the CTPB placement operation to establish a construction method for placement and compaction that does not cause degradation or segregation that is detrimental to base stability and drainability. Do not place CTPB beyond the limits of the control strip until an acceptable placement method is determined and verified.

Place the CTPB mixture in a single layer according to subsection 602.04 of the Standard Specifications for Construction using methods as demonstrated by the control strip. Do not use internal vibration. Protect the underdrain system from damage at all times.

Finish the surface of the CTPB smooth, uniform in appearance, and free of depressions, ruts, and ridges. Surface tolerance will be as specified in subsection 303.03.B of the Standard Specifications for Construction. Compact and trim CTPB to final grade within one-half hour after spreading. Do not cold mill the CTPB for correct surface variations and elevation. Fabricate all work progress test specimens.

Protect the fresh CTPB from being damaged by rain. Include specific provisions for curing, and protecting the CTPB during hot and cold weather in the concrete quality control plan. Do not place CTPB when the ambient temperature is below 45 degrees F. Membrane curing compound is not required.

Attain approval from the Engineer for intermittent access onto the CTPB surface to facilitate delivery

Reviewed by Construction Assistance	
Recommended for Approval	_____
Date: 06-12-09	Jeffrey M. Boush, PE
Accepted	_____
Date: 06-12-09	Michael V. Ashworth, PE

03CT303(A140)
06-12-09

C&T:JFS

3 of 4

of concrete during pavement construction. Include provisions to protect the CTPB surface against contamination with dirt, fines, or debris. Repair or remove and replace (at no additional expense to the Department) any damage induced by construction equipment, including surface deformations and contamination with dirt, fines, or debris. Do not use CTPB for a construction haul road.

When construction resumes after seasonal shutdown, the Engineer will inspect for approval all CTPB that was completed and not covered with concrete pavement during seasonal shutdown. Repair or remove and replace (at no additional expense to the Department) any damaged CTPB induced by the seasonal shutdown.

d. Testing and Acceptance. The Engineer will identify, in writing, the preferred sample location from those listed in subsection 303.03.E of the Standard Specifications for Construction, at the Pre-Construction meeting and at the Pre-Bid meeting, if applicable. However, the Engineer may designate a new preferred sample location should circumstances change during construction. All tests of materials will be performed according to methods specified in the contract documents. Mechanical methods may be used to assist in obtaining samples from the grade when layer thicknesses are greater than 4 inches. All sampling and testing must be performed by a Michigan Certified Aggregate Technician and Certified Concrete Technician, where applicable.

The Department will sample and test the OGDC aggregate prior to cement-treatment. The OGDC must conform to the physical and grading requirements prior to being incorporated into the CTPB mixture. The cement content of the CTPB mixture will be verified by Engineer after mixing is completed.

Repair, or remove and replace, as directed by the Engineer, (at no additional expense to the Department), areas of excessive random cracking in the in-situ CTPB attributed to proportioning of the mixture beyond a batching or metering tolerance of +/- 5 percent of the specified mixture proportions, as documented by the daily yield tests.

The Engineer will fabricate a minimum of three 6 x 12 inch cylinders during each day of production for each 7-day compressive strength acceptance test. Curing of the specimens will be according to ASTM C 31.

The Contractor is solely responsible for degradation and segregation during handling, placement and compaction of the OGDC aggregate and CTPB mixture.

Each day, the Engineer will monitor and document the construction method established during control strip placement is being followed.

e. Measurement and Payment. The completed work, as described, will be measured and paid for at the contract unit price using the following contract item (pay item):

Contract Item (Pay Item)	Pay Unit
Open-Graded Dr Cse, 5 inch, Cement-Treated	Square Yard

Open-Graded Dr Cse, 5 inch, Cement-Treated will be measured by area in square yards in place in accordance with subsection 303.04 of the Standard Specifications for Construction.

Open-Graded Dr Cse, 5 inch, Cement-Treated includes furnishing the crushed aggregate, mixing with Portland cement, placing, spreading, shaping, compacting, curing, maintaining the CTPB, constructing the test strip, and disposal of all surplus and unsuitable materials.

Reviewed by Construction Agreement	
Reviewed by Engineer	
Date: 06/01/2013	Reviewed by: [Signature]
Accepted:	Reviewed by: [Signature]
Date: 06/02/2013	Reviewed by: [Signature]

C&T:JFS

4 of 4

03CT303(A140)
06-12-09

Negative adjustments will be made for 7-day compressive strength below the class design strength (CDS) according to the following formula. Positive adjustments do not apply.

$$\text{Adjusted Unit Price} = \frac{\text{Tested Strength}}{\text{CDS}} \times (\text{Unit Price})$$

APPENDIX C: AASHTO (1993) DESIGN CHARTS

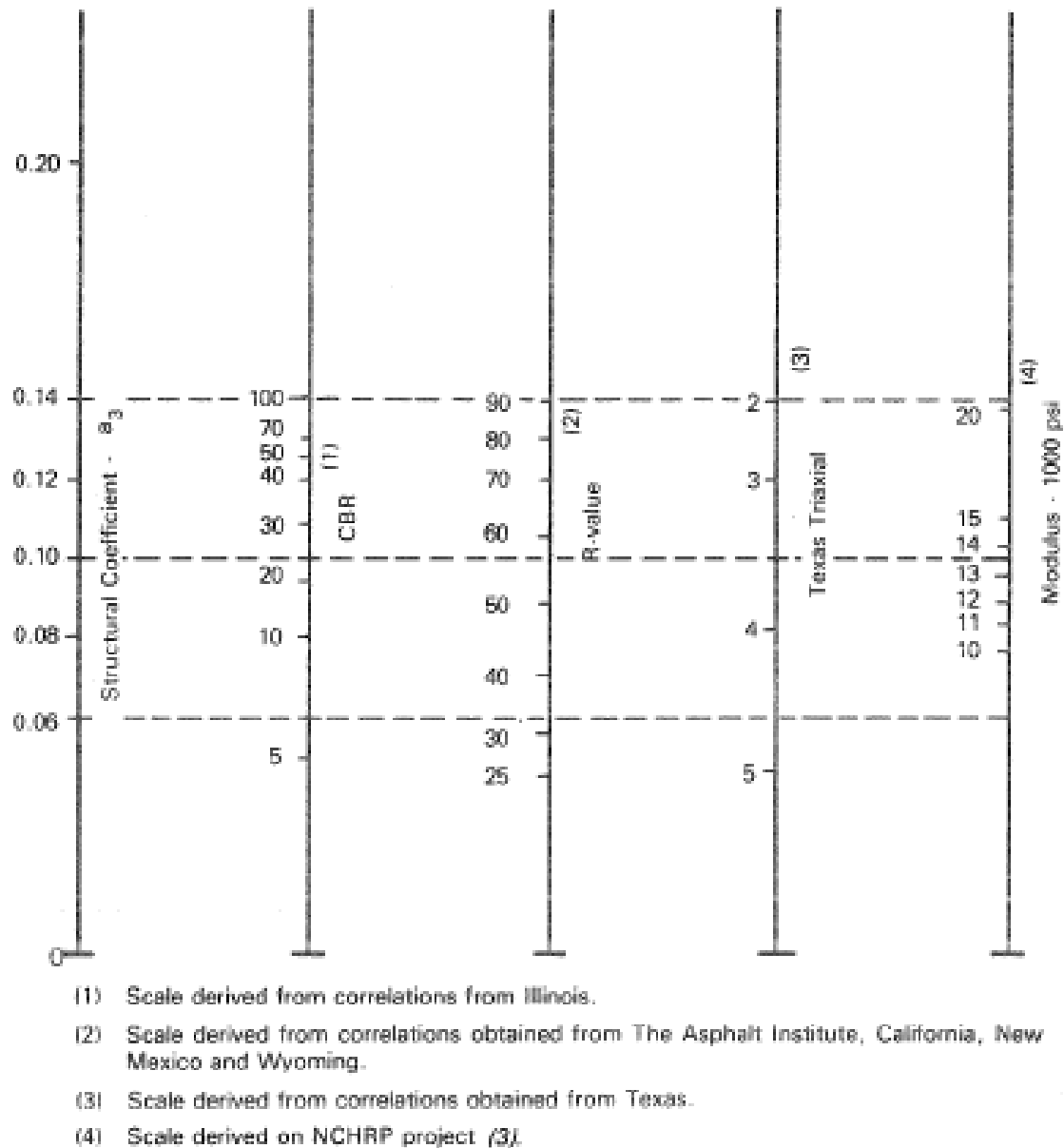
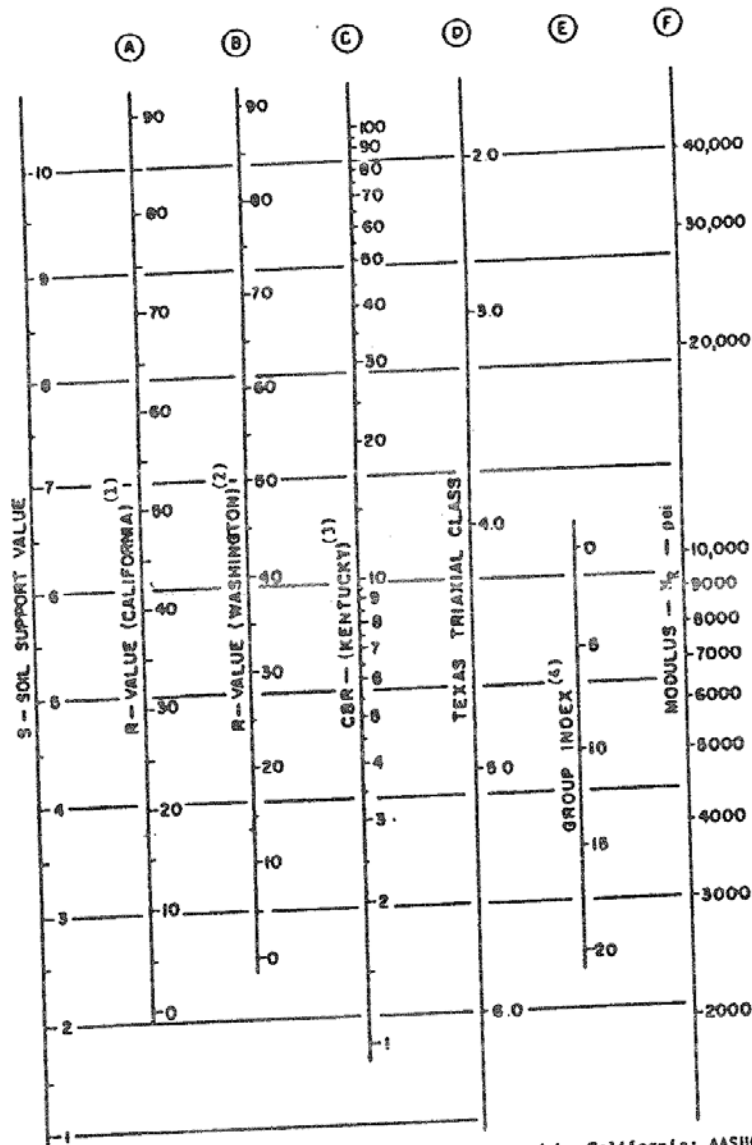


Figure 59. Chart to estimate modulus of subbase layer (E_{SB}) from CBR (from AASHTO 1993 based on results from van Til et al. 1972)



(1) The correlation is with the design curves used by California; AASHTO designation is T-173-60, and exudation pressure is 240 psi. See Hveem, F.H., and Carmany, R.M., "The Factors Underlying the Rational Design of Pavements." *Proc. HRB*, Vol. 28 (1948) pp. 101-136.

(2) The correlation is with the design curves used by Washington Dept. of Highways; exudation pressure is 300 psi. See "Flexible Pavement Design Correlation Study." *HRB Bull.* 133 (1956).

(3) The correlation is with the CBR design curves developed by Kentucky. See Drake, U.B., and Havens, J.H., "Re-Evaluation of Kentucky Flexible Pavement Design Criterion." *HRB Bull.* 233 (1959) pp. 33-56. The following conditions apply to the laboratory-modified CBR: specimen is to be molded at or near the optimum moisture content as determined by AASHTO T-99; dynamic compaction is to be used with a hammer weight of 10 lb dropped from a height of 18 in.; specimen is to be compacted in five equal layers with each layer receiving 10 blows; specimen is to be soaked for 4 days.

(4) This scale has been developed by comparison between the California R-value and the Group Index determined by the procedure in *Proc. HRB* Vol. 25 (1945) pp. 376-392.

Figure 60. Chart to estimate resilient modulus (M_r) of subgrade from CBR (from AASHTO 1993 Appendix FF based on results from van Til et al. 1972)

Example:

$D_{SB} = 6$ inches

$E_{SB} = 20,000$ psi

$M_R = 7,000$ psi

Solution: $k_{\infty} = 400$ pci

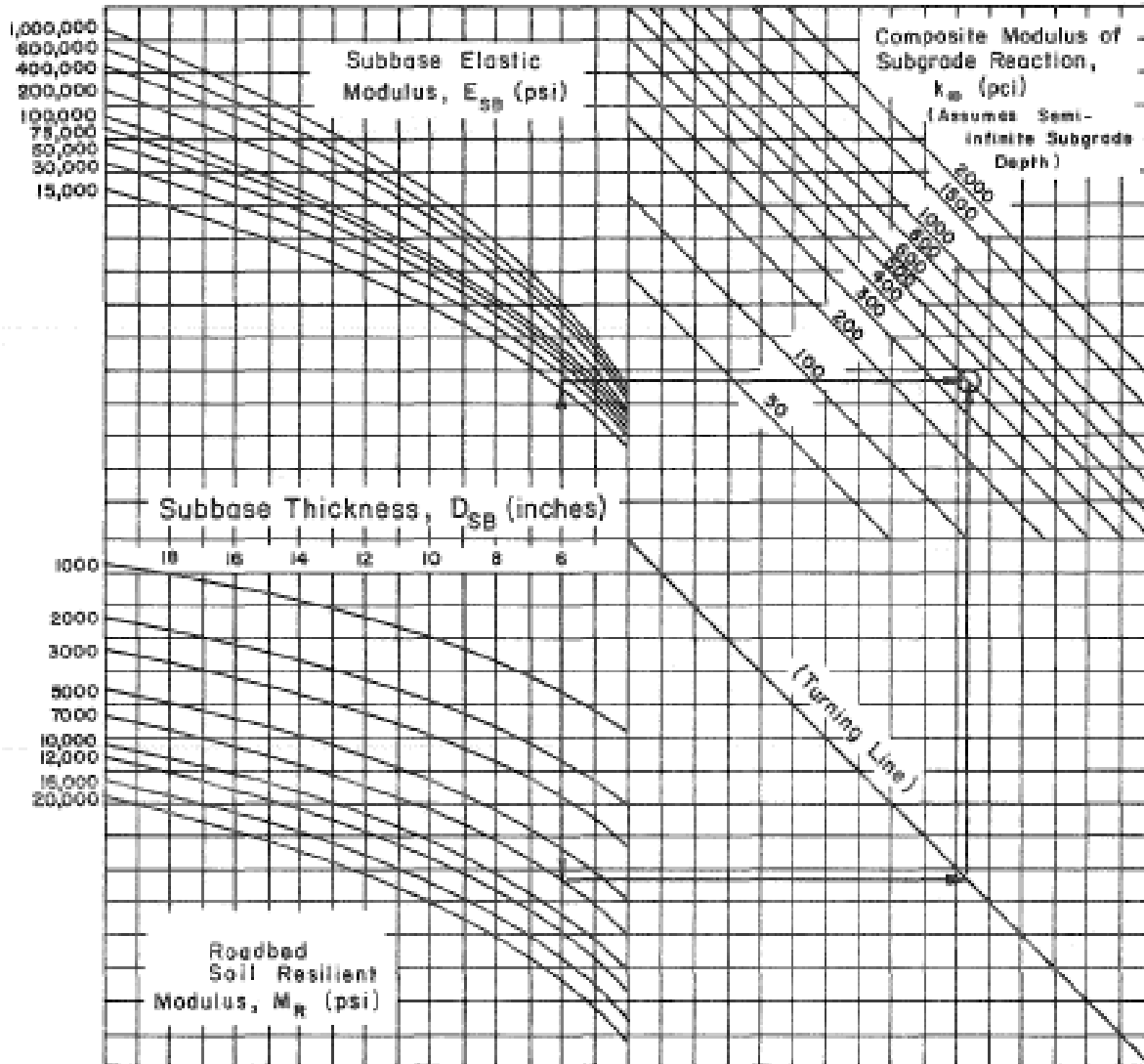


Figure 3.3. Chart for Estimating Composite Modulus of Subgrade Reaction, k_{∞} , Assuming a Semi-Infinite Subgrade Depth. (For practical purposes, a semi-infinite depth is considered to be greater than 10 feet below the surface of the subgrade.)

Figure 61. Chart for estimating composite modulus of subgrade reaction (k_{comp}) assuming a semi-infinite subgrade depth (from AASHTO 1993)

APPENDIX D: STRESS-STRAIN CURVES FROM RESILIENT MODULUS TESTS

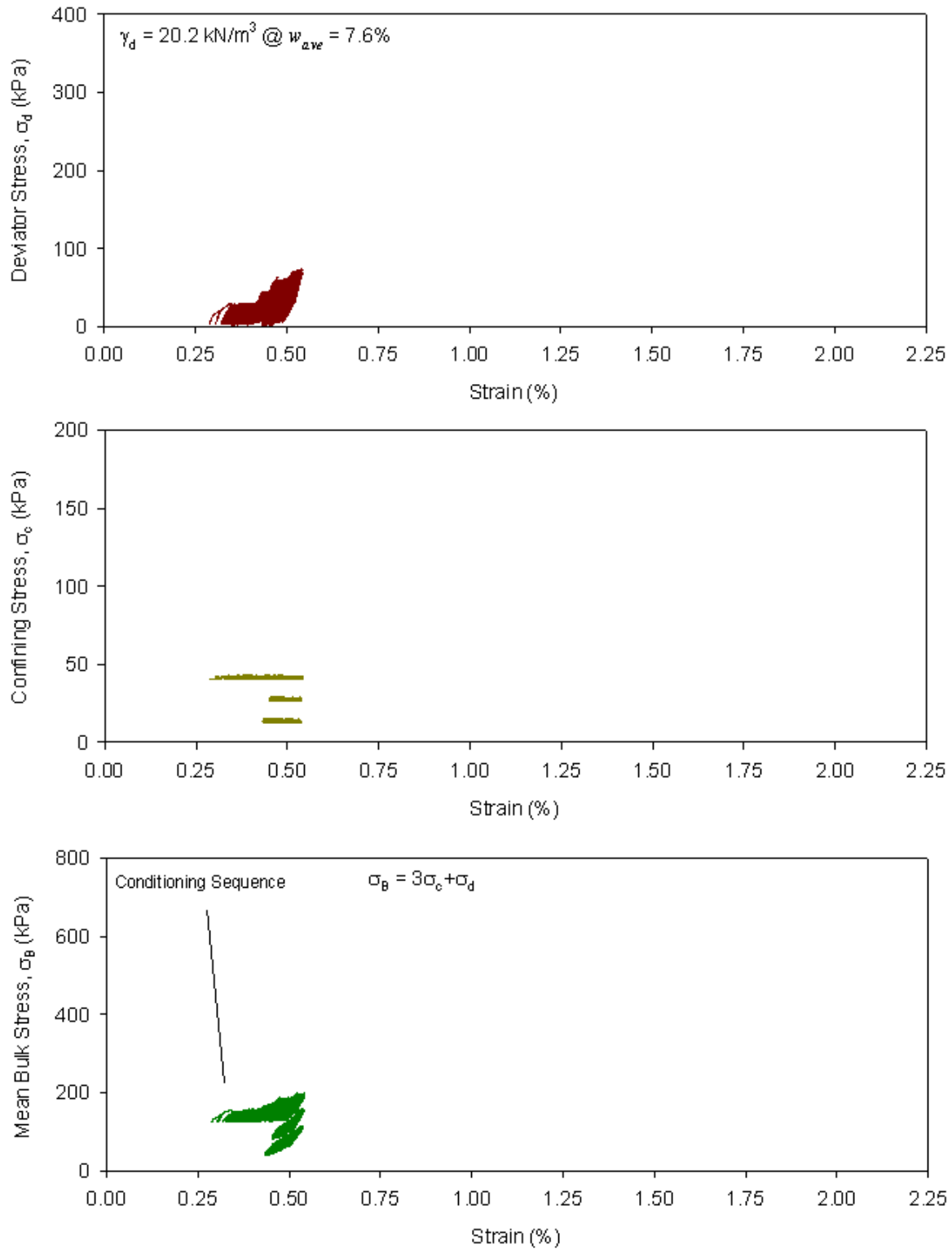


Figure 62. Cyclic stress-strain curves for subgrade sample # 1

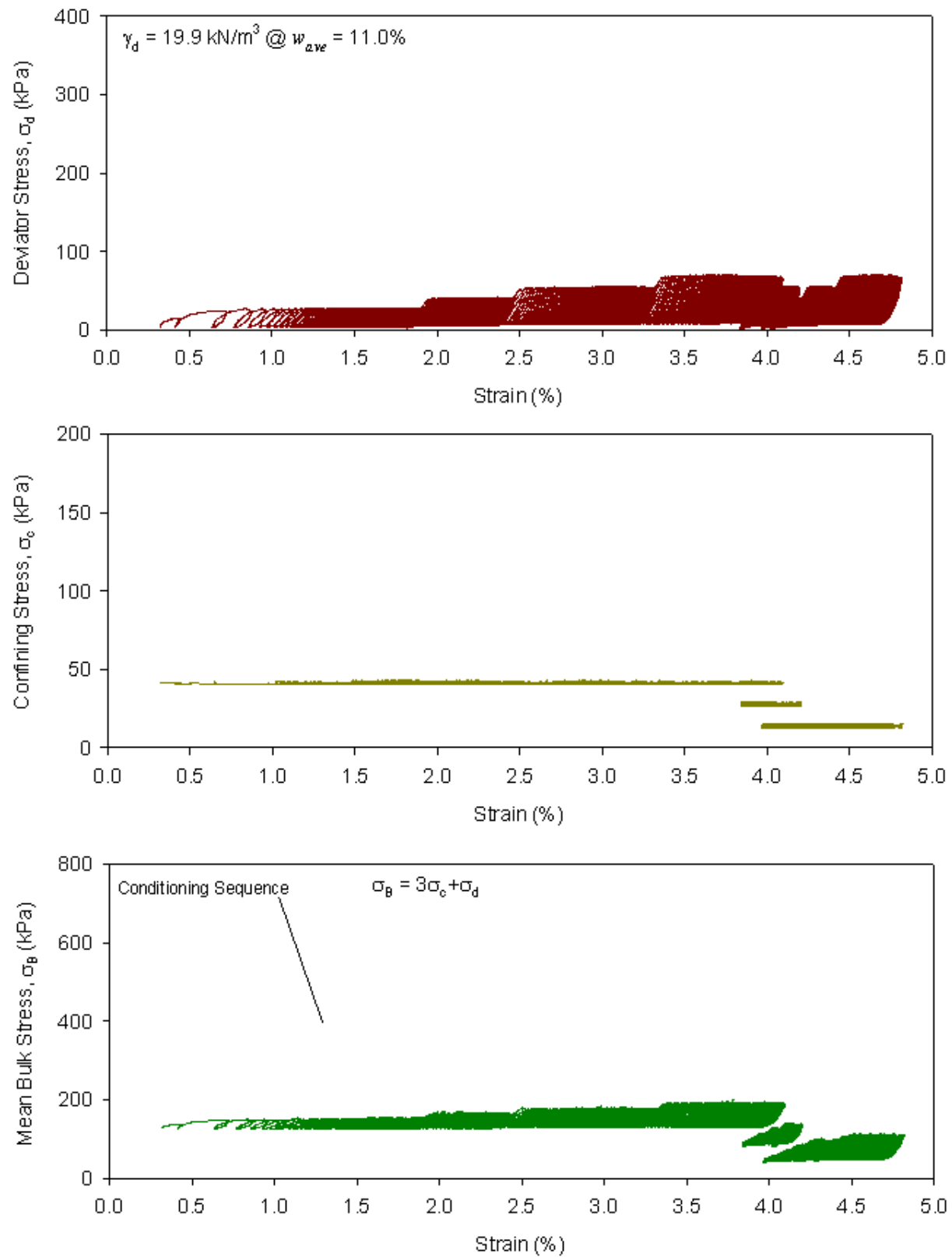


Figure 63. Cyclic stress-strain curves for subgrade sample # 2

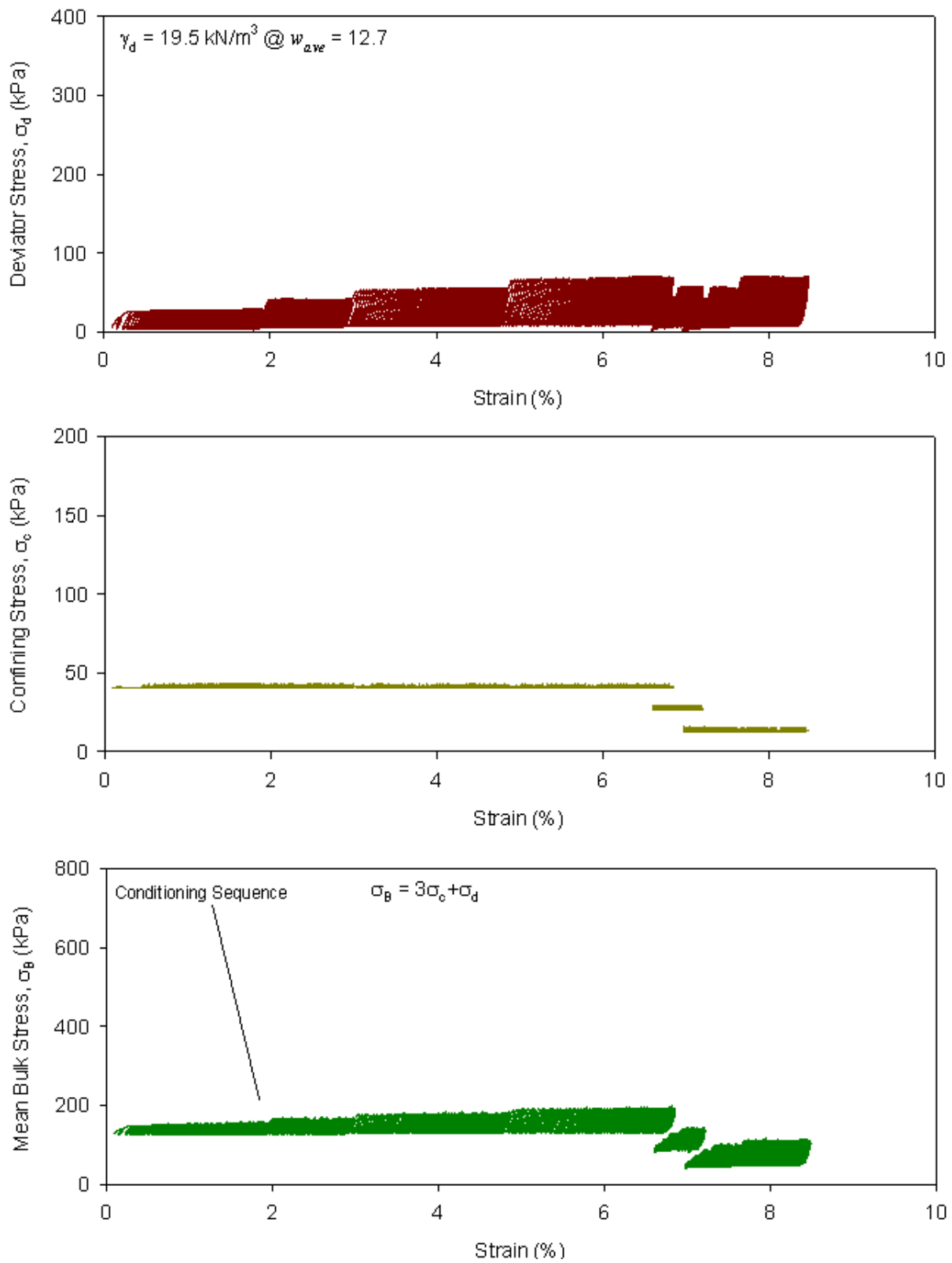


Figure 64. Cyclic stress-strain curves for subgrade sample # 3

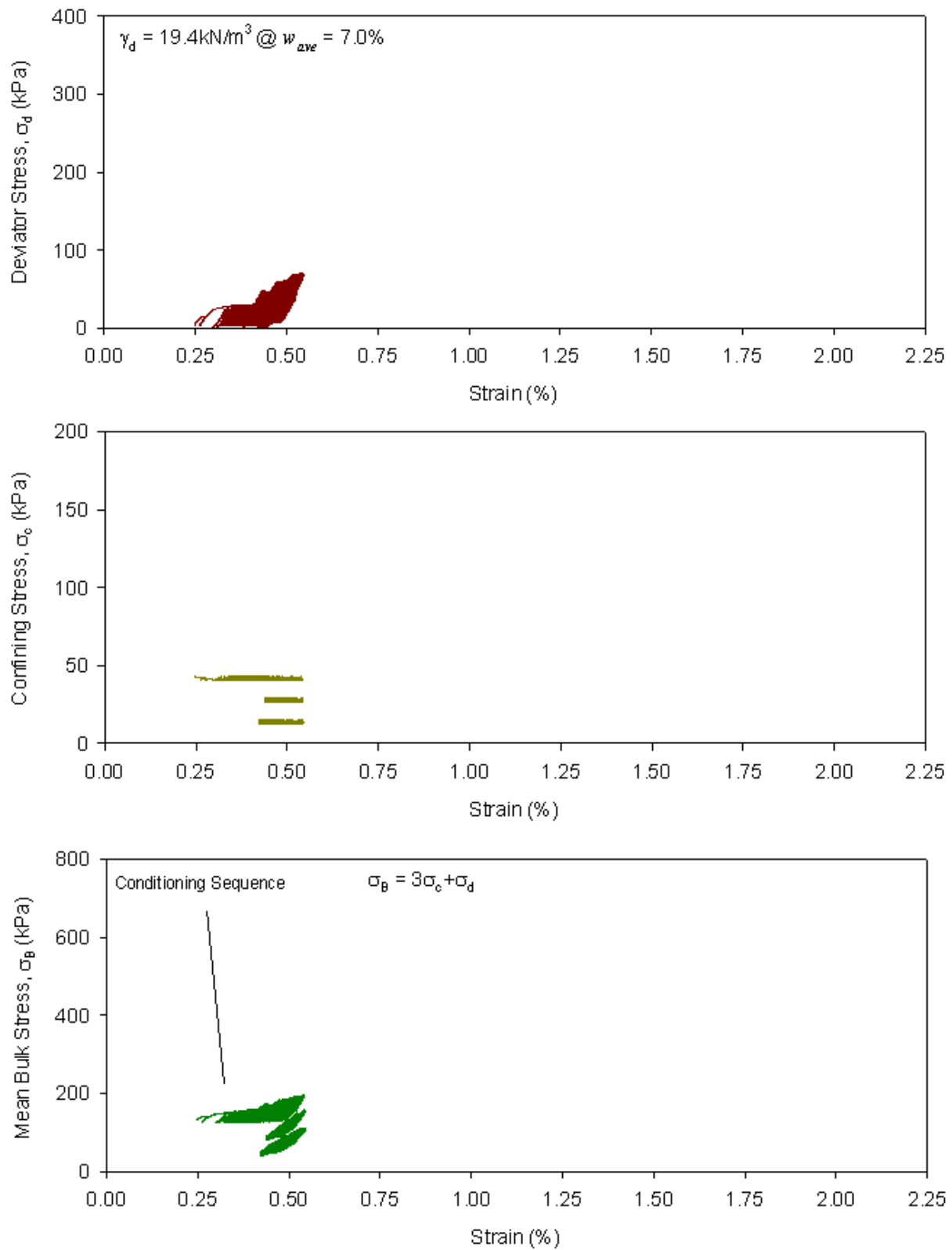


Figure 65. Cyclic stress-strain curves for subgrade sample # 4

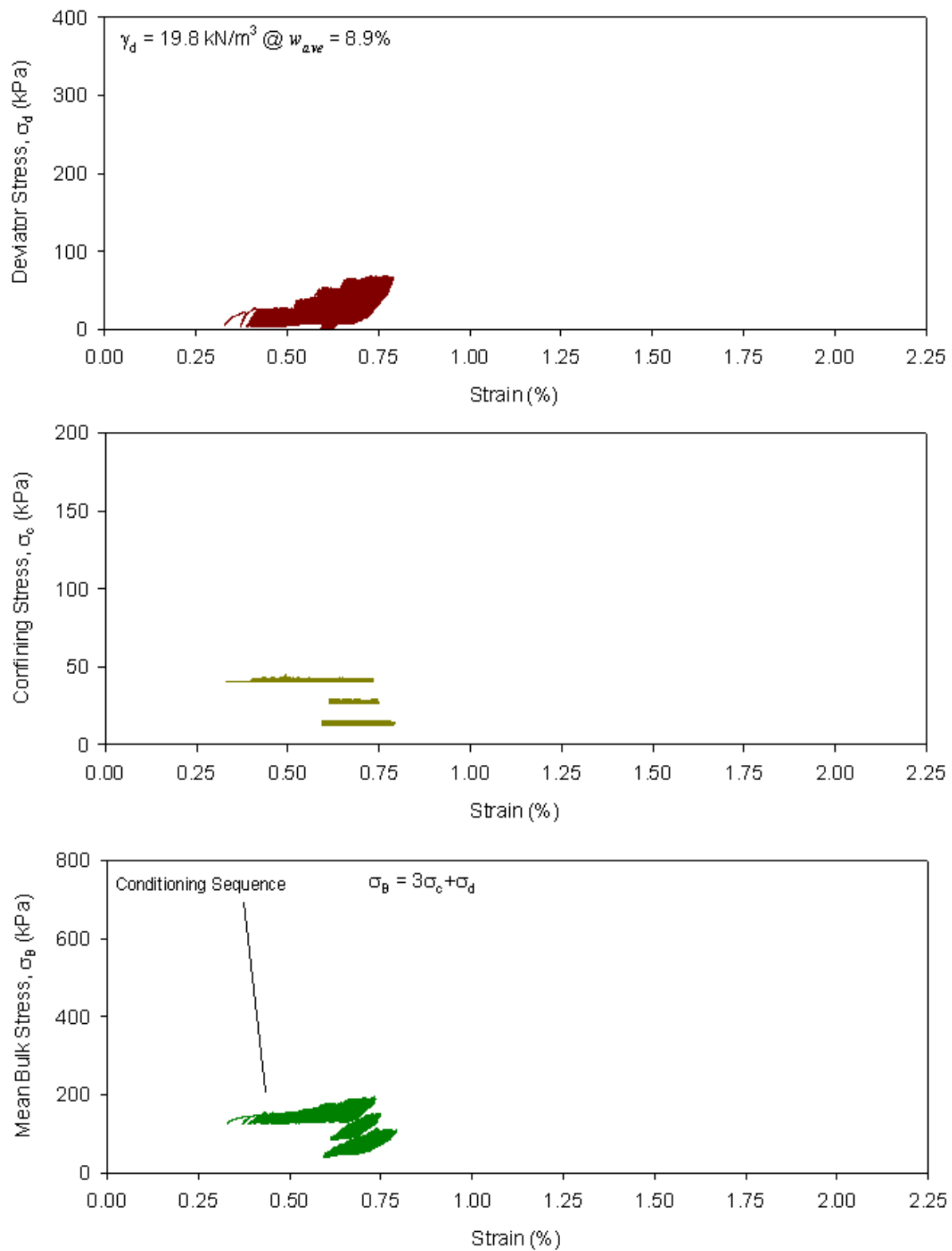


Figure 66. Cyclic stress-strain curves for subgrade sample # 5

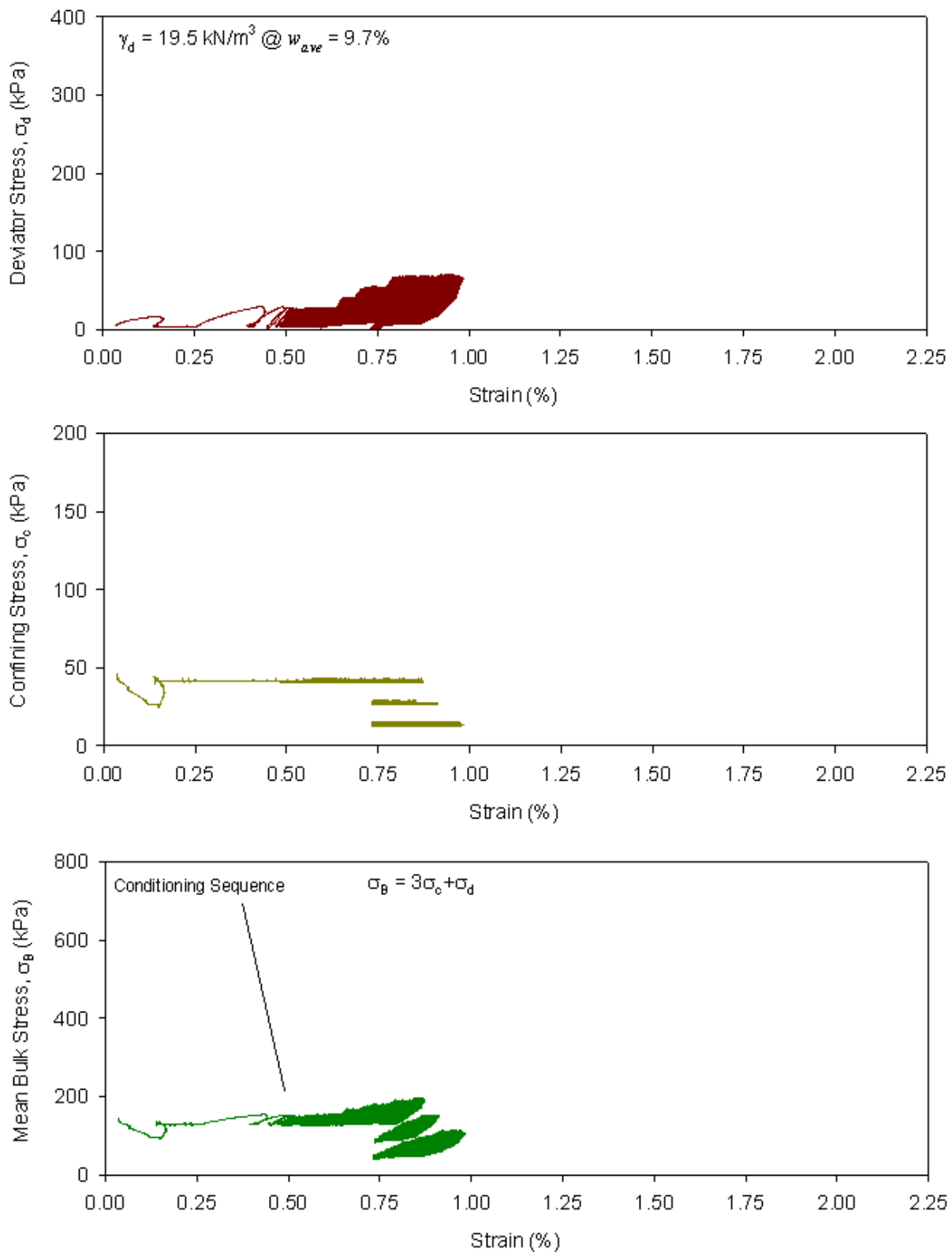


Figure 67. Cyclic stress-strain curves for subgrade sample # 6

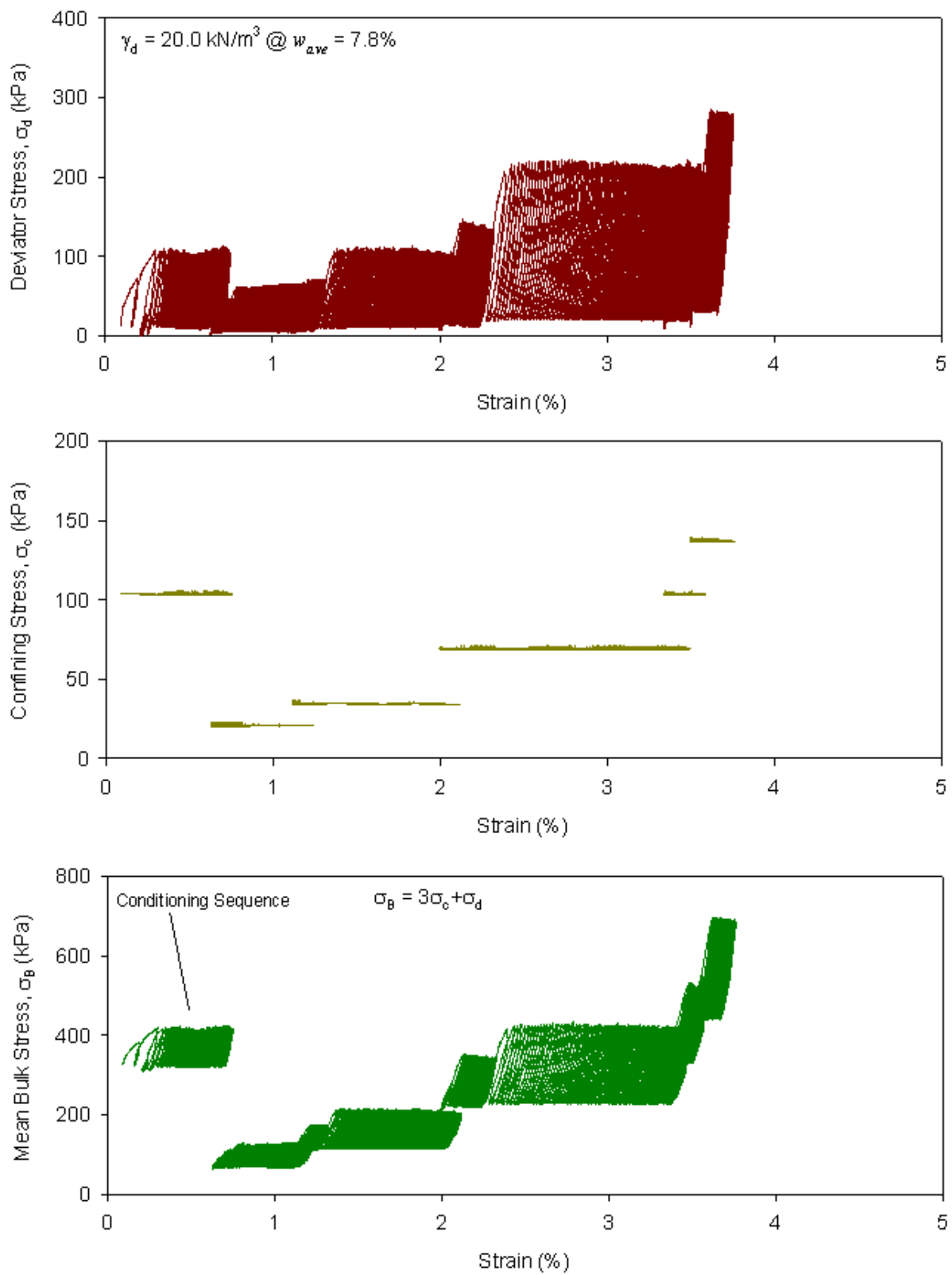


Figure 68. Cyclic stress-strain curves for subbase sample # 1

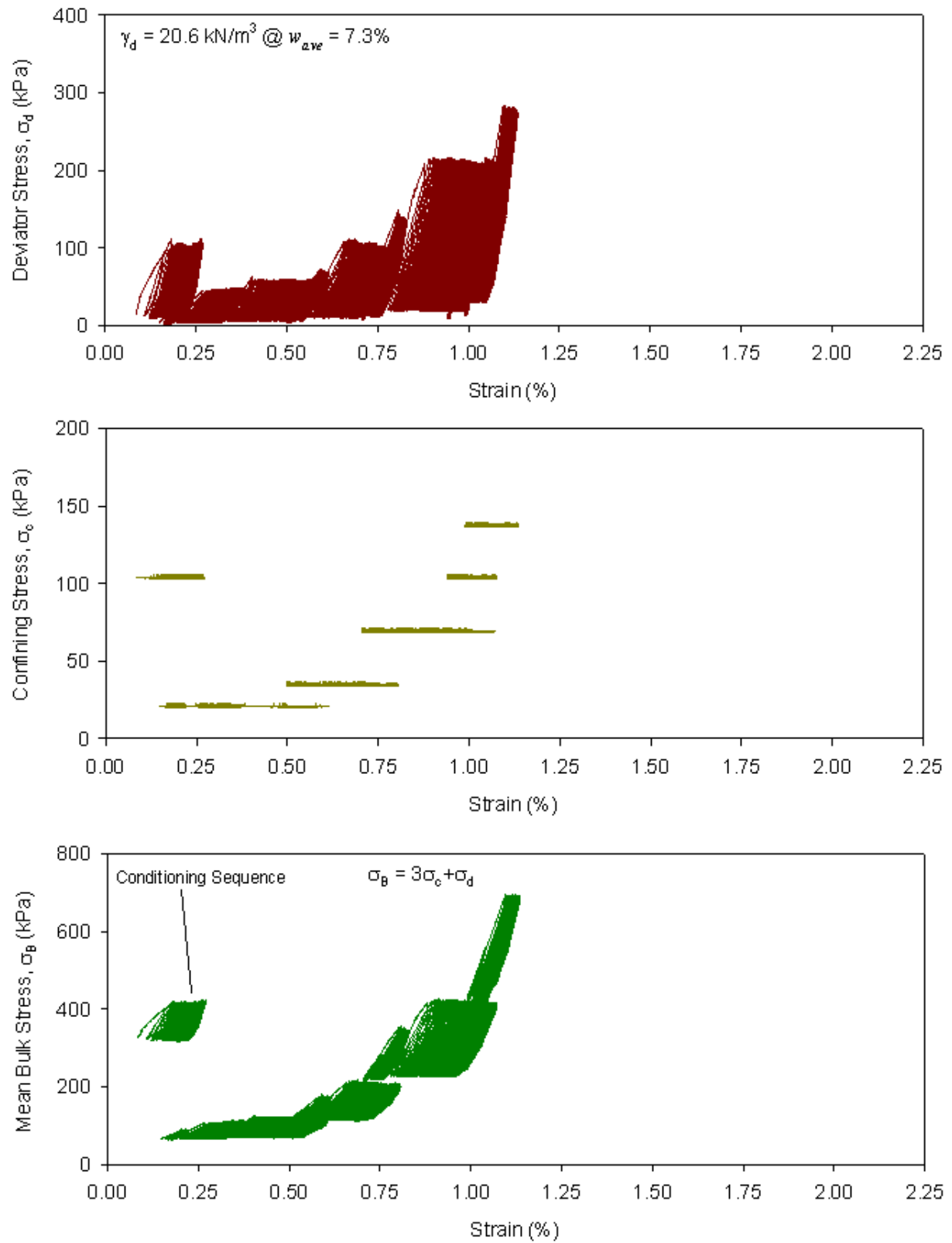


Figure 69. Cyclic stress-strain curves for subbase sample # 2

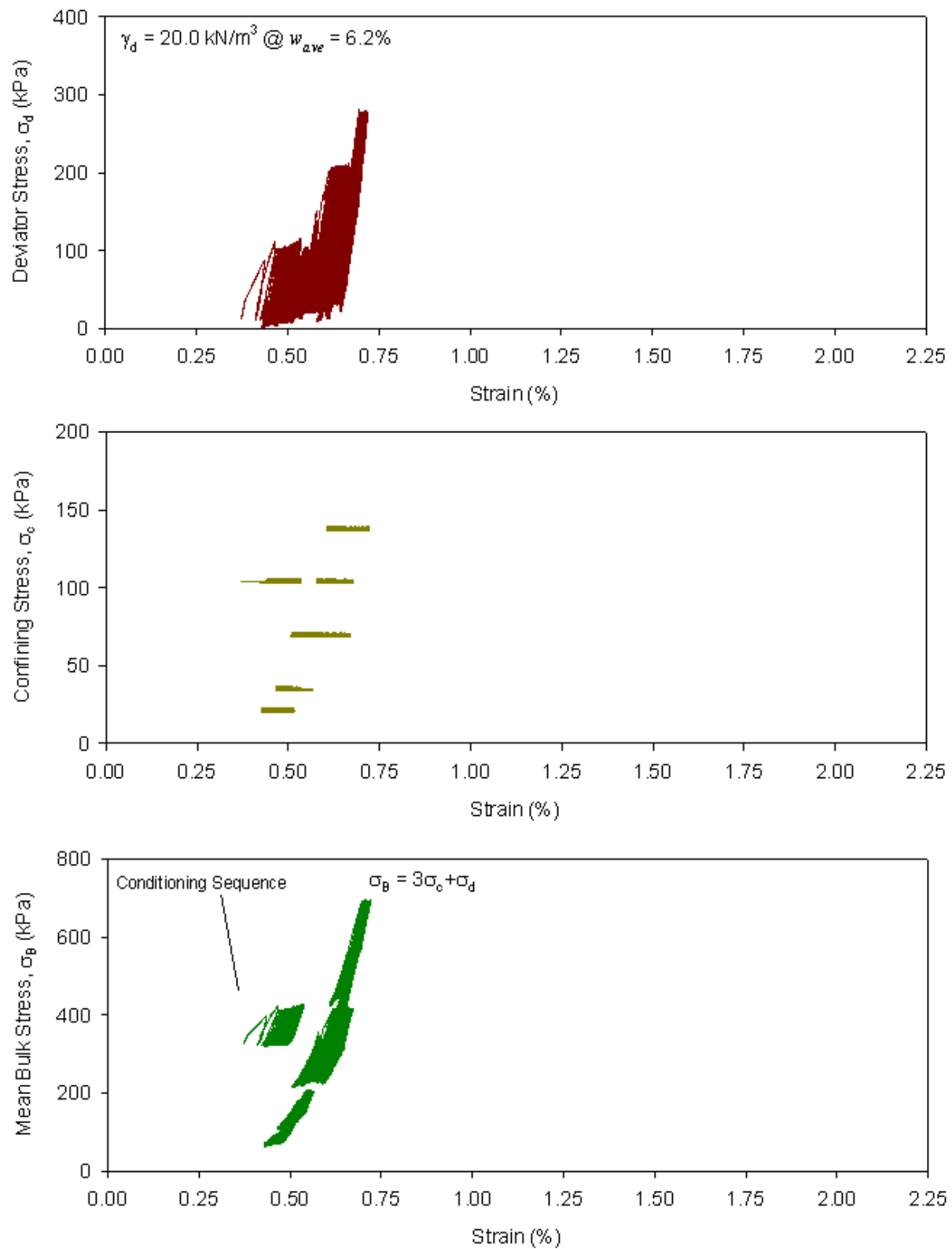


Figure 70. Cyclic stress-strain curves for subbase sample # 3

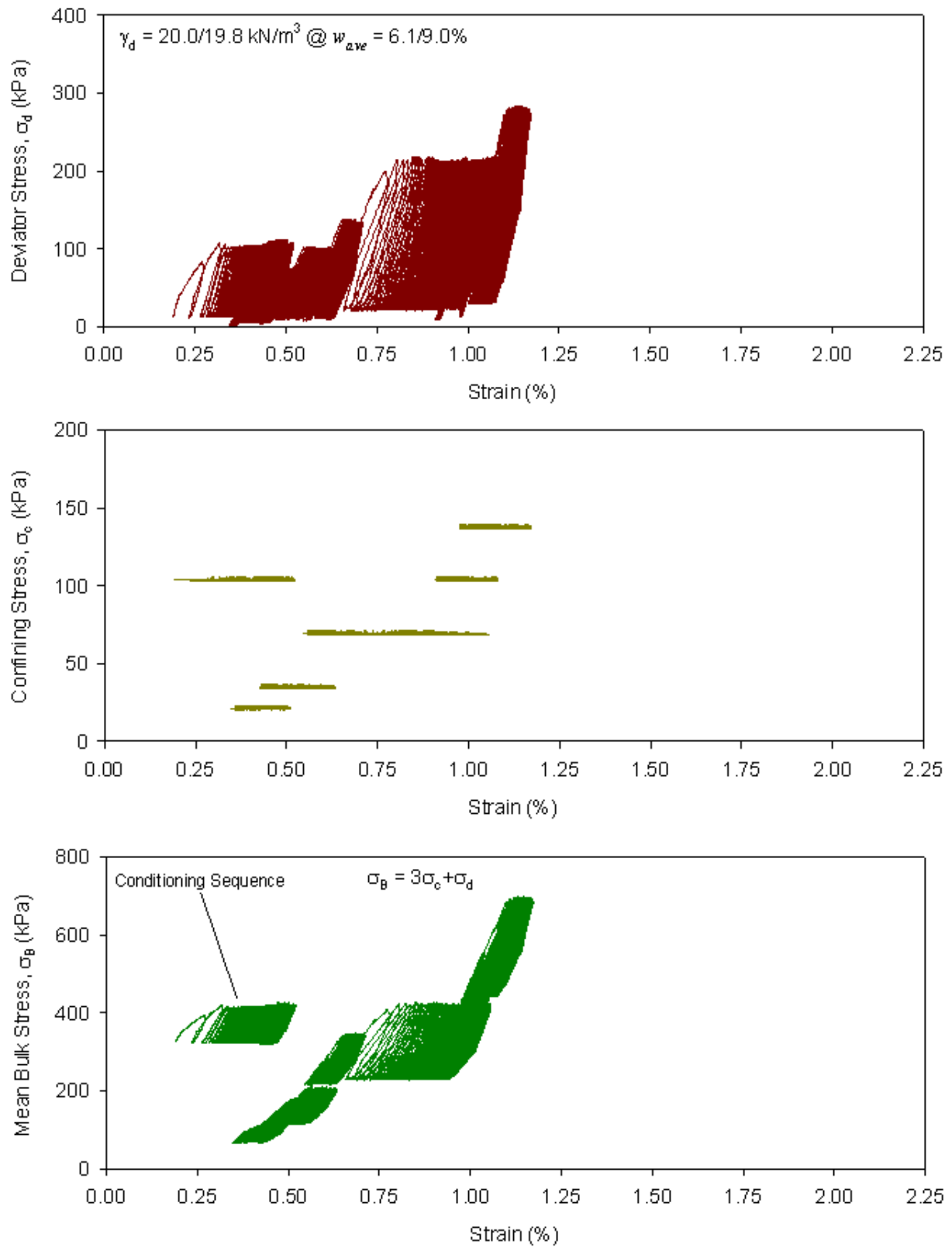


Figure 71. Cyclic stress-strain curves for subbase + subgrade composite sample